DEPARTMENT OF TRANSPORTATION

Pavement Thickness Evaluation Using 3D Ground Penetrating Radar

Lev Khazanovich, Principal Investigator
Department of Civil and Environmental Engineering
University of Pittsburg

June 2021

Research Project
Final Report 2021-19

To request this document in an alternative format, such as braille or large print, call 651-366-4718 or 1-800-657-3774 (Greater Minnesota) or email your request to ADArequest.dot@state.mn.us. Please request at least one week in advance.

Technical Report Documentation Page

1. Report No.	2.	3. Recipients Accession No.
MN 2021-19		

4. Title and Subtitle	5. Report Date
Pavement Thickness Evaluation Using 3D Ground Penetrating Radar	June 2021
	6.

7. Author(s)	8. Performing Organization Report No.
Lev Khazanovich	

9. Performing Organization Name and Address	10. Project/Task/Work Unit No.
Department of Civil and Environmental Engineering University of Pittsburgh Benedum Hall 3700 O'Hara Street Pittsburgh, PA 15261	11. Contract (C) or Grant (G) No. (c)1003327 (wo)1

12. Sponsoring Organization Name and Address	13. Type of Report and Period Covered
Minnesota Department of Transportation Office of Research & Innovation 395 John Ireland Boulevard, MS 330 St. Paul, Minnesota 55155-1899	Final Report
	14. Sponsoring Agency Code

15. Supplementary Notes

https://www.mndot.gov/research/reports/2021/202119.pdf

16. Abstract (Limit: 250 words)

The objective of this research was to develop a procedure for nondestructive assessment of pavement thickness using 3D ground penetrating radar (3D GPR). The software developed in this study can analyze the data sets collected with either 27- or 121- transmitting and receiving pair configurations. It uses two approaches to determine asphalt thickness: analysis of individual pairs of antennas time histories along with the user-provided dielectric constant for the asphalt layer; and analysis of groups of signals from transmitting and receiving antennas with various spacing but with a common mid-point using the Modified Extended Common Mid-Point (MXCMP) method. The MXCMP method is a generalization of the Extended Common Mid-Point (MXCMP) method for analysis of more than two antenna pair signals with the same mid-point.

17. Document Analysis/Descriptors	18. Availability Statement
Ground penetrating radar, Thickness, Antennas, Asphalt pavements	No restrictions. Document available from: National Technical Information Services, Alexandria, Virginia 22312

19. Security Class (this report)	20. Security Class (this page)	21. No. of Pages	22. Price
Unclassified	Unclassified	81	

PAVEMENT THICKNESS EVALUATION USING 3D GROUND PENETRATING RADAR

FINAL REPORT

Prepared by:

Lev Khazanovich
Department of Civil and Environmental Engineering
University of Pittsburgh

June 2021

Published by:

Minnesota Department of Transportation
Office of Research & Innovation
395 John Ireland Boulevard, MS 330
St. Paul, Minnesota 55155-1899

ACKNOWLEDGMENTS

The authors appreciate the participation of the members of the project technical advisory panel:

Shongtao Dai, MnDOT Research Operations Engineer

David Glyer, Project Coordinator, MnDOT Office of Research & Innovation

Timothy Andersen, MnDOT Pavement Design Engineer

Christine Dulian, MnDOT District 6 Engineer

Steven Henrichs, Assistant Pavement Design Engineer

Kyle Hoegh, Research Operations Scientist

Eyoab Zegeye Teshale, Senior Pavement Research Engineer

Special thanks to Dr. Eyoab Zegeye Teshale for collecting of the 3D GPR data.

TABLE OF CONTENTS

CHAPTER 1: Introduction 1

CHAPTER 2: GPR for Pavement Evaluation 2

2.1 GPR Types 2

2.1.1 Air Coupled Horn Antenna 2

2.1.2 Ultra-Wide Bowtie Antenna 3

2.1.3 Stepped Frequency Signal 4

2.1.4 Antenna Array 4

2.1.5 3D GPR 5

2.2 Determination of Asphalt Layer Thickness 6

2.2.1 Two-way travel method 6

2.2.2 Common Midpoint Method (CMP) 7

2.2.3 Common Source Method 9

2.2.4 Extended CMP Method (XCMP) 9

2.2.5 Accuracy of GPR for Pavement Layer Thickness Evaluation 12

CHAPTER 3: Evaluation of 3D GPR Signals Time Histories 14

CHAPTER 4: Development of the Asphalt Thickness Determination Procedure 25

4.1 Input Data 25

4.2 Input Data processing 25

4.3 Asphalt thickness Determination uisng individual antenna Pair data 28

4.4 Modfied Extended Common Mid-Point Method 29

4.5 Rudimentary Software 31

CHAPTER 5: Example with Field Data 33

CHAPTER 6: Conclusions 47

REFERENCES 48

Appendix A: User Guide

LIST OF FIGURES

Figure 1. FWD vehicle integrated with GSSI GPR and horn antenna (Uddin, 2006) 3

Figure 2. Illustration of a typical bowtie antenna (Zhao, 2015) 3

Figure 3. Stepped frequency signal example (Zhao, 2015) 4

Figure 4. APE vehicle outfitted with 3D GPR system 5

Figure 5. 3D GPR antenna array (Eide and Sala, 2012; Zhao, 2015) 6

Figure 6. Typical time history of GPR signal reflected from a pavement system (Zhao, 2015) 7

Figure 7. CMP method illustration 8

Figure 8. Signal time history (adapted from Zhao 2015) 9

Figure 9. Schematics of wave propagation and reflection from the bottom of asphalt layer 11

Figure 10. 3D GPR array system used in this study 14

Figure 11. Real part time histories for the signals transmitting by transmitting antenna 1 and recorded by receiving antennas 1 through 3. 16

Figure 12. Real part time histories for the signals transmitting by transmitting antenna 1 and recorded by receiving antennas 4 through 6. 16

Figure 13. Real part time histories for the signals transmitting by transmitting antenna 1 and recorded by receiving antennas 7 through 9. 17

Figure 14. Time history magnitudes for the signals transmitting by transmitting antenna 1 and recorded by receiving antennas 1 through 3. 17

Figure 15. Time history magnitudes for the signals transmitting by transmitting antenna 1 and recorded by receiving antennas 4 through 6. 18

Figure 16. Time history magnitudes for the signals transmitting by transmitting antenna 1 and recorded by receiving antennas 7 through 9 18

Figure 17. Signals from the antenna pairs with the same distances. 19

Figure 18. Signals from the antenna pairs Tx1 –Rx1 and Tx2-Rx2. 20

Figure 19. Example of oversampled real part time histories 21

Figure 20. Signal time histories from air calibration 22

Figure 21. Resulting time history after subtraction of the air calibration signal 22

Figure 22. Example of three antenna pairs with a common mid-point (top view) 29

Figure 23. Real part time histories for a non-dimensional time from 0 to 25. 34

Figure 24. Real part time histories w/o air calibration for non-dimensional time from 10 to 40. 35

Figure 25. Real part time histories with air calibration for non-dimensional time from 10 to 40. 36

Figure 26. Asphalt thicknesses for 27 pairs 38

Figure 27. Sensitivity of the computed asphalt thickness to the assumed dielectric constant for the asphalt layer. 39

Figure 28. Variation of the asphalt thickness along the project 40

Figure 29. Signal values of the reflections from the pavement surface for various assumed distances between antennas and pavement surface 41

Figure 30. Signal values of the reflections from the bottom asphalt surface for various assumed asphalt thicknesses and dielectric constant of asphalt equal to 6. 42

Figure 31. Total signal values of the reflections from the bottom asphalt surface for various assumed asphalt thicknesses and dielectric constants of asphalt equal to 4, 6, and 8. 43

Figure 32. The maximum values of the total signals and the corresponding asphalt thicknesses for various assumed values of the dielectric constants of asphalt. 44

Figure 33. Computed asphalt thicknesses and dielectric values from time histories from every antenna pair groups and the same trigger. 45

Figure 34. Computed asphalt thicknesses for one antenna group but different triggers 46

LIST OF TABLES

Table 1. Data collection protocol with 27 transmitting and receiving pairs. 24

Table 2. Determination of the time of the arrival of the reflection signal from the top pavement surface. 36

Table 3. Determination of the time of the arrival of the reflection signal from the top pavement surface. 37

Table 4. Determination of the time of the arrival of the reflection signal from the top pavement surface. 37

Table 5. Thicknesses of the top asphalt layer computed using tine histories from the individual antenna pairs..... 37

EXECUTIVE SUMMARY

Developing cost-effective pavement rehabilitation strategies requires knowledge of the existing pavement thickness. Currently, thickness assessment is done by the Minnesota Department of Transportation (MnDOT) either by core removal or with single antenna ground penetrating radar (GPR) testing. Conventional GPRs provide a nondestructive evaluation of pavement thickness but restrict testing during one pass to a single test line.

The objective of this research was to develop a procedure for nondestructive assessment of pavement thickness using 3D ground penetrating radar (3D GPR). The 3D RADAR step-frequency linear array system provides coverage of a 1.5-meter wide area at 75-mm spacing in the transverse direction, which improves data collection productivity and coverage. The 3D GPR has been incorporated into the RoadDoctor vehicle to further advance MnDOT's capabilities in continuous roadway evaluation technologies.

The developed software can analyze the data sets collected using all 121 transmitting and receiving pairs. However, to improve the efficiency of data collection, a data collection protocol with 27 sending and receiving pairs was proposed. This protocol permits the determination of the asphalt layer thicknesses along 9 paths 6 inches apart.

Two procedures for the determination of the asphalt layer thickness using the data collected with the 3D Radar system were incorporated into the software. The first procedure uses signal time histories recorded by individual antennas. The second procedure uses the Modified Extended Common Mid-Point (MXCMP) method to simultaneously analyze groups of signals collected with transmitting and receiving antennas at various distances. The MXCMP method was developed in this study to generalize the Extended Common Mid-Point method for the analysis of more than two signals collected by antenna pairs having a common mid-point.

The software reports the resulting asphalt layer thicknesses in comma-separated text files that can be later analyzed by the user using Excel or other tools. The use of multiple antenna pairs focused on the same point of the pavement surface and two analysis methods provides redundancy and increases reliability of the computed thicknesses compared to the results obtained with a single GPR antenna.

To validate the procedure developed in this study, it is recommended to perform demonstration projects for a variety of existing pavement types and ambient conditions and compare the results of the program with the asphalt thicknesses from cores. Then the current *Pavement Design Manual* can be modified to allow reduction of the number of cores if a 3D GPR evaluation is conducted.

The use of the proposed tool would facilitate the use of continuous asphalt thickness evaluation at highway speed and minimize the amount of coring. Whereas coring indicates thickness only in the location of the core and a traditional GPR provides a depiction of thickness along the line of survey, one pass of a 3D GPR corresponds to multiple passes of a traditional GPR. Therefore, 3D GPR scans provide a full depiction of thickness for the entire scanned region. The tool developed in this study will enable MnDOT to reduce the number of cores taken to assess pavement thickness and provide a more comprehensive evaluation of thickness for the entire scanned region.

CHAPTER 1: INTRODUCTION

An accurate determination of the asphalt layer thickness is important both as a quality assurance/ quality control (QA/QC) measure and as a step in renewing pavement systems. For QA/QC, assessing thickness ensures that the pavement is structurally capable of providing the intended roadway service life and performance; for pavement renewal, the design of many rehabilitation/reconstruction options (e.g., full-depth reclamation, cold in-place recycling, and whitetopping) is strongly influenced by the existing pavement thickness.

Currently, the Minnesota Department of Transportation (MnDOT) uses core removal to assess thickness of the asphalt pavements. In this study, the procedure was developed to determine the asphalt layer thickness, using data collected from the 3D ground penetrating radar (3D GPR) data. 3D GPR is a nondestructive device with a step-frequency linear array GPR system. The 3D GPR has been incorporated into the RoadDoctor vehicle to further advance MnDOT's capabilities in continuous roadway evaluation technologies. Use of the proposed procedure will enable MnDOT to conduct continuous asphalt thickness evaluation at highway speed and minimize the amount of coring.

The following five chapters of the report describe the project work:

Chapter 2 provides background on GPR technology and the various methods used for determining asphalt pavement thickness using GPR.

Chapter 3 describes the evaluation of the data collected with the 3D GPR system and the procedure to determine asphalt layer thickness using time histories from individual antenna.

Chapter 4 presents the development of the generalization of the common mid-point (CMP) method for determining asphalt layer thickness using data from a group of antenna pairs with the same common mid-point.

Chapter 5 presents an illustration of the procedure with the 3D GPR data collected at MnROAD.

Chapter 6 concludes the report and provides recommendations for future work.

Appendix A provides a user's guide to the developed software for 3D GPR data analysis and the source code for the developed analysis and software.

CHAPTER 2: GPR FOR PAVEMENT EVALUATION

GPR (Ground Penetrating Radar) is the general term applied to techniques that employ electromagnetic waves. GPR uses electromagnetic fields to probe non-metallic materials to detect layers and changes in material properties within the structure. GPRs were invented more than 100 years ago in Germany. According a compilation by Olhoeft and Smith III (2000), at the end of 1999 there were more than 260 articles, patents, and standards related to the use of the GPR technology to evaluate concrete and asphalt pavements. The Minnesota Department of Transportation (MnDOT) has an established history of using GPR technology in pavement assessment for such tasks as determining layer thicknesses, locating subsurface objects, and evaluation compaction uniformity (Cao et al, 2007; Hoegh et al 2015).

GPR works by emitting a pulse into the pavement and recording the echoes. The transmitting antenna emits a signal that travels through air and is partially reflected when it meets the pavement surface. The receiver antenna then picks up the wave that has been reflected. The returned signal received by the antenna is saved by the GPR system for later processing and visualization. Grote et al. (2005) state that GPR can be equipped with antennas for sending and registering different frequency classes. By using high-frequency antennas, the results appear in high resolution, however the depth range is low. On the other hand, low frequency antennas provide deeper penetration with a consequent lower resolution. Most commercial GPR offer antenna with frequencies between 50 MHz and 1.5 GHz (Daniels, 1996).

2.1 GPR TYPES

In order to convert electrical signals from transmission lines to empty space – and vice versa –, antennas designed to radiate or to receive electromagnetic waves are used as transducers (IEEE 1993). GPR uses antenna in different arrangements to locate targets or interfaces within a medium (Daniels 2005). There are two major types of GPR: ground coupled or air coupled. The antennas can be in contact with the ground in what is referred to as ground coupled GPR or they can be above the ground which is air coupled GPR.

2.1.1 Air Coupled Horn Antenna

Air coupled antenna quickly became one of the most popular GPR systems due to the ability to collect data on pavement and bridges with a moving vehicle. This enables the collection of GPR data at normal highway speed thus significantly decreasing the interference on traffic. Figure 1 shows a JILS 20T FWD (back of the vehicle) integrated with GSSI RoadScan GPR and 2-GHz model 4105 horn antenna (Uddin, 2006). This type of GPR system also presents highly satisfactory directivity due to antenna having gains larger than 15 dB (Stutzman and Thiele 2012).

Figure 1. FWD vehicle integrated with GSSI GPR and horn antenna (Uddin, 2006)

2.1.2 Ultra-Wide Bowtie Antenna

GPRs equipped with low frequency antenna are widely used for locating structures placed deep underground like utilities, drainage devices, and others. A horn antenna usually has a moderate range for operation frequency. For activities such as pavement thickness evaluation, which are performed closer to the surface, antenna with high frequency, like a broadband antenna, perform better due to the superior time domain resolution provided.

To enable finer time domain resolutions, an ultra-wideband antenna like the bowtie antenna can be used (Eide, 2000). Since the bandwidth is one of the most important features for adequate resolution, bowtie antennas also have the advantage of presenting finer lateral resolutions (Jol 2008). Bowtie antenna are designed with an angle between two metal pieces as illustrated in Figure 2.

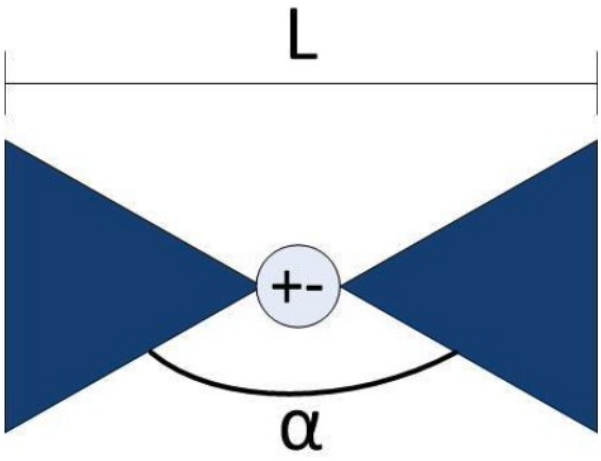

Figure 2. Illustration of a typical bowtie antenna (Zhao, 2015)

2.1.3 Stepped Frequency Signal

Broadband antennas might radiate waves at a stepped frequency because of the radiation pattern developed over wider frequency bands. This effect causes signals to have successive pulses linearly increasing frequency in discrete steps. As illustrated in Figure 3, frequency, which is emitted in dwell times (duration), increases with time by the frequency step.

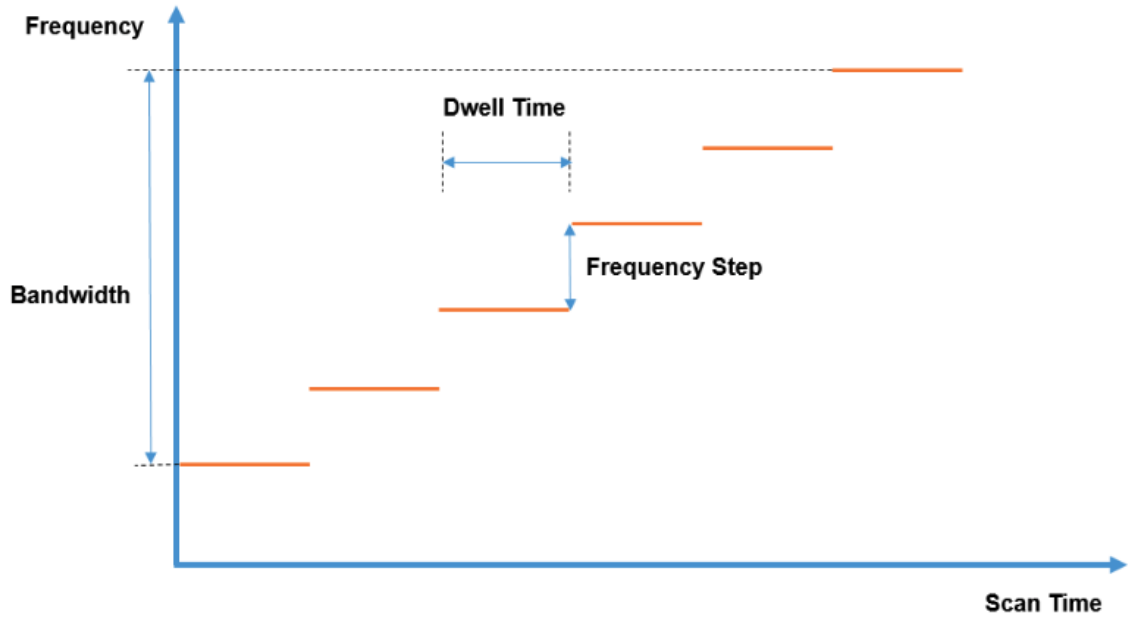

Figure 3. Stepped frequency signal example (Zhao, 2015)

The stepped frequency signal is collected in the frequency domain. By calculating the inverse Fourier transform of the frequency, the signal's time domain can be estimated. As dwell time increases, a more adequate signal to noise ratio (SNR) can be estimated. Still, with a longer dwell time, the survey speed of a single stepped frequency system will be slower than in a pulsed system (Zhao, 2015).

2.1.4 Antenna Array

Using a combination of multiple antenna elements in an array has many advantages. Most of all, the radiation patter, which is simultaneously transmits and receives by all the elements in the array, is controllable. When using an antenna array, the adjustment of each element's spacing and phasing can control the resulting radiation pattern.

In this system, the array factor is described as the array's radiation patter considering an isotropic point source as a replacement for the actual elements whereas the element pattern is the radiation of a single element. The product of both features, the array factor and the element patter, is defined as the total pattern of the array.

The GPR array element is defined by the type of antenna needed. As mentioned, a horn antenna array can provide moderate bandwidth needing fewer array elements which are more widely spaced limiting the number of scans. Conversely, a bowtie antenna element presents a wider beam, simple structure, and a broad bandwidth (Stutzman and Thiele, 2012).

A synthetic aperture radar (SAR) is a single antenna moving from one position to another (Blahut, 2004). While this results in a similar performance of an antenna array, the SAR antenna transmits the pulse and receives the reflection at each position individually in succession. This results in the electromagnetic wave being doppler-shifted because the data is collected while the device is moving. When compared to a conventional antenna array, SAR provides less information than when a signal is transmitted and received by two different antenna elements and tends to miss relevant information.

2.1.5 3D GPR

In 2014, MnDOT outfitted a vehicle from the Federal Highway Administration (FHWA) with a step-frequency ground penetrating radar system (manufactured by 3D Radar) referred to as 3D GPR as shown in Figure 4. Later, a 3D GPR antenna was incorporated into the RoadDoctor vehicle. A 3D GPR system is composed of an array of electronically switched transmitting and receiving bowtie antenna pairs. The DX antenna system used in this study has 11 transmitting (T) and receiving (R) antennas as shown is Figure 5. Each receiving antenna may record signals from any transmitting antenna in the assembly.

Figure 4. APE vehicle outfitted with 3D GPR system

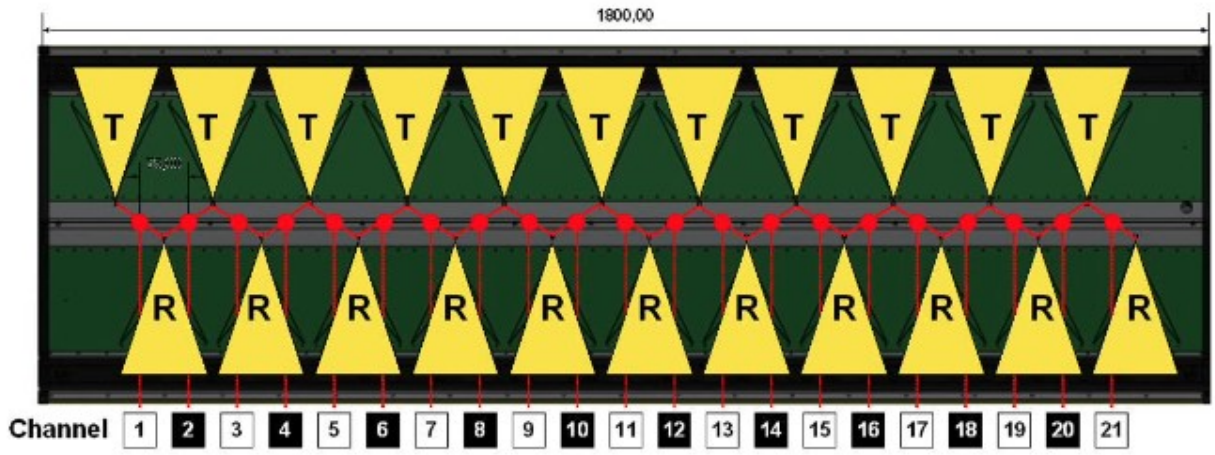

Figure 5. 3D GPR antenna array (Eide and Sala, 2012; Zhao, 2015)

While the data collection with 3D GPR is very efficient, the analysis of the collected data is complex. This research was initiated to evaluate and develop methods for determining asphalt layer thickness from the data collected using the 3D Radar ground penetrating radar (3D GPR) equipment. The following methods have been used in the past for determining pavement layer thicknesses.

2.2 DETERMINATION OF ASPHALT LAYER THICKNESS

Below we will provide a brief overview of the available methods for determination of asphalt layer thickens using GPR data.

2.2.1 Two-way travel method

Two-way travel method is a common method for the calculation asphalt surface layer thickness from single antenna GPR measurements. Figure 6 shows a typical GPR signal reflected from a pavement system consisting of a surface layer whose dielectric constant is ε_1 and a second layer whose dielectric constant is ε_2. Tx/Rx represents the location of the monostatic antenna, and A_0 and A_1 are the amplitudes of the reflection from the surface and the bottom of the surface layer, respectively.

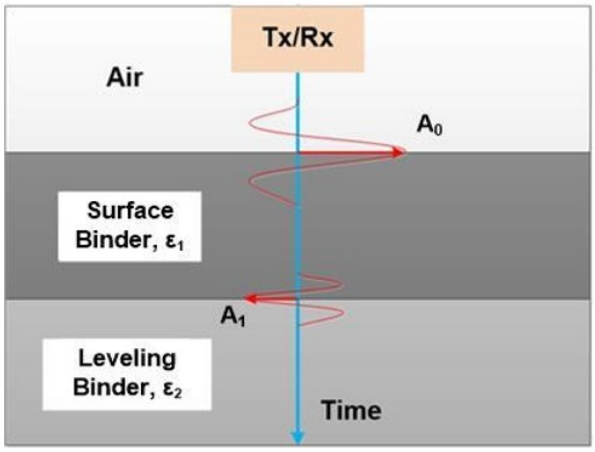

Figure 6. Typical time history of GPR signal reflected from a pavement system (Zhao, 2015)

The two-way travel method determines the thickness of the surface layer using the following equation:

$$h = \frac{\Delta t\, v}{2} \quad (1)$$

where h is the layer thickness, Δt is the two-way travel time of the electromagnetic wave within the surface layer, and v is the velocity of the electromagnetic waves in the surface layer that can be determined as follows:

$$v = c/\sqrt{\varepsilon} \quad (2)$$

where c is speed of light of in vacuum. Dielectric constant is a characteristic of an electrical insulating material quantifying the degree to which a material stores and transmits electromagnetic energy. The velocity at which electromagnetic waves propagate through a dielectric medium decreases with an increase in dielectric constant. The dielectric constant of air is close to 1, for water it is 81, and for asphalt it is between 4 and 8. Dialectic constant cores need to be taken for each new mix at locations with measured dielectric constant is determine from cores or from the ratios of the magnitude of the signal reflection from the pavement surface to the magnitude of the signal reflection from a steel plate using the following equation (Saarenketo and Scullion 2000):

$$\varepsilon = \left(\frac{1+\left(\frac{A_0}{A_i}\right)}{1-\left(\frac{A_0}{A_i}\right)}\right)^2 \quad (3)$$

2.2.2 Common Midpoint Method (CMP)

Common Midpoint Method (CMP) is a layer thickness determination method based on increasing an offset between Transmitter (Tx) and Receiver (Rx). An increase in the offset increases the two-way travel time in the layer. The Tx-Rx offset is centered on the mid-point (Figure 7). The travel time depends

on the ray path that the GPR signal travels from the Tx to the Rx, specifically: direct, refracted, or reflected. The method assumes that the pavement is thick enough and/or the frequency band of the electromagnetic wave is wide enough so the two pulses reflected from the surface and the bottom of the layer can be distinguished. The layer thickness can be obtained from the known offsets between the antennas and the two-way travel times of both antenna systems.

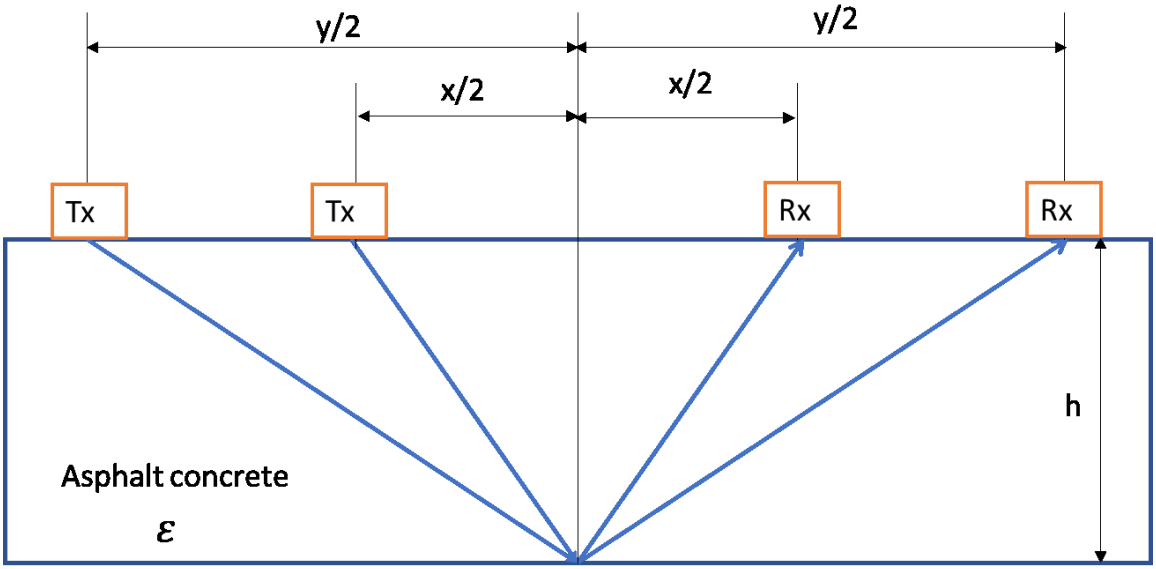

Figure 7. CMP method illustration

From Figure 7 the following equations can be written:

$$v\,t_1 = 2\sqrt{h^2 + \left(\frac{x}{2}\right)^2} \tag{4}$$

$$v\,t_2 = 2\sqrt{h^2 + \left(\frac{y}{2}\right)^2} \tag{5}$$

where t_1 is travel time from transmitter T_1 to receiver R_1 through the surface layer reflecting at point P, and t_2 is travel time from transmitter T_2 to receiver R_2 through the surface layer reflecting at point P.

From Equations 4 and 5, the layer thickness h and electromagnetic wave velocity can be calculated as follows:

$$h = \frac{1}{2}\frac{\sqrt{t_1{}^2 y^2 - t_2{}^2 x^2}}{\sqrt{t_2{}^2 - t_1{}^2}} \tag{6}$$

$$v = \frac{\sqrt{\frac{t_2{}^2 (y^2 - x^2)}{t_2{}^2 - t_1{}^2}}}{t_2} \tag{7}$$

2.2.3 Common Source Method

The common source method involves GPR measurements with one transmitter and at least two receivers as shown in Figure 7. If the layer thickness does not change between the transmitter and the second receiver, the layer thickness can be determined using Equation 6. If more than 2 receivers are available, the layer thickness can be obtained from averaging thicknesses calculated for both pairs of receivers.

2.2.4 Extended CMP Method (XCMP)

The CMP method assumes that the two antenna systems are all ground-coupled systems. Leng and Al-Qadi (2014) developed an extended CMP (XCMP) method that can be applied to two air-coupled bistatic antenna systems. This method uses the following information obtained from each Tx/Rx pair signal time history as exemplified in Figure 8:

1. The travel times of the direct coupling pulse, t_{01} and t_{02}, for the for the first and second Tx/Rx pairs, respectively.

2. The travel times for reflection from the surface of the pavement, t_{11} and t_{12}, for the first and second Tx/Rx pairs, respectively.

3. The travel times for reflection from the bottom of the pavement layer, t_{21} and t_{22}, for the for the first and second Tx/Rx pairs, respectively.

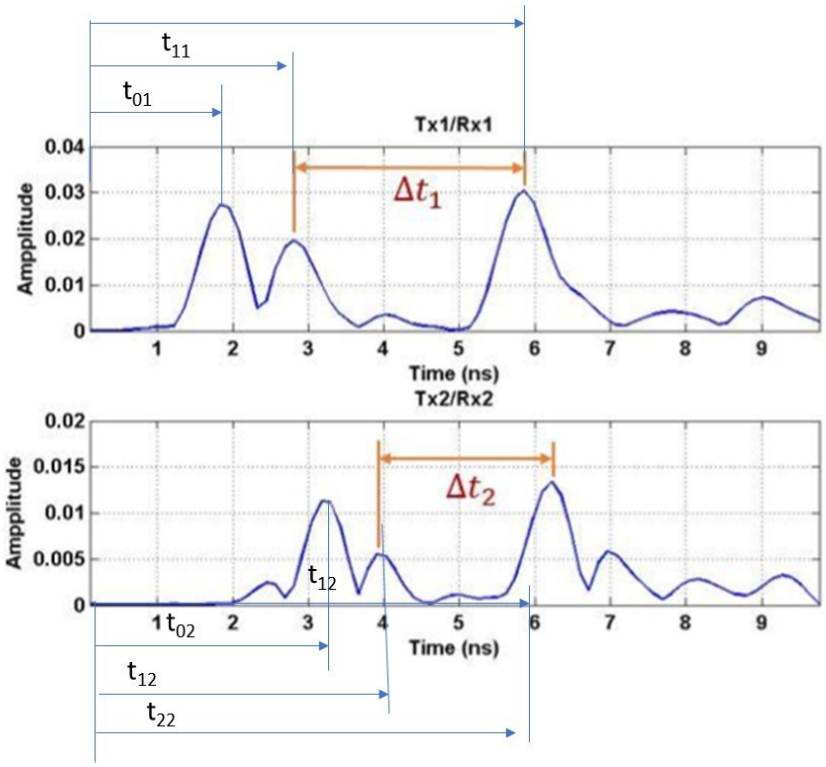

Figure 8. Signal time history (adapted from Zhao 2015)

The direct signal travel time depends only on the distance between the transmitting and receiving antennas. If x_0 and y_0 are distances between the first and second Tx/Rx pairs, respectively, then the direct travel times are:

$$t_{01} = \frac{x_0}{c} \tag{8}$$

$$t_{02} = \frac{y_0}{c} \tag{9}$$

where c is the speed of the electromagnetic waves in the air assumed to be equal to the speed of light in free space.

The travel time for reflection from the surface of the pavement between the air-coupled antennas depend on the distance between antenna and the surface. If the antenna are placed at the distance *d* from the surface, then the signal from the transmitter is expressed by:

$$t_{11} = \frac{2}{c}\sqrt{d^2 + \frac{{x_0}^2}{4}} \tag{10}$$

$$t_{12} = \frac{2}{c}\sqrt{d^2 + \frac{{y_0}^2}{4}} \tag{11}$$

The travel times for reflection from the bottom of the pavement layer consists of two components:

1. Signal travel times in the air from the transmitting antenna to the surface and from the surface to the receiving antenna, t_{1a} and t_{2a}, for the first and second Tx/Rx pairs, respectively.

2. Two-way travel times of the signal in the asphalt layer, t_1 an t_2, for the first and second Tx/Rx pairs, respectively.

Therefore,

$$t_{21} = t_1 + t_{1a} \tag{12}$$

$$t_{22} = t_2 + t_{2a} \tag{13}$$

Denote the distances at which the signal travels in the asphalt layer from its entrance to its exit into the air as *x* and *y* for the first and second Tx/Rx pairs, respectively. Then, similar to the CMP method, two-way travel times of the signal in the asphalt layer, t_1 an t_2, can be determined as follows:

$$t_1 = \frac{2}{v}\sqrt{h^2 + \left(\frac{x}{2}\right)^2} = \frac{2\sqrt{\epsilon}}{c}\sqrt{h^2 + \left(\frac{x}{2}\right)^2} \tag{14}$$

$$t_2 = \frac{2}{v}\sqrt{h^2 + \left(\frac{y}{2}\right)^2} = \frac{2\sqrt{\epsilon}}{c}\sqrt{h^2 + \left(\frac{y}{2}\right)^2} \tag{15}$$

Combining equations 14 and 15 yields:

$$\varepsilon = \frac{c^2(t_2{}^2 - t_1{}^2)}{y^2 - x^2} \tag{16}$$

The following expressions can be derived from Figure 9 for the incident angle and transmission angles:

$$\sin\theta_{i1} = \frac{(x_0 - x)/2}{\sqrt{d^2 + \frac{(x_0 - x)^2}{4}}} \tag{17}$$

$$\sin\theta_{i2} = \frac{(y_0 - y)/2}{\sqrt{d^2 + \frac{(y_0 - y)^2}{4}}} \tag{18}$$

$$\sin\theta_{t1} = \frac{x/2}{vt_1/2} = \frac{x\sqrt{\epsilon}}{c\ t_1} \tag{19}$$

$$\sin\theta_{t2} = \frac{y/2}{vt_2/2} = \frac{y\sqrt{\epsilon}}{vt_2} \tag{20}$$

Where θ_{i1} and θ_{i2} are incidental angels for the first and second Tx/Rx pairs, respectively; t_{i1} and θ_{t2} are transmittal angels for the first and second Tx/Rx pairs, respectively.

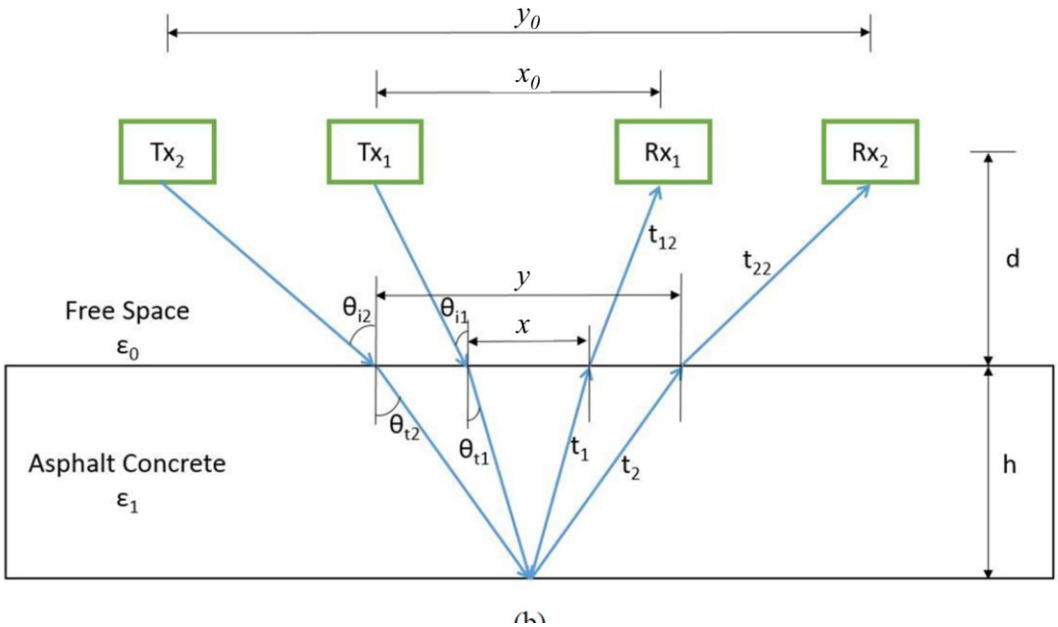

Figure 9. Schematics of wave propagation and reflection from the bottom of asphalt layer

According to Snell's law of transmission, the incident angle and transmission angle have the following relationship (Jin 2011):

$$\frac{\sin\theta_{i1}}{\sin\theta_{t1}} = \frac{\sin\theta_{i2}}{\sin\theta_{t2}} = \sqrt{\varepsilon} \tag{21}$$

Using equations (16), (17), (19) and (21) leads to the following relationships:

$$\frac{(x_0-x)/2}{\sqrt{d^2+\frac{(x_0-x)^2}{4}}} = \frac{x}{c\,t_1}\frac{c^2({t_2}^2-{t_1}^2)}{y^2-x^2} \quad (22)$$

Using equations (16), (18), (20) and (21) we get:

$$\frac{(y_0-y)/2}{\sqrt{d^2+\frac{(y_0-y)^2}{4}}} = \frac{y}{c\,t_2}\frac{c^2({t_2}^2-{t_1}^2)}{y^2-x^2} \quad (23)$$

Denote the time difference between the reflections from the top and the bottom surfaces of the top layer for the first and second sensor pairs as Δt_1 and Δt_2, respectively. Then using Equations (12) and (13) we obtain the following relationships:

$$\Delta t_1 = t_{21} - t_{11} = t_1 + t_{1a} - t_{11} \quad (24)$$

$$\Delta t_2 = t_{22} - t_{21} = t_2 + t_{2a} - t_{21} \quad (25)$$

Substitution equations (10) and (11) into equations (24) and (25) leads to

$$\Delta t_1 = t_1 + \frac{2}{c}\sqrt{d^2+\frac{(x_0-x)^2}{4}} - \frac{2}{c}\sqrt{d^2+\frac{{x_0}^2}{4}} \quad (26)$$

$$\Delta t_2 = t_2 + \frac{2}{c}\sqrt{d^2+\frac{(y_0-y)^2}{4}} - \frac{2}{c}\sqrt{d^2+\frac{{y_0}^2}{4}} \quad (27)$$

The system of four equations (22), (23), 25) and (27) has four unknown variables: *x*, *y*, t_1, and t_2. Solving it, the asphalt layer thickness can be determined using the same equation as it in the CMP methods:

$$h = \frac{1}{2}\frac{\sqrt{{t_1}^2y^2-{t_2}^2x^2}}{\sqrt{{t_2}^2-{t_1}^2}} \quad (28)$$

2.2.5 Accuracy of GPR for Pavement Layer Thickness Evaluation

The GPR primary evaluative function evidenced in international studies was for determining the layer thickness of both asphalt and concrete pavements (Al-Qadi et al., 2005; Scullion, 2006; Tompkins *et al*., 2008). Saarenketo and Scullion (2000) were able to assess with a certain precision the subgrade soil, the layers thickness, the granular base quality, the presence of sub-surface distresses, asphalt pavement voids, and mixture segregation through the dielectric response of the studied material.

Al-Qadi et al. (2003), using the two-way travel time method in newly constructed pavements composed of 100 to 250 mm thick asphalt layers, observed a minimal thickness error of around 3%. Lahouar et al. (2002), using the CMP reported a higher average error (around 7%) with individual points presenting error from 1% to 15%. Liu and Sato (2014) used the common source method for asphalt layer found that the error of asphalt layer thickness estimation is less than 6mm (10%). The same level of error (11%) was report by Hu et al (2015) when using the dielectric gauge values as an input for the data evaluation. However, the researchers were able to reduce the error to about 4% by calibrating the GPR with core

thicknesses. Uddin (2014) affirms that indeed calibration with cores improves the accuracy of GPR data for layer thickness.

CHAPTER 3: EVALUATION OF 3D GPR SIGNALS TIME HISTORIES

The 3D GPR system that MnDOT uses contains two arrays of 11 transmitting and 11 receiving antennas. Figure 10 shows the configuration of this system. The antenna are numbered from left to right. The transmitting antennas are denoted as Tx and the receiving antennas are denoted as Rx. The distance between transmitting and receiving arrays is 17.3 in (440 mm). The distance between adjacent transmitting and receiving antennas is 6 in (150 mm) so that has a total width of 5 ft (see Figure 10). The transmitting and receiving antennas are shifted in transverse direction by 3 in (75 mm).

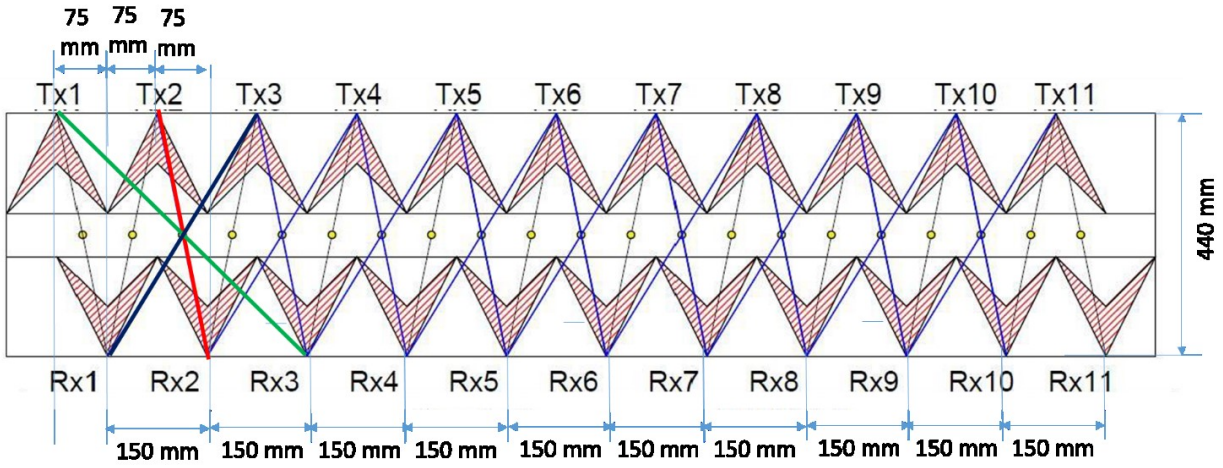

Figure 10. 3D GPR array system used in this study

The radar collects data in the frequency domain by measuring the phase and amplitude on each frequency. Those signals can be converted into time histories using the 3D GPR software, Examiner (Sala and Linford 2012, 3D-Radar 2018). For each transmitting and receiving pair and for each location (trigger), Examiner reports the real and imaginary parts of the signal time histories.

Figure 12, Figure 13, and Figure 13 present an example of the real part signal time histories for the signals transmitted by antenna Tx1 and recorded by 9 receiving antennas at various distances. It should be noted that these pairs have the same transmitting antenna but do not have a common mid-point. All the signals were recorded at the same trigger, i.e. location along the direction of traffic, and plotted against normalized time, t^*, defined as a ratio of the time from the signal transmission to the sampling time increment:

$$t^* = \frac{t}{t_{sampling}} \tag{29}$$

In this example the sampling time increment, $t_{sampling}$, was equal to 1.2207031E-10 seconds.

It can be observed from Figure 11 that the signals from closely spaced antenna exhibited distinct peaks that can be attributed to antenna-antenna signals, top surface reflection signals, and reflections from the bottom surface. The signal time history recorded by receiving antenna 1 shown a string peak at t*=

14 indicating the time of the direct arrival of the signal from the transmitting antenna, the second peak at t* = 29 indicating the arrival time of the signal due to reflection from the top pavement surface layer, and the third peak at t* = 36 indicting the arrival time of the signal due to reflection from the bottom of the top pavement layer.

The signals recorded by the second and third receiving antenna exhibit weak direct arrival signals indicating the direct paths are blocked by the antenna system, but still show very strong distinctive peaks due to reflections from the top and bottom surfaces of the pavement layer.

Figure 12 and Figure 13 show that the signals from antenna spaced at significant distances (greater than 500 mm) exhibit distinct peaks of much lower magnitudes that the peaks from the more closely spaced antenna. This makes determination of the travel time less reliable.

Similar conclusions can be made from the analysis of the instantaneous magnitude, $|Z(t^*)|$, of the time histories defined as follows:

$$|Z(t^*)| = \sqrt{Re(Z(t^*))^2 + Im(Z(t^*))^2} \quad (30)$$

Where $Re(Z(t^*))$ is the real part of the signal, $Im(Z(t^*))$ is the imaginary part of the signal.

It can be observed from Figure 14, Figure 15, and Figure 16, the magnitude of the signal reflections decrease with an increase in the distance between antenna. Therefore, it can be concluded that for determination of the asphalt layer thickness, it is preferable to collect and analyze signals only from closely spaced antenna. Transmitting, receiving, and recording signals for individual antenna pairs takes valuable survey time and hard drive space. If the information is not collected for the sensor pairs located at larger distances, readings for the remaining sensor pairs for the same trigger is collected faster. Therefore, if fewer transmitting and receiving pairs are used then the measurements can be taken at smaller distances in the longitudinal direction (direction of vehicle travel) at the same vehicle speed or at higher speed for the same distances between the triggers. That may in fact increase the accuracy of the thickness determination over the pavement project length.

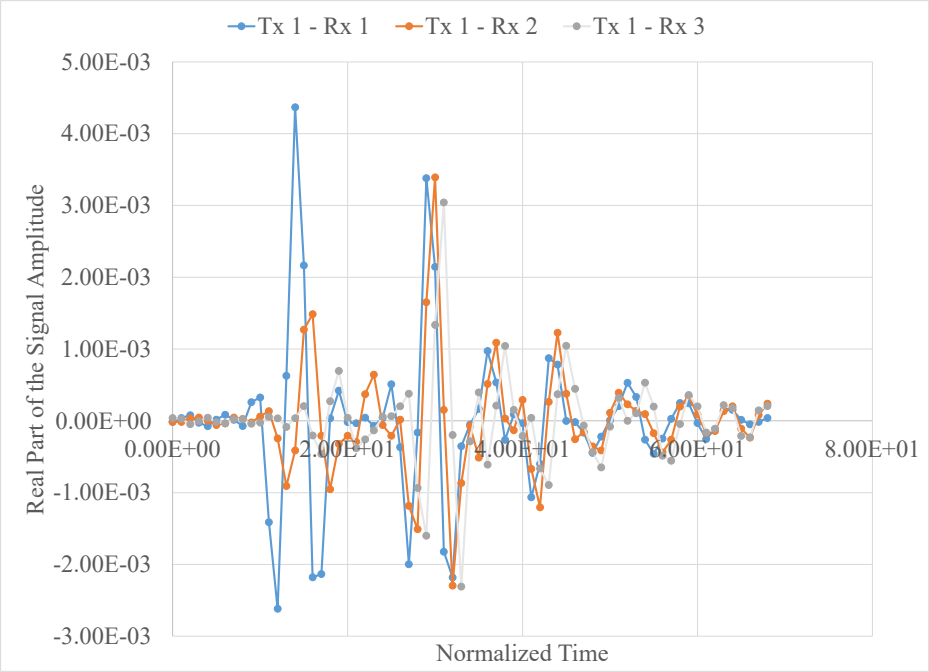

Figure 11. Real part time histories for the signals transmitting by transmitting antenna 1 and recorded by receiving antennas 1 through 3.

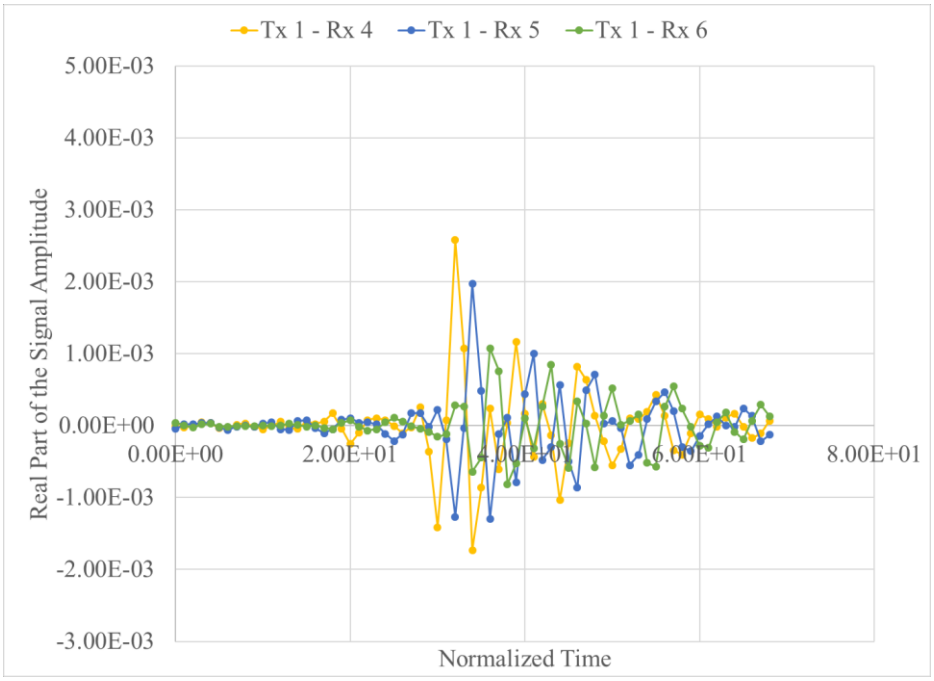

Figure 12. Real part time histories for the signals transmitting by transmitting antenna 1 and recorded by receiving antennas 4 through 6.

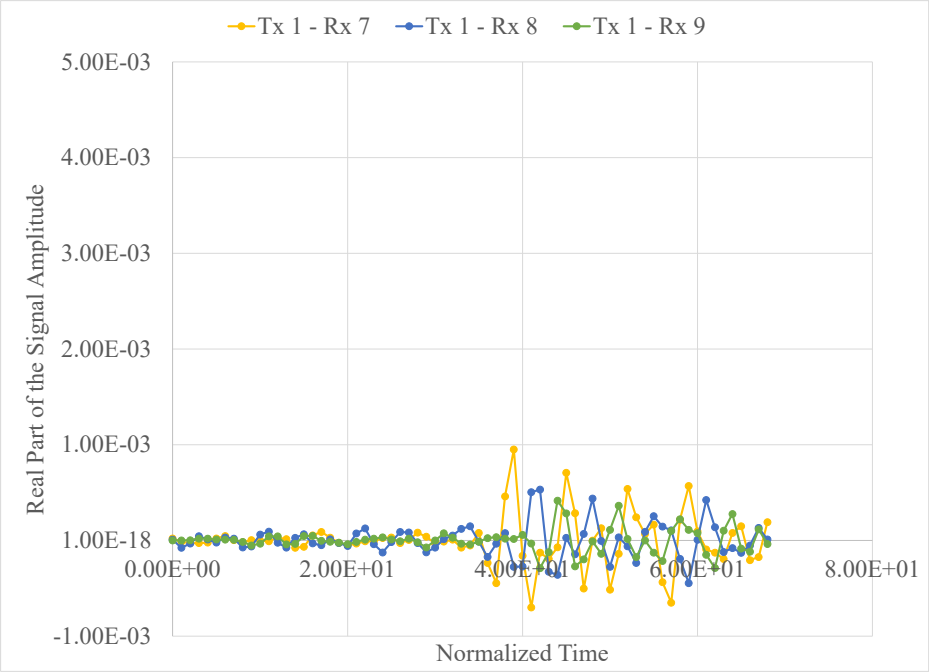

Figure 13. Real part time histories for the signals transmitting by transmitting antenna 1 and recorded by receiving antennas 7 through 9.

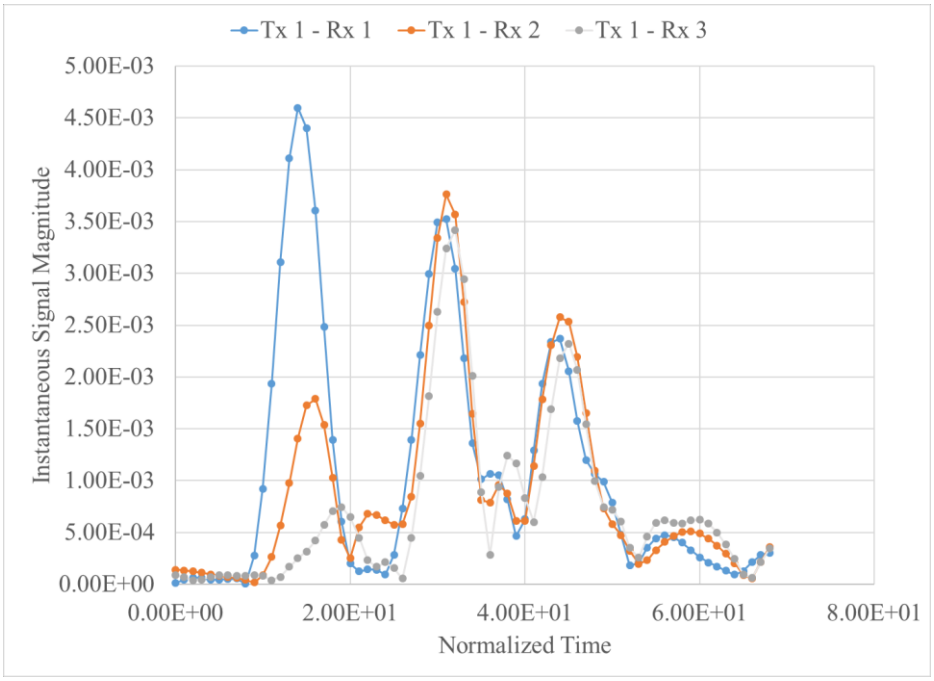

Figure 14. Time history magnitudes for the signals transmitting by transmitting antenna 1 and recorded by receiving antennas 1 through 3.

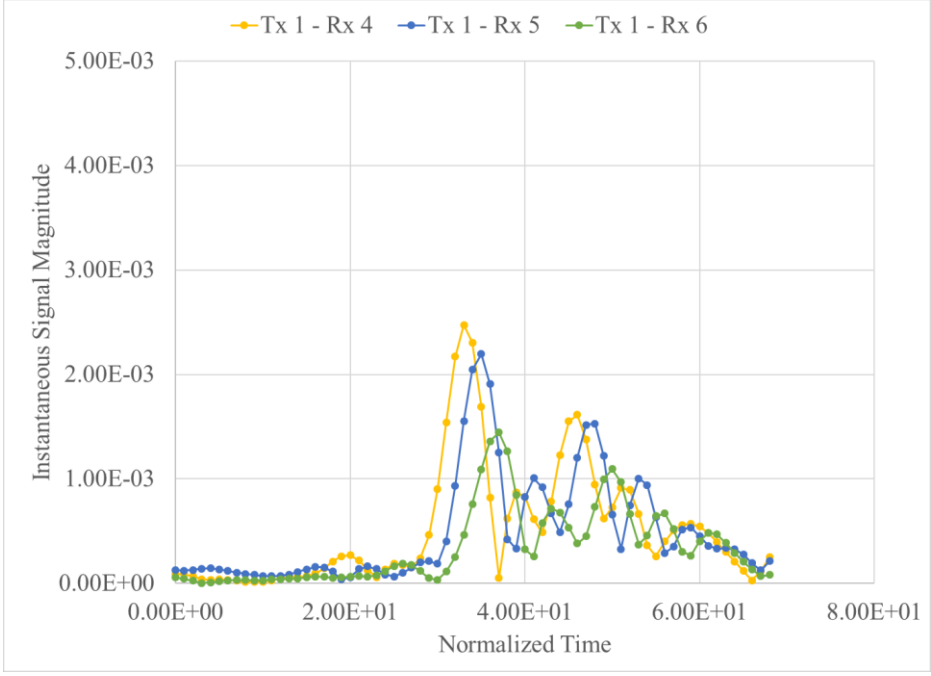

Figure 15. Time history magnitudes for the signals transmitting by transmitting antenna 1 and recorded by receiving antennas 4 through 6.

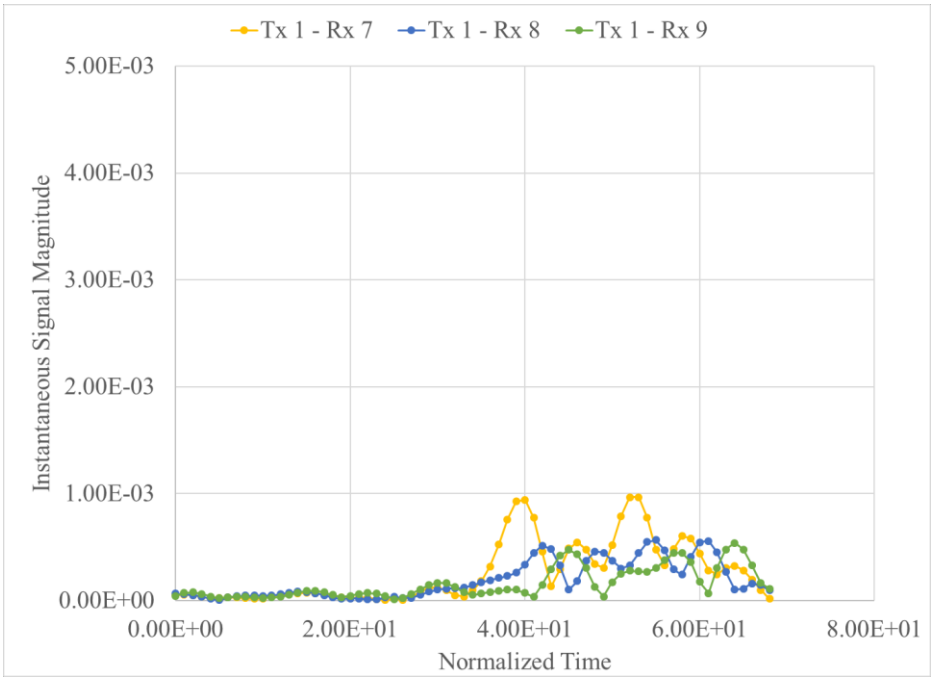

Figure 16. Time history magnitudes for the signals transmitting by transmitting antenna 1 and recorded by receiving antennas 7 through 9

Although the recorded signals significantly differ for the antenna pairs located at various distances, the signals from the antennas spaced at the same distances and taken for the same trigger are quite similar.

Figure 17 shows six time histories from the antenna spaced 3 in in the transverse direction. Although it can be observed that some variability in the magnitude of the recorded real parts of the system the times of the reflection peaks are very close. This suggests that the 3D Radar system produces reliable measurements of the times of the reflections from the top and bottom surfaces of the top pavement layer.

To determine the top layer thickness, it is important to determine accurately the time difference between signals peaks due to reflections from the top and bottom surfaces of the top pavement layer. The analysis of Figure 17 shows that the sampling rate may significantly affect the results. Indeed, the signals from Tx 1 – Rx 1 pair and Tx 2 – Rx 2 are very similar and have the same time of second peak corresponding to the reflections from the top pavement surface (t* = 29). The peaks corresponding to the reflections from the bottom surface of the asphalt layer occur at t* = 43 for Tx 1 – Rx 1 pair and t* =44 for Tx 2 – Rx 2 pair. Therefore, the discrepancy between the differences in the time peaks from these two antenna pairs is almost 8%. However, the magnitudes of the signals at t* = 44 for pair Tx 1 – Rx 1 is only slightly lower than at t* =43. Similar, for pair Tx 2 – Rx 2 the magnitude at t*= 44 is only slightly higher than at t* =43 as can be observed from Figure 18. Therefore, it can be concluded that the actual peaks occur at 43<t*<44 and an improvement in accuracy of determination of the times of the peaks would decrease the discrepancy between the results from these two pairs.

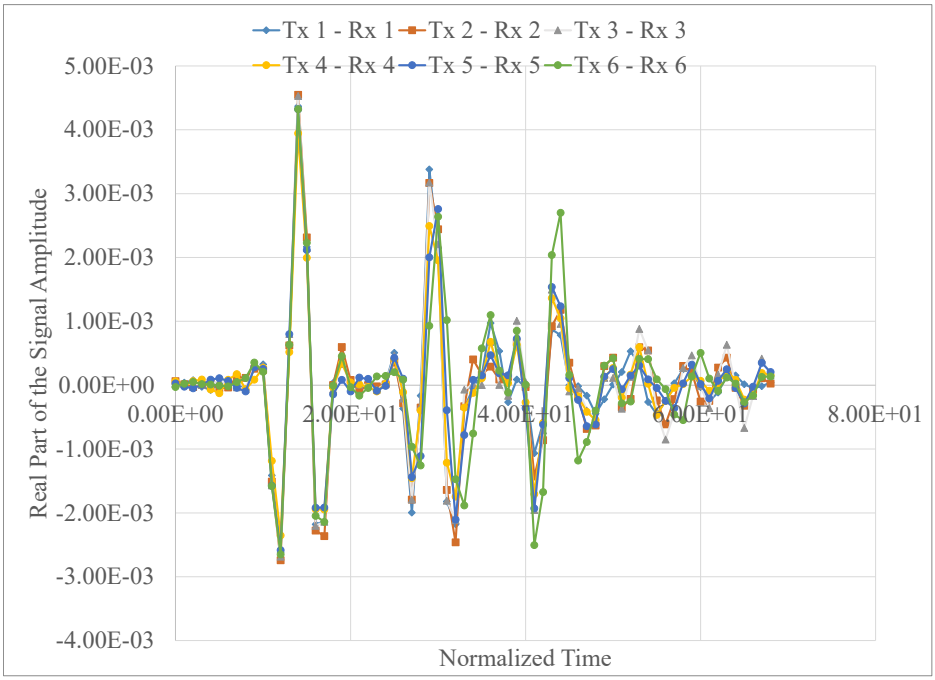

Figure 17. Signals from the antenna pairs with the same distances.

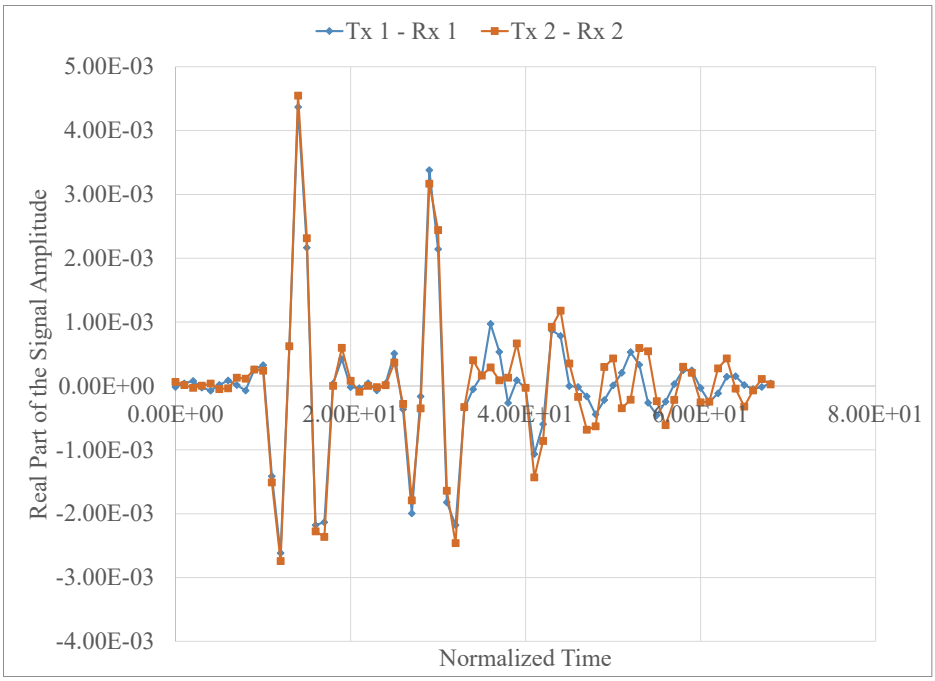

Figure 18. Signals from the antenna pairs Tx1 –Rx1 and Tx2-Rx2.

To improve the accuracy of the analysis, the research team has implemented an oversampling procedure that uses the inverse and forward Fourier transforms to improve resolution, reduce noise, and avoid aliasing and phase distortion by relaxing anti-aliasing filter performance requirements. The implemented procedure performs the following steps:

1. Select the value of oversampling factor F. It is recommended to use the oversampling factor equal to 8.
2. If the length of the recorded time history is n, the determine the smallest value of k such as $2^k > n$.
3. Introduce a new time history, $Z'(t_i)\ such\ as$

$$Z'_i = \begin{bmatrix} Z(t_i) & if\ \ i \le n \\ 0 & if\ \ \ n < i \le n' = 2^k \end{bmatrix}$$

4. Computes the Fourier coefficients, c_i of a complex periodic sequence, $Z'(t_i)$

$$c_m = \sum_{i=1}^{n'} Z'_i e^{-2\,m\,(i-1)(m-1)/n'} \quad , \ m = 1,\ 2,\ \cdots, n'$$

5. Computes the complex periodic sequence of the oversampled signal from its Fourier coefficients

$$Z"_m = \sum_{i=1}^{n'} c_i e^{-2\,m\,(i-1)(m-1)/n'} \ , \ m = 1,\ 2,\ \cdots, F \times n'$$

6. Obtain the real part and the magnitude of each component of the oversampled signal.

Figure 19 shows oversampled signals for antenna pairs Tx 1 – Rx 3, Tx 2 – Rx 2, and Tx 3 – Rx3. It can be observed that the use of oversampling permits determining the signal values at with a smaller time step. It significantly improves accuracy of determination of the times of peaks.

Although the closely-spaced pair have higher amplitudes of the peaks of corresponding to the reflections from the bottom surface of the asphalt layer, the signal-to-noise ratio is lower than for the peaks due to reflections from the top pavement surface. A portion of the signal is noise is recorded by the receiving antenna. A portion of the noise can be identified using the air calibration. The air calibration involves sending the electromagnetic into a direction such that most the signals will not meet any object and reflect back. This might be achieved by firing the waves vertically in the direction opposite to the pavement surface. In this case, the signals recorded by the transmitting antenna are the signals arriving directly from the transmitting antennas, or due to reflections from other elements of the array assembly system, or just the noise.

Figure 20 shows an example of such signals that will be referred to as the air calibration signals. Subtracting such signals from the signals obtained from the waves emitted toward the pavement helps to extract the portion of the signal arrived due to reflections from the pavement layers and increase the signal-to-noise ratio. Figure 21 shows the resulting signal. Comparison of Figure 21 and Figure 19 reveals that subtraction of the air calibration signal eliminates the first peak due to direct arrival as well as slightly reduces the noise in the remaining portion of the signal.

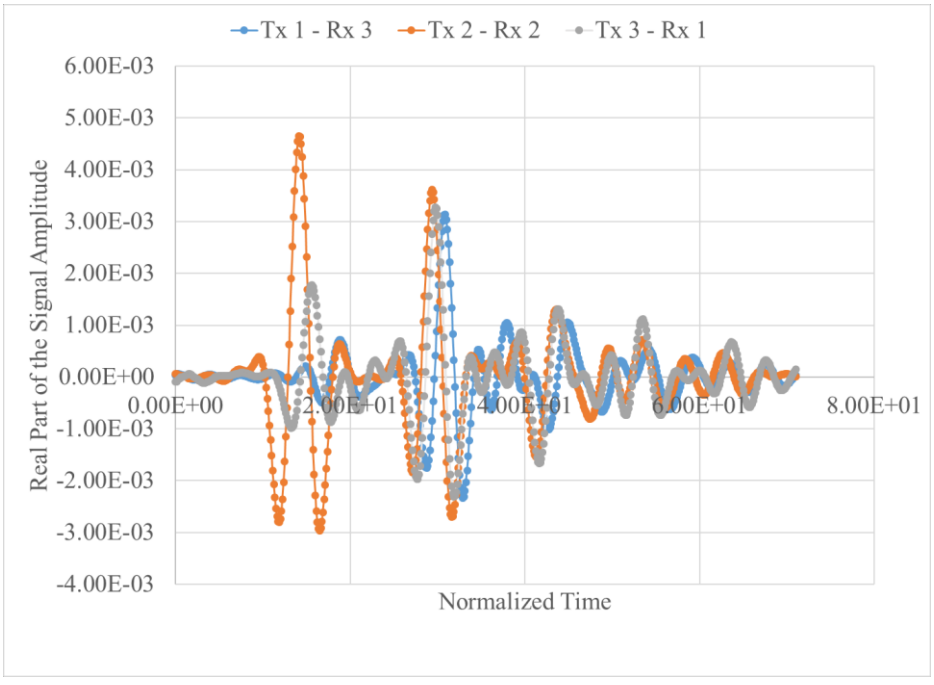

Figure 19. Example of oversampled real part time histories

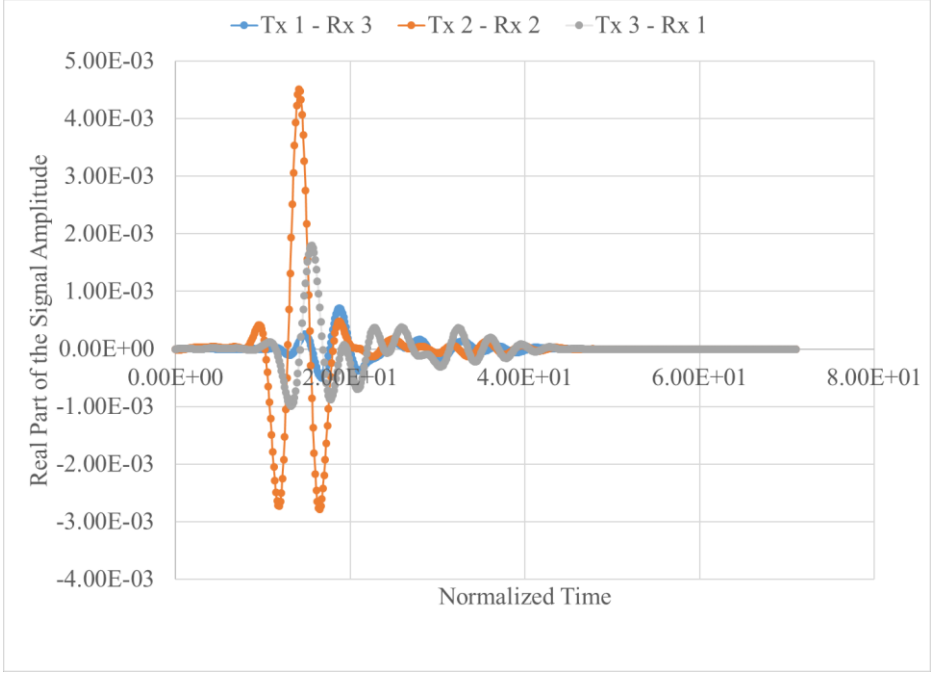

Figure 20. Signal time histories from air calibration

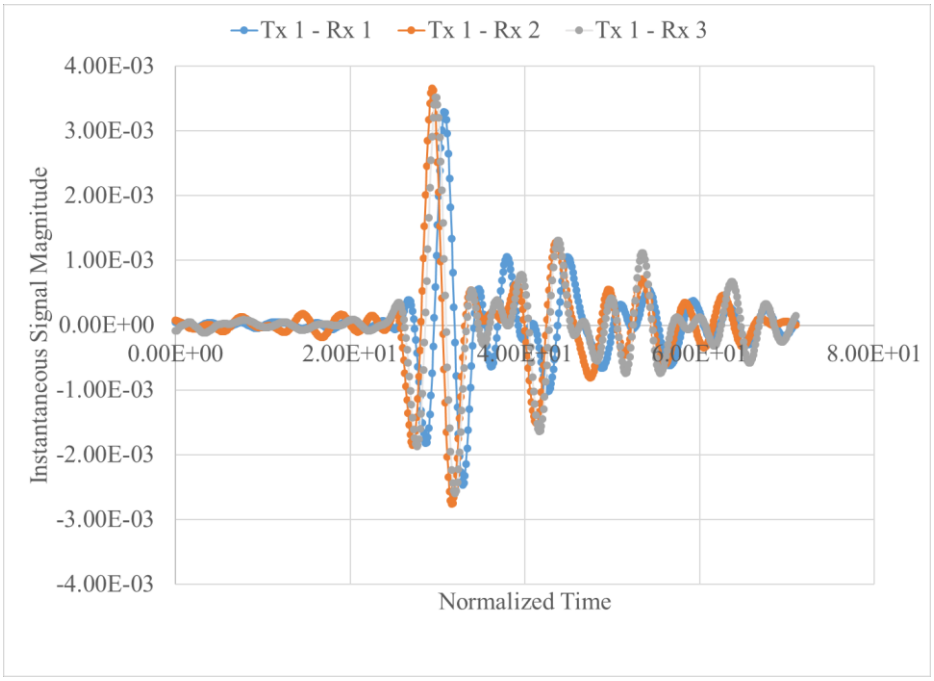

Figure 21. Resulting time history after subtraction of the air calibration signal

Based on this analysis it can be concluded that oversampling an air calibration significantly improve quality of the collected data. The oversampling procedure was implemented into a FORTRAN code to enable the use of the oversampled signal time histories in the asphalt thickness determination

procedure described in the next chapter. The air calibration option is also implemented in the FORTAN code.

The DX antenna system used in this study has 11 transmitting (T) and receiving (R) antennas. Each receiving antenna may record signals from any transmitting antenna in the assembly. The software developed in this study can analyze the 3D GPR data collected for all 121 transmitting and receiving pairs. However, if all 121 measurements have to be made for one location it makes the data collection process unnecessary slow.

To address this limitation, it was proposed to collect data using the 27 transmitting and receiving pairs. This set of pair consists of 9 groups of transmitting and receiving pairs. Each group has 3 pair spaced and different distances but having the same mid-point. Table 1 presents the information on the transmitting receiving pairs, their groups, distances between antennas and the order in which these signals should be collected. The option to analyze this sensor configuration was added to the software.

Table 1. Data collection protocol with 27 transmitting and receiving pairs.

Pair Group	Antenna		Distance mm	Collection order
	Transmitting	Receiving		
1	1	3	578.1	1
1	2	2	446.4	2
1	3	1	394.2	4
2	2	4	578.1	3
2	3	3	446.4	5
2	4	2	394.2	7
3	3	5	578.1	6
3	4	4	446.4	8
3	5	3	394.2	10
4	4	6	578.1	9
4	5	5	446.4	11
4	6	4	394.2	13
5	5	7	578.1	12
5	6	6	446.4	14
5	7	5	394.2	16
6	6	8	578.1	15
6	7	7	446.4	17
6	8	6	394.2	19
7	7	9	578.1	18
7	8	8	446.4	20
7	9	7	394.2	22
8	8	10	578.1	21
8	9	9	446.4	23
8	10	8	394.2	25
9	9	11	578.1	24
9	10	10	446.4	26
9	11	9	394.2	27

CHAPTER 4: DEVELOPMENT OF THE ASPHALT THICKNESS DETERMINATION PROCEDURE

The research team developed the asphalt layer thickness determination procedures using the data collected with 3D GPR system. The procedure utilized two methods: based on the analysis of time histories from the individual transmitting and receiving antenna pairs and using time histories from groups of antenna pairs. The first method requires assuming the dielectric constant for the asphalt layer, the second method determines simultaneously the asphalt layer thickness and dielectric constant. The latter method is based on a generalization of the extended common mid-point (XCMP) method. This chapter documents both procedures.

4.1 INPUT DATA

To determine asphalt layer thickness using the procedures developed in this study, the user should provide the following information:

- The 3D Radar time histories for each transmitting and receiving antenna pair to be used in the analysis as well as the sampling. This information is stored in the *.vol files created by 3D GPR Examiner software.
- The type of time history data to be used in the analysis: real portion of the signal or signal amplitude.
- The air calibration time histories if the air calibration option is selected by the user.
- The reference dielectric constant for determination of asphalt thicknesses from the individual antenna pairs, ε_{ref}
- The lower and upper bound estimates for the asphalt layer thickness, h_{min} and h_{max}, respectively, and the number of thickness values to be used in the analysis, n_h
- The lower and upper bound estimates for the asphalt layer dielectric constant, ε_{min} and ε_{max} respectively, and the number of dielectric constant values to be used in the analysis, n_ε
- The lower and upper bound estimates for the distance between the 3D GPR antenna and the pavement surface, d_{min} and d_{max}, respectively, and the number of distance values to be used in the analysis, n_d.

4.2 INPUT DATA PROCESSING

In the beginning of the analysis, the software performs the following input data processing operations for each transmitting and receiving antenna pairs:

1. Perform oversampling. It is recommended to use the oversampling factor equal to 8. It computes the signal values with the time step equal to 1/8 the sampling rate.

2. If the signal magnitude is going to be used in the analysis, compute the signal magnitudes for all time histories using equation (30).
3. Compute the theoretical normalized travel time for the electromagnetic wave from the transmitting to receiving antenna,t_0, as follows:

$$t_0 = \frac{x_0}{c\ t_{sampling}} \tag{31}$$

where x_0 is the distance between antennas, c is the speed of light and $t_{sampling}$ is the sampling interval.

4. Determine the normalized time for the peak corresponding to the direct arrival of the signal from the transmitting to the receiving antenna, t_{01}, by finding the normalized time with the maximum value of the signal within the interval (t_0, t_0+5).
5. Compute $\Delta t_{1,min}$ and $\Delta t_{1,max}$, the lower and upper estimates, respectively, for difference between the normalized travel time for an electromagnetic wave to travel from the transmitting sensor toward the pavement and get reflected from the top surface of the pavement, and reach the receiving antenna and the normalized time to travel directly using equation the following equations:

$$\Delta t_{1,min} = \frac{2}{c\ t_{sampling}} \left(\sqrt{{d_{min}}^2 + \frac{x_0^2}{4}} - x_0 \right) \tag{32}$$

$$\Delta t_{1,max} = \frac{2}{c\ t_{sampling}} \left(\sqrt{{d_{max}}^2 + \frac{x_0^2}{4}} - x_0 \right) \tag{33}$$

where x is the distance between the transmitting and receiving antennas

6. Determine the normalized time for the peak corresponding to the reflection of the wave from top of the pavement surface, t_{11}, by finding the normalized time with the maximum value of the signal within the interval ($t_{01}+\Delta t_{1,min}$ $t_{01}+\Delta t_{1,max}$).
7. Compute the distance between the antennas and the pavement surface, d:

$$d = \sqrt{\left(\frac{(t_{11} - t_{10}) c\ t_{sampling} + x}{2} \right)^2 - \frac{x^2}{4}} \tag{34}$$

8. Compute $\Delta t_{2,min}$ and $\Delta t_{2,max}$, the lower and upper estimates, respectively, for difference between the normalized travel time for the electromagnetic wave reflected from the bottom surface of the asphalt layer and the top surface of the asphalt layer using the following equations:

$$\Delta t_{2,min} = 2\frac{\sqrt{\left(\frac{x_{11}^2}{4} + h_{min}^2\right)\varepsilon_{\min}} + \sqrt{d^2 + \frac{(x_0 - x_{11})^2}{4}}}{c \quad t_{sampling}} \tag{35}$$

$$\Delta t_{2,max} = 2\frac{\sqrt{\left(\frac{x_{22}^2}{4} + h_{max}^2\right)\varepsilon_{\max}} + \sqrt{d^2 + \frac{(x_0 - x_{22})^2}{4}}}{c \quad t_{sampling}} \tag{36}$$

where

$$x_{11} = \frac{1}{2}\sqrt{-\frac{-\frac{16h_{min}^2 x}{\varepsilon_{\min} - 1} - \frac{8p_{11}x}{\varepsilon_{\min} - 1} + 8x^3}{4\sqrt{p_{41}}} - \frac{4p_{11}}{3(\varepsilon_{\min} - 1)} - \frac{\sqrt[3]{p_{31}}}{3\sqrt[3]{2}(\varepsilon_{\min} - 1)} - \frac{\sqrt[3]{2}p_{11}^2}{3\sqrt[3]{p_{31}}(\varepsilon_{\min} - 1)} + 2x^2} - \frac{\sqrt{p_{41}}}{2} + \frac{x}{2}$$

$$p_{11} = -x^2 - h_{\min}^2 + 4d^2\varepsilon_{\min} + x^2\varepsilon_{\min}$$

$$p_{21} = -4p_{11}^6 + (2p_{11}^3 + 108x^2h_{\min}^4(-1 + \varepsilon_{\min}) + 108x^2h_{\min}^2p_{11}(-1 + \varepsilon_{\min}) - 108x^4h_{\min}^2(-1 + \varepsilon_{\min})^2)^2$$

$$p_{31} = 2p_{11}^3 + \sqrt{p_{21}} + 108x^2h_{\min}^4(-1 + \varepsilon_{\min}) + 108x^2h_{\min}^2p_{11}(-1 + \varepsilon_{\min}) - 108x^4h_{\min}^2(-1 + \varepsilon_{\min})^2$$

$$p_{41} = x^2 - \frac{2p_{11}}{3(-1 + \varepsilon_{\min})} + \frac{2^{1/3}p_{11}^2}{3p_{31}^{1/3}(-1 + \varepsilon_{\min})} + \frac{p_{31}^{1/3}}{32^{1/3}(-1 + \varepsilon_{\min})}$$

$$x_{22} = \frac{1}{2}\sqrt{-\frac{-\frac{16h_{max}^2 x}{\varepsilon_{\max} - 1} - \frac{8p_{22}x}{\varepsilon_{\max} - 1} + 8x^3}{4\sqrt{p_{42}}} - \frac{4p_{12}}{3(\varepsilon_{\max} - 1)} - \frac{\sqrt[3]{p_{32}}}{3\sqrt[3]{2}(\varepsilon_{\max} - 1)} - \frac{\sqrt[3]{2}p_{12}^2}{3\sqrt[3]{p_{31}}(\varepsilon_{\max} - 1)} + 2x^2} - \frac{\sqrt{p_{42}}}{2} + \frac{x}{2}$$

$$p_{22} = -x^2 - h_{\min}^2 + 4d^2\varepsilon_{\min} + x^2\varepsilon_{\min}$$

$$p_{22} = -4p_{12}^6 + (2p_{12}^3 + 108x^2h_{\max}^4(-1+\varepsilon_{\max}) + 108x^2h_{\max}^2p_{12}(-1+\varepsilon_{\max}) - 108x^4h_{\max}^2(-1+\varepsilon_{\max})^2)^2$$

$$p_{32} = 2p_{12}^3 + \sqrt{p_{22}} + 108x^2h_{\max}^4(-1+\varepsilon_{\max}) + 108x^2h_{\max}^2p_{12}(-1+\varepsilon_{\max}) - 108x^4h_{\max}^2(-1+\varepsilon_{\max})^2$$

$$p_{42} = x^2 - \frac{2p_{12}}{3(-1+\varepsilon_{\max})} + \frac{2^{1/3}p_{12}^2}{3p_{32}^{1/3}(-1+\varepsilon_{\max})} + \frac{p_{32}^{1/3}}{2^{1/3}\,3\,(-1+\varepsilon_{\max})}$$

9. Determine the normalized time for the peak corresponding to the reflection of the wave from the bottom of the bottom layer, t_{22}, by finding the normalized time with the maximum value of the signal within the interval ($t_{11} + \Delta t_{2,min}$ $t_{01} + \Delta t_{2,max}$).

4.3 ASPHALT THICKNESS DETERMINATION UISNG INDIVIDUAL ANTENNA PAIR DATA

Using the reference dielectric constant for the asphalt layer provided by the user, find the asphalt layer thickness, h_{ac}, by solving iteratively the following system of equations:

$$\sqrt{\left(\frac{x_1^2}{4}+h^2\right)\varepsilon_{ref}} + \sqrt{d^2+\frac{(x_0-x_1)^2}{4}} - \sqrt{d^2+\frac{x_0^2}{4}} = \frac{t_{22}-t_{11}}{2}\; c\; t_{sampling} \tag{37}$$

$$x_{1r} = \frac{1}{2}\sqrt{-\frac{-\frac{16\,h^2x}{\varepsilon_{\min}-1}-\frac{8p_{1r}x}{\varepsilon_{\min}-1}+8x^3}{4\sqrt{p_{41}}} - \frac{4p_{1r}}{3(\varepsilon_{\min}-1)} - \frac{\sqrt[3]{p_{3r}}}{\sqrt[3]{2}\,3(\varepsilon_{\min}-1)} - \frac{\sqrt[3]{2}p_{1r}^2}{3\sqrt[3]{p_{31}}(\varepsilon_{\min}-1)} + 2x^2} - \frac{\sqrt{p_{4r}}}{2} + \frac{x}{2} \tag{38}$$

where

$$p_{1r} = -x^2 - h^2 + 4d^2\varepsilon_{\text{ref}} + x^2\varepsilon_{\text{ref}}$$

$$p_{2r} = -4p_{11}^6 + (2p_{1r}^3 + 108x^2h^4(-1+\varepsilon_{\text{ref}}) + 108x^2h^2p_{1r}(-1+\varepsilon_{\text{ref}}) - 108x^4h^2(-1+\varepsilon_{\text{ref}})^2)^2$$

$$p_{3r} = 2p_{1r}^3 + \sqrt{p_{2r}} + 108x^2h^4(-1+\varepsilon_{\text{ref}}) + 108x^2h^2p_{1r}(-1+\varepsilon_{\text{ref}}) - 108x^4h^2(-1+\varepsilon_{\text{ref}})^2$$

$$p_{4r} = x^2 - \frac{2p_{1r}}{3(-1+\varepsilon_{\text{ref}})} + \frac{2^{1/3}p_{1r}^2}{3p_{3r}^{1/3}(-1+\varepsilon_{\text{ref}})} + \frac{p_{3r}^{1/3}}{2^{1/3}\,3\,(-1+\varepsilon_{\text{ref}})}$$

4.4 MODFIED EXTENDED COMMON MID-POINT METHOD

To address the limitations of the XCMP method, a Modified Extended Common Mid-Point (MXCMP) method is proposed. In this method, more than two pairs of transmitting and receiving antennas can be used, as long as these pairs have the same mid-points of the lines connecting these antennas as illustrated in Figure 22.

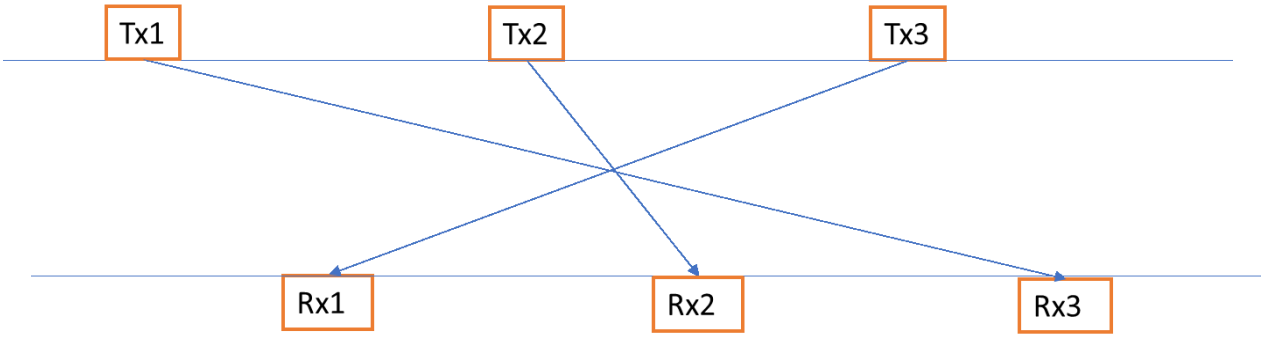

Figure 22. Example of three antenna pairs with a common mid-point (top view)

The first stage in the MXCMP method requires determination of the distance between the mid-point connecting the transmitting and receiving pairs and the asphalt surface, d. The following procedure is used:

1. Assign n_d values of potential distances, d_i, within the interval between the user-specified minimum and maximum values for the distance between the 3D GPR antennas and the pavement surface using the following equation:

$$d_i = d_{min} + (i-1) * \frac{d_{max} - d_{min}}{n_d} i, \qquad i = 1, \cdots, n_d \tag{39}$$

2. For each potential distance, d_i, and antenna pair *k* within the antenna group, determine the normalized travel time , $t_1^{(k)}(d_i)$, for the signal to travel from the transmitting antenna toward the pavement, get reflected from the top surface of the pavement, and reach the receiving antenna:

$$t_1^{(k)}(d_i) = \frac{2}{c\, t_{sampling}} \sqrt{\left(\frac{t_1^{(k)}}{2}\right)^2 + {d_i}^2} \tag{40}$$

where x_k is the distance between transmitting and receiving antenna pair *k*

3. For each potential distance d_i and antenna pair *k* within the antenna group, determine the arrival time, $t_{11}^{(k)}(d_i)$, for the signal to reflected from the top surface of the pavement, and reach the receiving antenna:

$$t_{11}^{(k)}(d_i) = t_1^{(k)}(d_i) - t_0^{(k)} - t_{01}^{(k)} \tag{41}$$

where $t_0^{(k)}$ is the theoretical normalized travel time for the electromagnetic wave from the transmitting to receiving antenna for the pair k, $t_{01}^{(k)}$is the normalized time for the peak corresponding to the first arrival of the signal for the antenna pair k.

4. For each normalized time $t_{11}^{(k)}(d_i)$ find the corresponding value of recorded signal for the antenna pair k, $S_k\left(t_{11}^{(k)}(d_i)\right)$. Depending on the signal type used in the analysis, the oversampled real part time history or the oversampled signal magnitude is used. To improve the accuracy of the analysis, the cubic spline interpolation is utilized.

5. For each potential distance. d_i, find the total value of recorded signals corresponding to the apparent reflection from the surface from all antenna pairs in the group:

$$R(d_i) = \sum_{k=1}^{M} S_k\left(t_{11}^{(k)}(d_i)\right)$$

where M is the number antenna pairs in the group.

6. Find the maximum value of the apparent reflectivity function $R(d_i)$. The value of d_i corresponding to the maximum value of R is assumed to be the distance between the antenna pairs and the asphalt surface, $d^{(k)}$.

The second stage in the MXCMP method requires determination of the asphalt layer thicknesses for each of the following values of the dielectric constant for the asphalt layer:

$$\varepsilon_i = \varepsilon_{min} + (i-1) * \frac{\varepsilon_{max} - \varepsilon_{min}}{n_\varepsilon} i, \qquad i = 1, \cdots, n_\varepsilon \tag{42}$$

The asphalt layer thickness is selected from the following set of the potential asphalt layer thicknesses.

$$h_j = h_{min} + (j-1) * \frac{h_{max} - h_{min}}{n_h} j, \qquad j = 1, \cdots, n_h \tag{43}$$

using the following procedure:

1. For each combination of the potential asphalt thickness, h_j, dielectric constant, ε_i, and antenna pair *k* within the antenna group, determine the normalized difference between the travel time for the signal to travel from the transmitting antenna toward the pavement, get reflected from

the bottom surface of the asphalt layer pavement, and reach the receiving antenna , $t_2^{(k)}(d^{(k)})$, and the travel time for the signal to travel from the transmitting antenna toward the pavement, get reflected from the top surface of the asphalt layer pavement, and reach the receiving antenna:

$$\Delta t_2^{(i,j,k)} = \Delta t_2(\varepsilon_i, h_j, x_0^{(k)}, d^{(k)}) \quad (44)$$

2. For each combination of the potential asphalt thickness, h_j, dielectric constant, ε_i, and antenna pair *k* within the antenna group, determine the normalized time for the signal to travel from the transmitting antenna toward the pavement, get reflected from the bottom surface of the asphalt layer pavement, and reach the receiving antenna:

$$t_2^{(i,j,k)} = \Delta t_2^{(i,j,k)} + t_{11}^{(k)}(d^{(k)}) \quad (45)$$

3. For each normalized time $t_2^{(i,j,k)}$ find the corresponding value of recorded signal for the antenna pair k, $S_k\left(t_2^{(i,j,k)}\right)$. Depending on the signal type used in the analysis, the oversampled real part time history or the oversampled signal magnitude is used. To improve the accuracy of the analysis, the cubic spline interpolation is utilized.

4. For each potential asphalt thickness and dielectric constant, find the total value of recorded signals corresponding to apparent reflections from the bottom asphalt surface from all antenna pairs in the group :

$$R(\varepsilon_i, h_j) = \sum_{k=1}^{M} S_k\left(t_2^{(i,j,k)}\right)$$

where M is the number antenna pairs in the group.

5. For each potential combination of the dielectric constant value and the asphalt thickness find the combination of these parameters corresponding to the largest value of $R(\varepsilon_i, h_j)$. This combination is the asphalt layer thickness and the dielectric constant for the asphalt layer located under the common point for this antenna group.

4.5 RUDIMENTARY SOFTWARE

This procedure described in this chapter has been implemented into a rudimentary software consisting of the two components:

- A Graphical User Interface (GUI) coded in JAVA. To execute the program, the Java Runtime Environment (JRE) 8 should be installed.
- A computational engine program coded in FORTRAN.

The GUI enables the user to provide appropriate inputs, such as the ranges for the asphalt layer thickness and dielectric constant, the files with the 3D radar data, and data the type of the signal to be used in the analysis (real part of the signal or signal magnitude). The user can also specify the use of air calibration and the file with air calibration data. When the require information is provided the GUI program can execute the computational engine program and open output files.

The computational engine reads the raw 3D GPR time histories data, performs oversampling and, if specified, air calibration, and computes asphalt layer thicknesses using two methods:

- Analysis of individual antennas pairs time histories along with the user-provided dielectric constant for the asphalt layer
- Analysis of groups of signals from transmitting and receiving antennas with various spacing but with a common mid-point using the Modified Extended Common Mid-Point (MXCMP) method.

The software performs the analysis of the data provided by the user and reports the results of the analysis in comma separated text files that can be later analyzed by the user using Excel or other tools.

Appendix A provides the User Guide for the software.

The next chapter presents example of the analysis performed using the developed software.

CHAPTER 5: EXAMPLE WITH FIELD DATA

To illustrate the procedures described above we will consider the data collected with 3D Radar by MnDOT personnel for Cell 127 at the MnROAD test facilities on August 8, 2020. The reference dielectric constant for the determination of asphalt thicknesses from the individual antenna pairs is assumed to be equal to 6. The lower and upper bound estimates for the asphalt layer thickness was assumed to be equal to 2 in and 6 in, respectively. The number of thickness values to be used in the analysis was assumed to be equal to 41. The lower and upper bound estimates for the asphalt layer dielectric constant were assumed to be equal to 4 and 8, respectively, and the number of dielectric constant values to be used in the analysis was assumed to be equal to 21. Finally, the lower and upper bound estimates for the distance between the 3D GPR antenna and the pavement surface were set to 14 in and 23 in, respectively, and the number of distance values to be used in the analysis was assumed to be equal to 40.

The analysis will be illustrated with the oversampled time histories of the air-calibrated real part signals collected with the antenna pairs Tx1-Rx3, Tx2-Rx2, and Tx3-Rx1 at trigger 100. All three pairs have the same mid-point of the lines connecting the corresponding sending and receiving antennas shown in Figure 22.

Using distances geometry in Figure 10, compute the distances between antennas.

Tx1 – Rx3: $x_0^{(1)} = \sqrt{(440\ mm)^2 + (75\ mm + 2 \times 150)^2} = 578.1\ mm$

Tx2 – Rx2: $x_0^{(2)} = \sqrt{(440\ mm)^2 + (75\ mm)^2} = 446.4\ mm$

Tx3 – Rx1: $x_0^{(3)} = \sqrt{(440\ mm)^2 + (75\ mm + 150)^2} = 494.2\ mm$

Since the speed of light c = 299,792,458 m/s and the sampling time equal to 1.2207031E-10 s then the theoretical non-dimensional travel times between the sensors are:

$$t_0^{(1)} = \frac{x_0^{(1)}}{c\ t_{sampling}} = \frac{0.5781\ m}{299{,}792{,}458\ \text{m/ s} \times\ 1.2207031 \times 10^{-10}\ \text{s}} = 15.8$$

$$t_0^{(2)} = \frac{x_0^{(2)}}{c\ t_{sampling}} = 12.2$$

$$t_0^{(3)} = \frac{x_0^{(3)}}{c\ t_{sampling}} = 13.5$$

Therefore, the peaks due to the direct arrival of the waves traveling directly from the transmitting to receiving antennas should be located within the non-dimensional time intervals (15.5, 20.5), (12.2, 17.2) and (13.5,18.5) for antenna pairs Tx1 – Rx3, Tx2 – Rx2, and Tx3 – Rx1, respectively. Figure 23 shows real part time histories for these antenna pairs for non-dimensional time from 0 to 25. It can be observed from this figure that the non-dimensional times for the first peaks for

antenna pairs Tx1 – Rx3, Tx2 – Rx2, and Tx3 – Rx1 signal time histories are 18.8375, 14.1625, and 15.5125, respectively, i.e. within the identified interval.

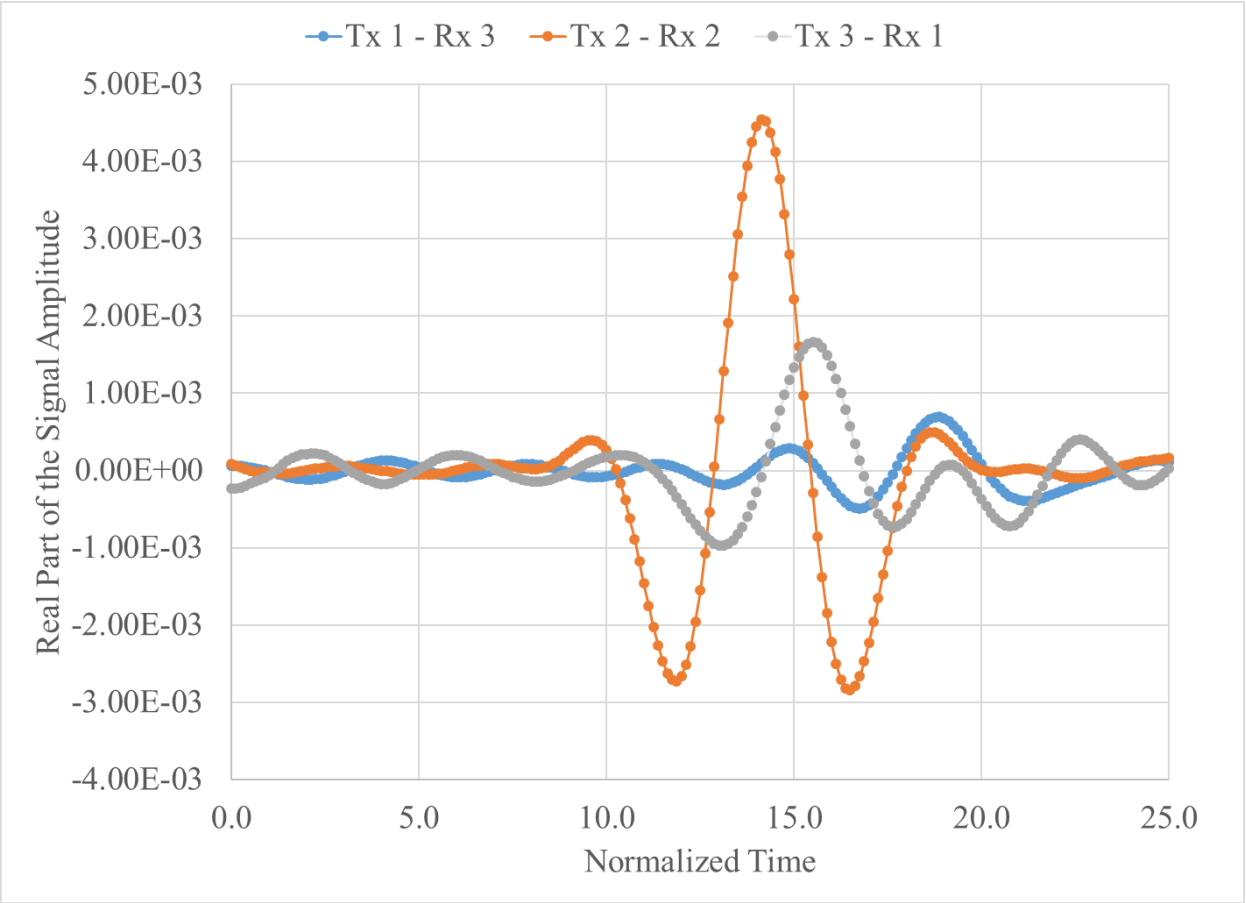

Figure 23. Real part time histories for a non-dimensional time from 0 to 25.

Since the air calibration option was specified, the air calibration signals were subtracted from the signals collected at trigger 19. Figure 24 and Figure 25 show portions of the time histories for a non-dimensional time between 10 and 40. It can be observed that the air calibration reduced the effect of the signal due to direct arrival from the transmitting to receiving antennas as well as somewhat reduced noise in the signals.

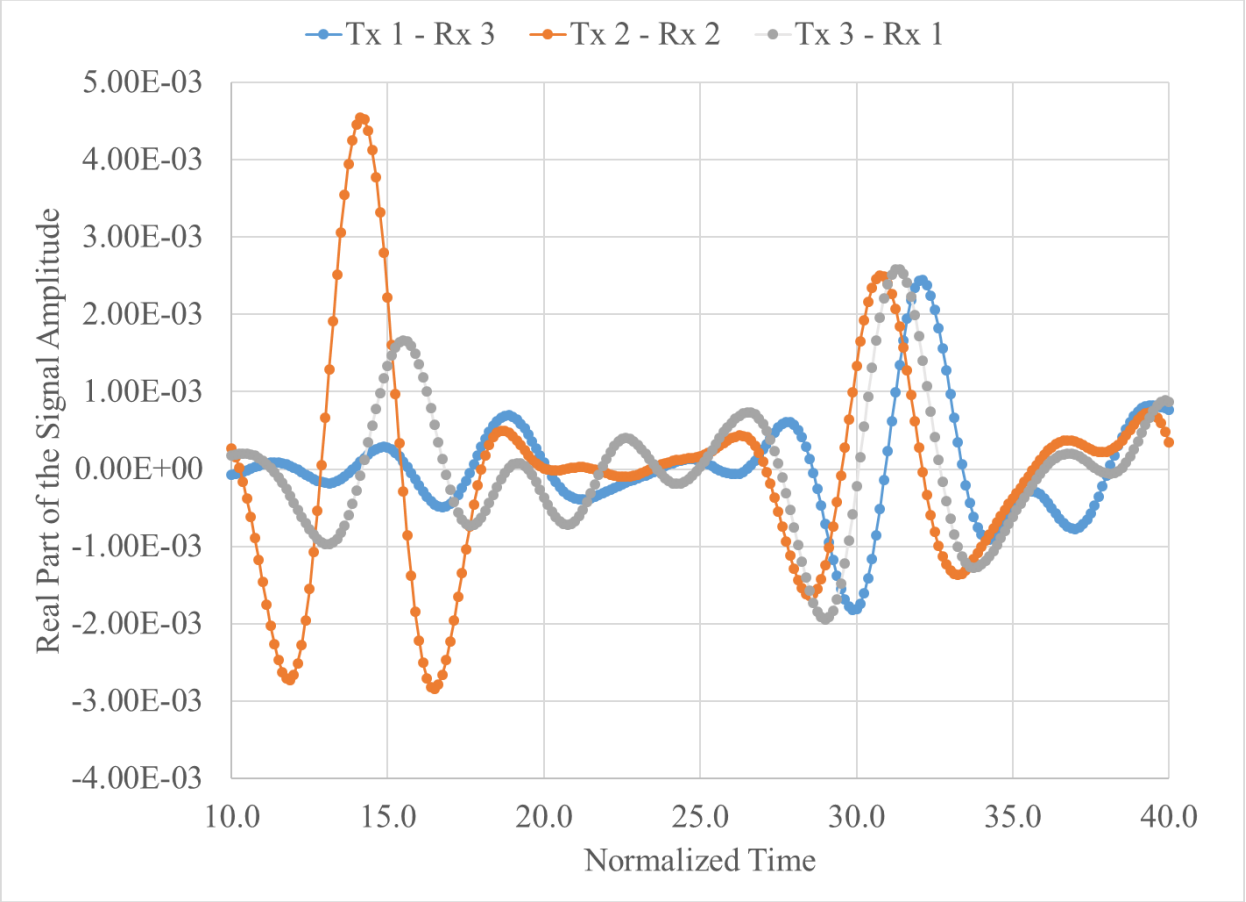

Figure 24. Real part time histories w/o air calibration for non-dimensional time from 10 to 40.

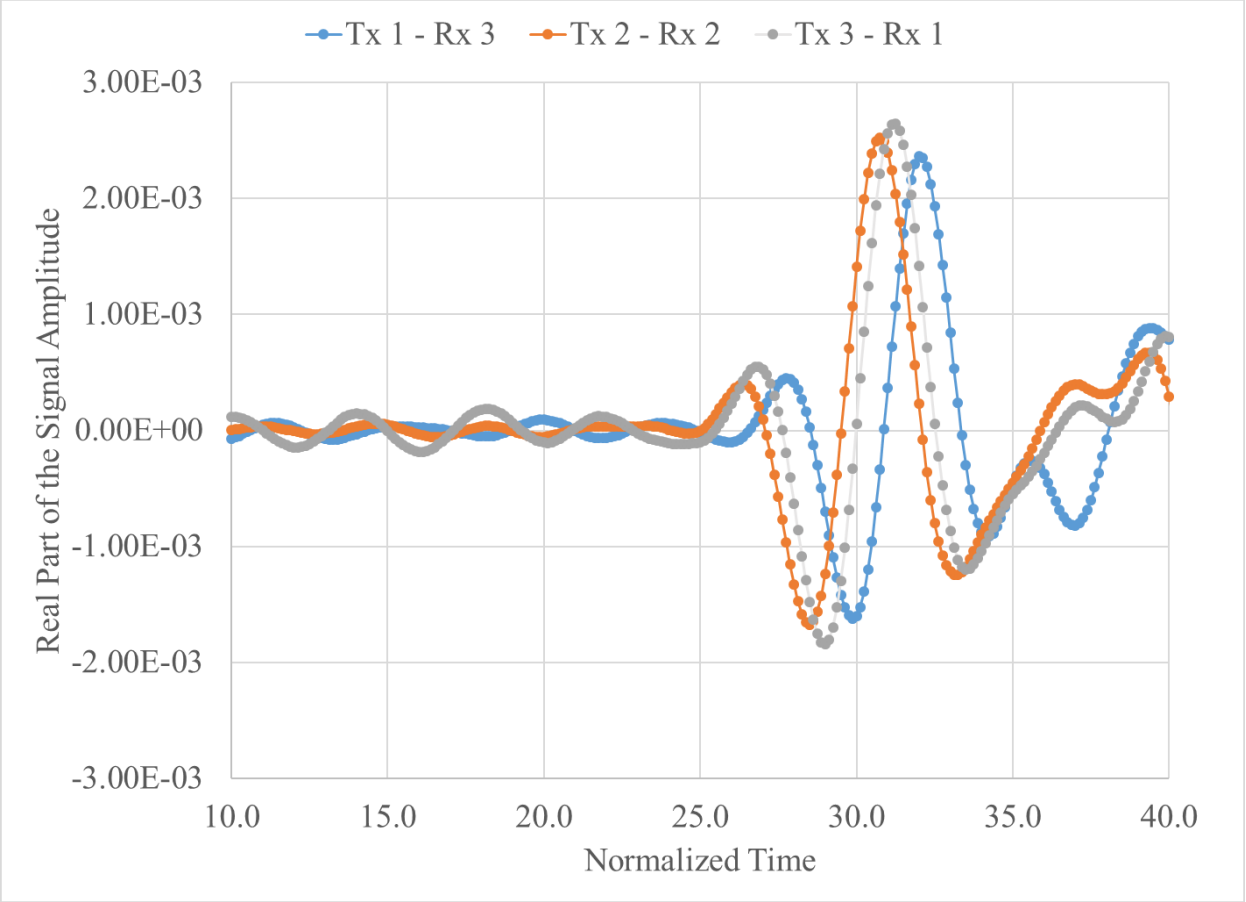

Figure 25. Real part time histories with air calibration for non-dimensional time from 10 to 40.

The results of the determination of $\Delta t_{1,min}$ and $\Delta t_{1,max}$ for each transmitting and receiving pair using equations 32 and 33 are shown in Table 2. The time ranges for the peaks due to reflections from the top surface of the pavements are calculated by adding the corresponding times for the direct arrivals presented above. These values are also shown in Table 2. Finally, the last two columns of Table 2 show the determined non-dimensional times for the peaks due to reflections from the top surface obtained for the signals without and with air calibration. It can be observed that for each antenna pair the peak times obtained without and with air calibration are similar and within the determined intervals.

Table 2. Determination of the time of the arrival of the reflection signal from the top pavement surface.

Antenna pair	$\Delta t_{1,min}$	$\Delta t_{1,max}$	$t_0 + \Delta t_{1,min}$	$t_0 + \Delta t_{1,max}$	t_{11}	
					w/o air calibration	w air calibration
Tx1 – Rx3	8.95	19.825	27.625	38.5	32.075	32.05
Tx2 – Rx2	10.4875	21.9875	24.625	36.125	30.775	30.75
Tx3 – Rx1	9.975	21.225	25.625	36.875	31.325	31.20

Using equation (34) we now can determine the distance between the antennas and the pavement surface. The results of these calculations are summarized in Table 3. In can be observed that the determined distances differ by up to 1 in.

Table 3. Determination of the time of the arrival of the reflection signal from the top pavement surface.

Antenna pair	GPR Antenna Height, in
Tx1 – Rx3	17.53
Tx2 – Rx2	18.78
Tx3 – Rx1	18.64

The results of the determination of $\Delta t_{2,min}$ and $\Delta t_{2,max}$ for each transmitting and receiving pair using equations 35 and 35 are shown in Table 4. The time ranges for the peaks due to reflections from the bottom surface of the pavements are calculated by adding the corresponding times for the direct arrivals presented above. These values are also shown in Table 4. Finally, the last column of Table 4 shows the determined non-dimensional times for the peaks due to reflections from the bottom surface obtained for the signals without air calibration. It can be observed that for each antenna pair the peak times are within the determined intervals.

Table 4. Determination of the time of the arrival of the reflection signal from the top pavement surface.

Antenna pair	$\Delta t_{2,min}$	$\Delta t_{2,max}$	$t_1 + \Delta t_{2,min}$	$t_1 + \Delta t_{2,max}$	t_{22}
Tx1 – Rx3	5.35	21.61	37.725	53.985	43.75
Tx2 – Rx2	5.43	21.78	36.4425	52.7925	41.125
Tx3 – Rx1	5.41	21.72	36.8475	53.1575	45.25

Finally, the thickness of the asphalt layer is determined from the individual antenna time histories by solving the system of non-linear equation (37) and (38). The asphalt layer dielectric constant was set to 6 for the analysis. The results of this analysis is presented in Table 5. It can be observed that the thicknesses are differ by 1.1 in. This can be attributed to the Figure 26 show the computed thicknesses for all 27 antenna pair measurements collected for this trigger.

Table 5. Thicknesses of the top asphalt layer computed using tine histories from the individual antenna pairs.

Antenna pair	Hac Thickness, in
Tx1 – Rx3	3.52
Tx2 – Rx2	3.09
Tx3 – Rx1	4.2

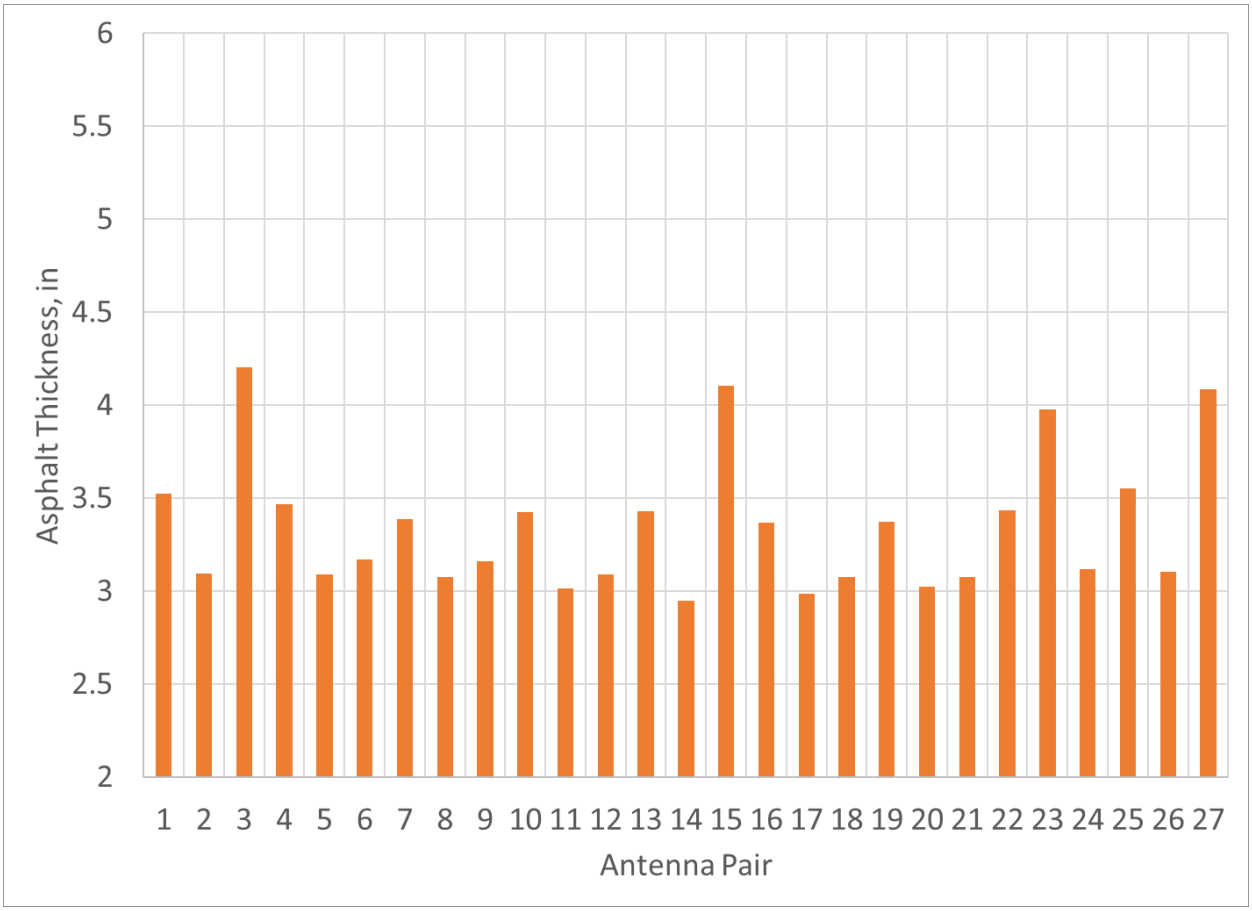

Figure 26. Asphalt thicknesses for 27 pairs

Figure 27 presents the computed asphalt thicknesses for the dielectric constants varied from 4 to 7. It can be observed that an increase in the assumed dielectric constant for the asphalt layer leads to an increase in the competed asphalt thickness for every sensor pair in this antenna group. Figure 28 shows the computed asphalt thicknesses for the first 100 triggers. It can be observed that the computed thicknesses from pairs TX1-RX3 and TX2-RX2 are similar, while the thicknesses from pair TX3-RX1 may differ from those thicknesses by 0.25 in. Overall, these results confirm that 3D Radar data produce consistent asphalt thicknesses.

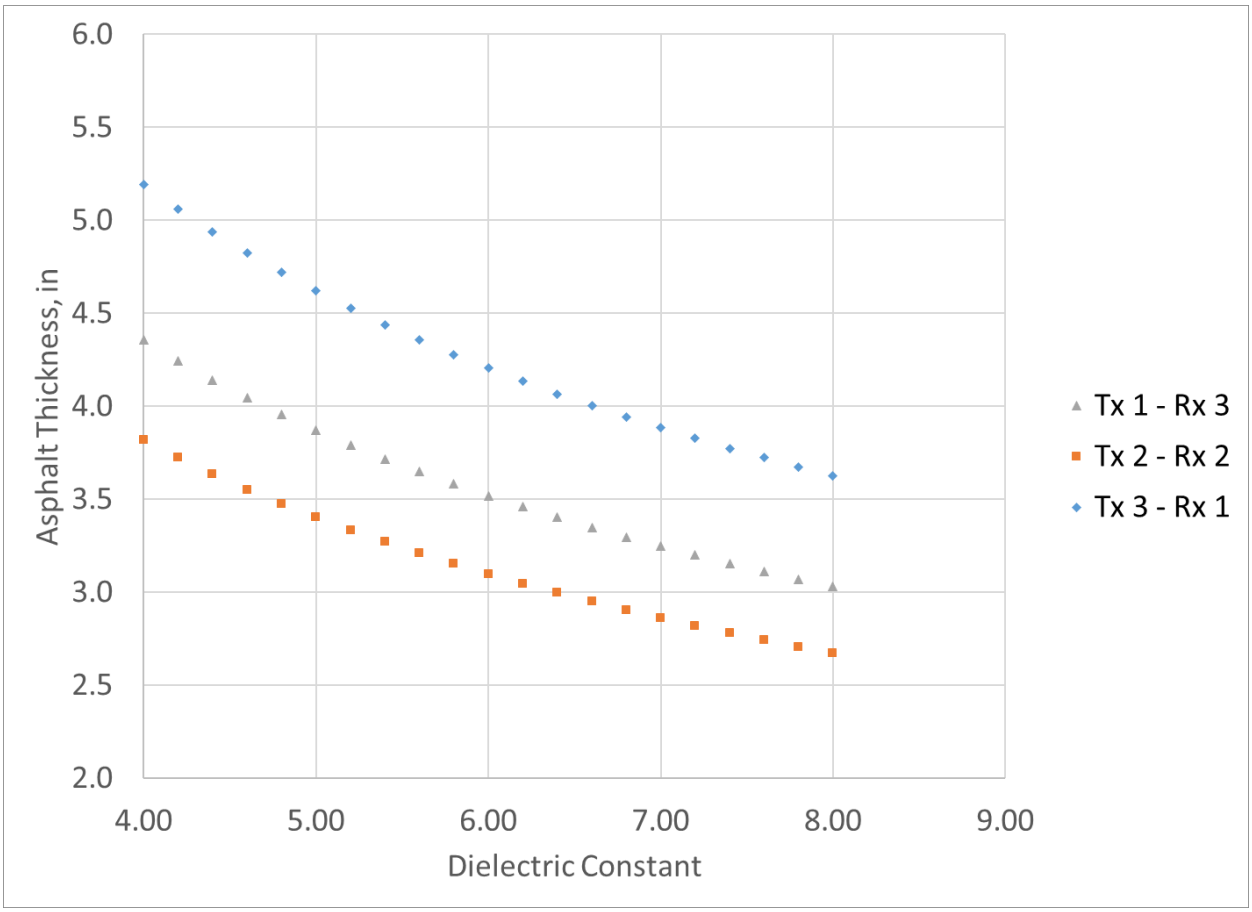

Figure 27. Sensitivity of the computed asphalt thickness to the assumed dielectric constant for the asphalt layer.

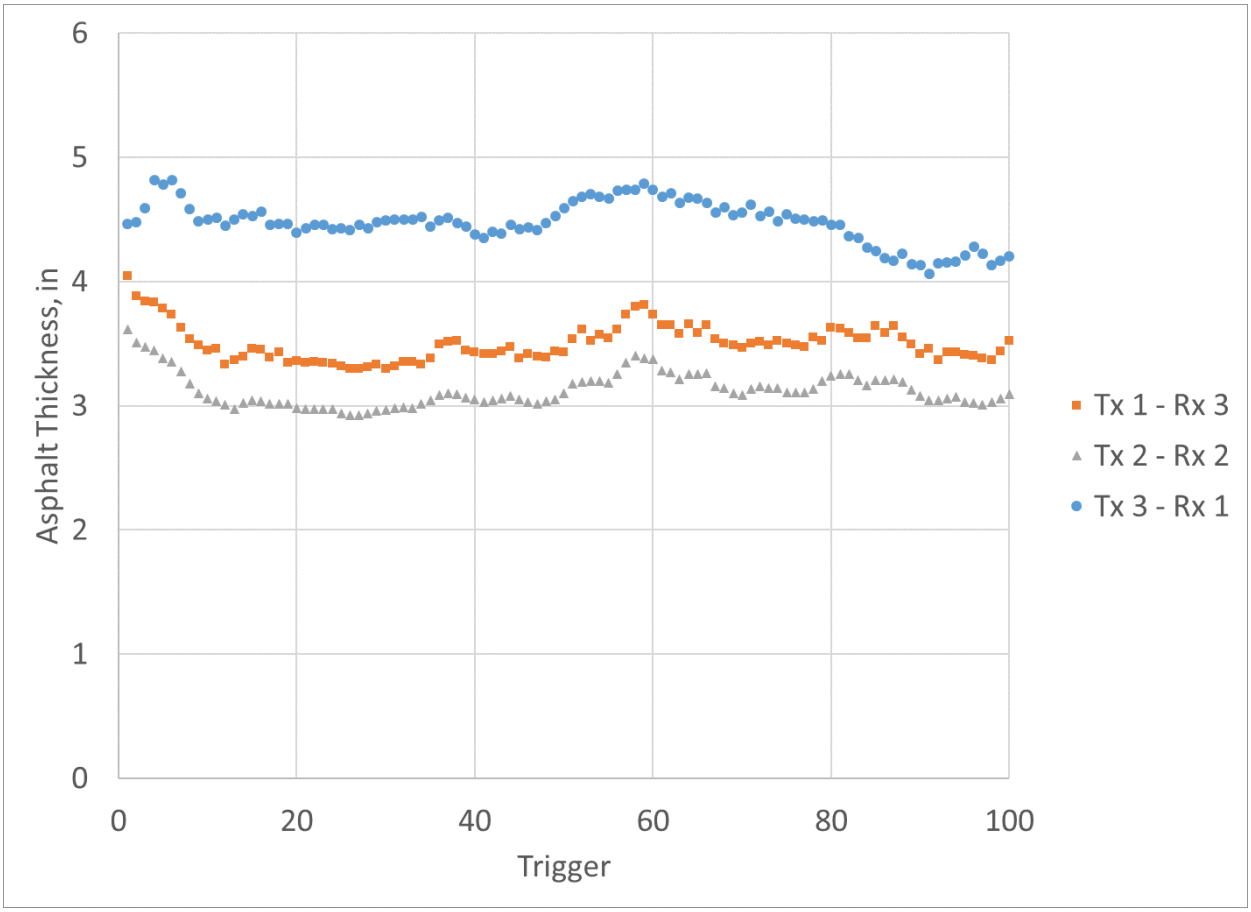

Figure 28. Variation of the asphalt thickness along the project

After computing the asphalt thicknesses from the individual pairs time histories, the software developed in this study uses time histories from antenna pairs having the same common point to determine simultaneously the dielectric constant of the asphalt layer and its thickness using the Modified Extended Common Mid-Point (MXCMP).

The first step in the MXCMP requires determining the distance between the antenna group and the pavement surface. The range of the possible distance was assumed to be between 14 in and 23 in with 40 equally spaced possible distances within this interval. For each possible distance and each antenna pair the time of the anticipated arrival of the refection from the pavement surface was determined using equations (39)-(41).

Figure 29 presents the real part signal values corresponding to the reflections from the pavement surface for various assumed distances between antennas and pavement surface determined from the individual antennas in one antenna group with a common mid-point. Figure 29 also presents the total signal magnitudes for all three antennas obtained by summation of the magnitudes for the individual antennas for each assumed distance. It can be observed that the maximum total magnitude occurs for the distance between antennas and the pavement surface equal to 0.461 m or 11.7 in. This distance is used in the subsequent analysis.

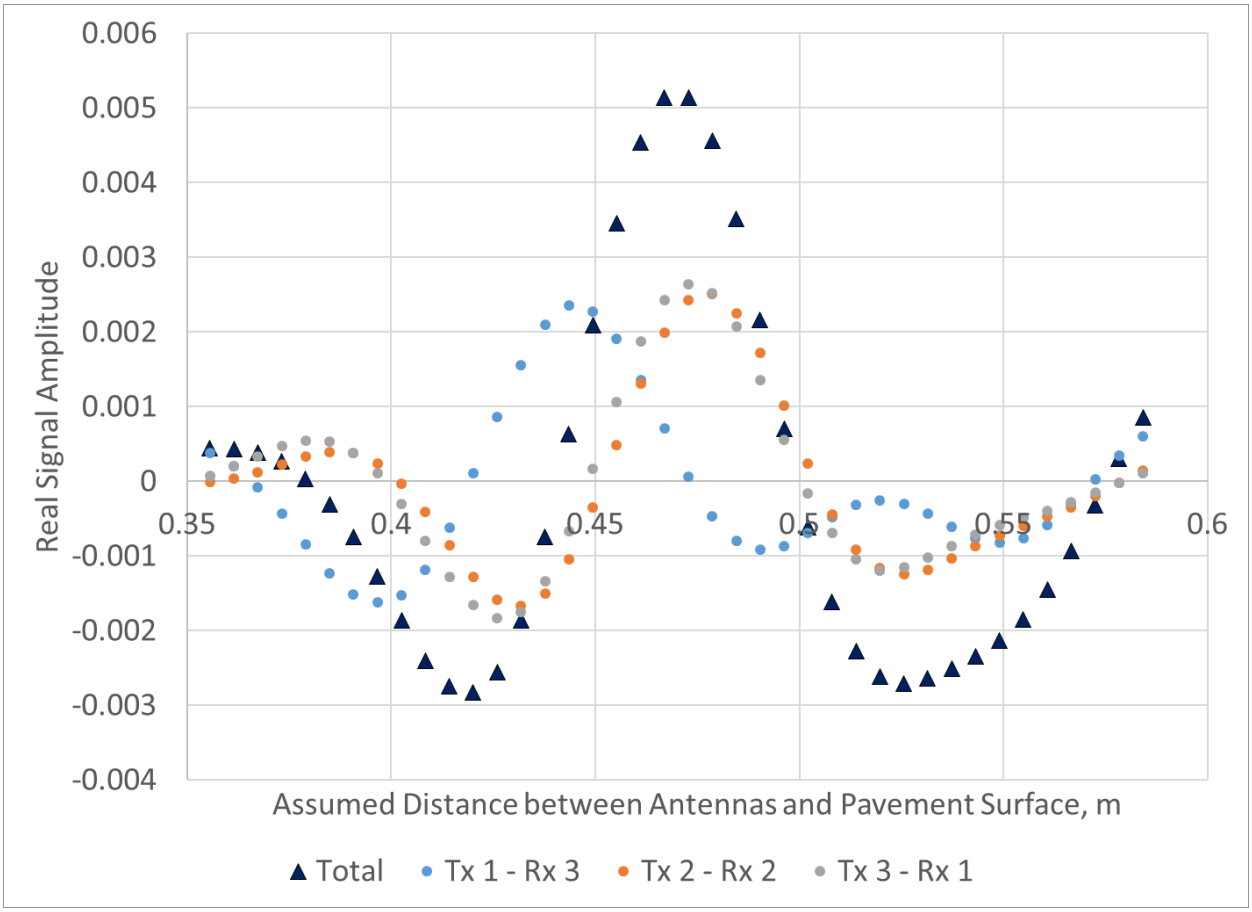

Figure 29. Signal values of the reflections from the pavement surface for various assumed distances between antennas and pavement surface

The next step in the MXCMP involves determining the signal magnitudes corresponding to the reflections from the bottom surface of the asphalt layer for various assumed asphalt thicknesses and dielectric constants. In the example the range of the possible asphalt thickness was assumed to be between 2 and 6 with 41 equally spaced values within this interval and the range of the possible dielectric constants was assumed to be between 4 and 8 with 21 values within this interval. For each possible combination of the asphalt thickness and dielectric constant and each antenna pair the time of the anticipated arrival of the refection from the bottom of the asphalt layer w was determined using equations (44) and (45).

Figure 30 presents the real part signal values corresponding to the reflections from the bottom surface of the asphalt layer for various assumed asphalt thicknesses and dielectric constant for the asphalt layer equal to 6. The real part signal values computed for the individual antenna pairs in the antenna group with a common mid-point. Figure 30 also presents the total signal magnitudes for all three antennas obtained by summation of the magnitudes for the individual antennas for each assumed asphalt thickness. It can be observed that the maximum total

magnitude occurs for the asphalt thickness equal to 3.8 in. Figure 31 shows the total values of the reflections for the dielectric values equal to 4, 6, and 8. It can be observed that for dielectric values of 4 and 8 the maximum values of the reflections correspond to asphalt thicknesses equal to 4.9 and 3.4 in, respectively.

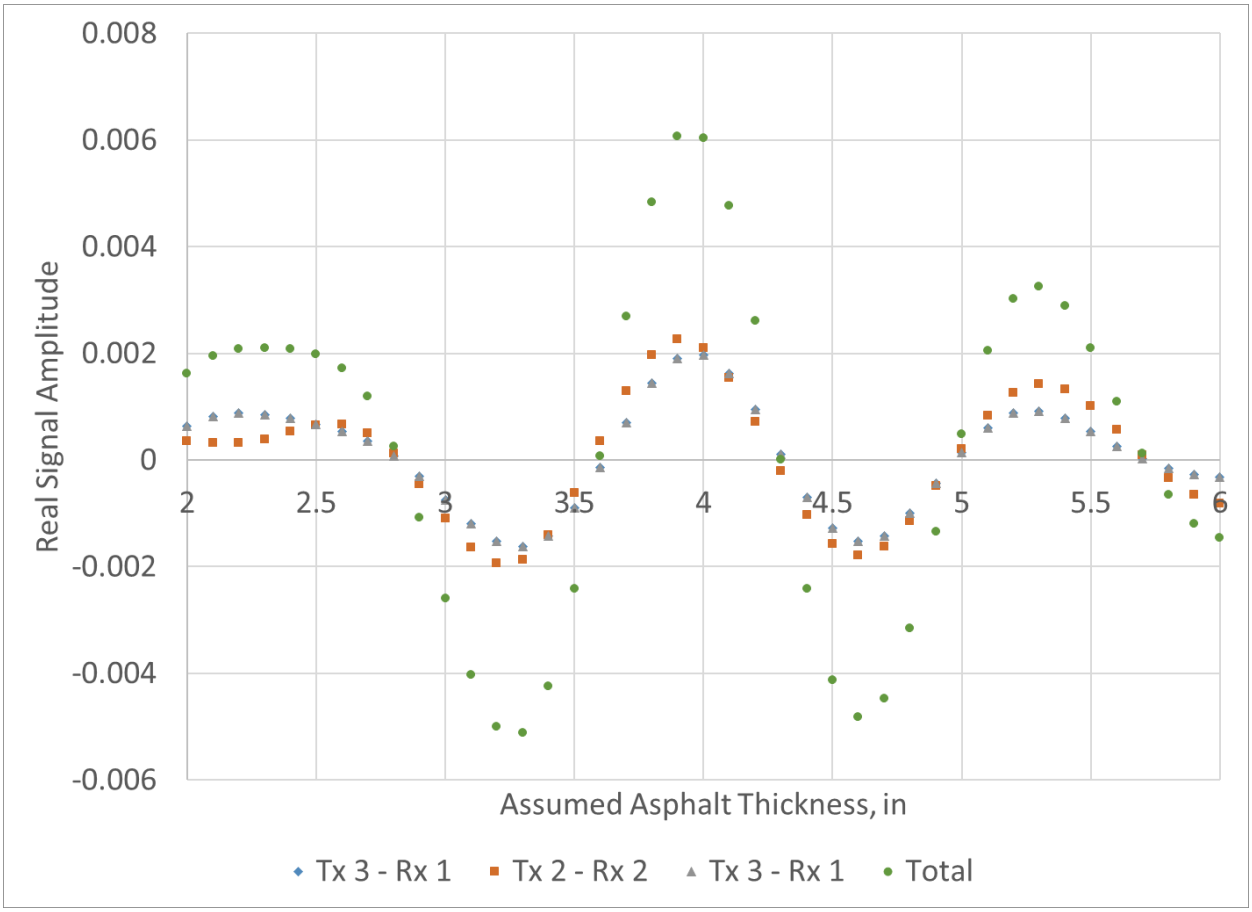

Figure 30. Signal values of the reflections from the bottom asphalt surface for various assumed asphalt thicknesses and dielectric constant of asphalt equal to 6.

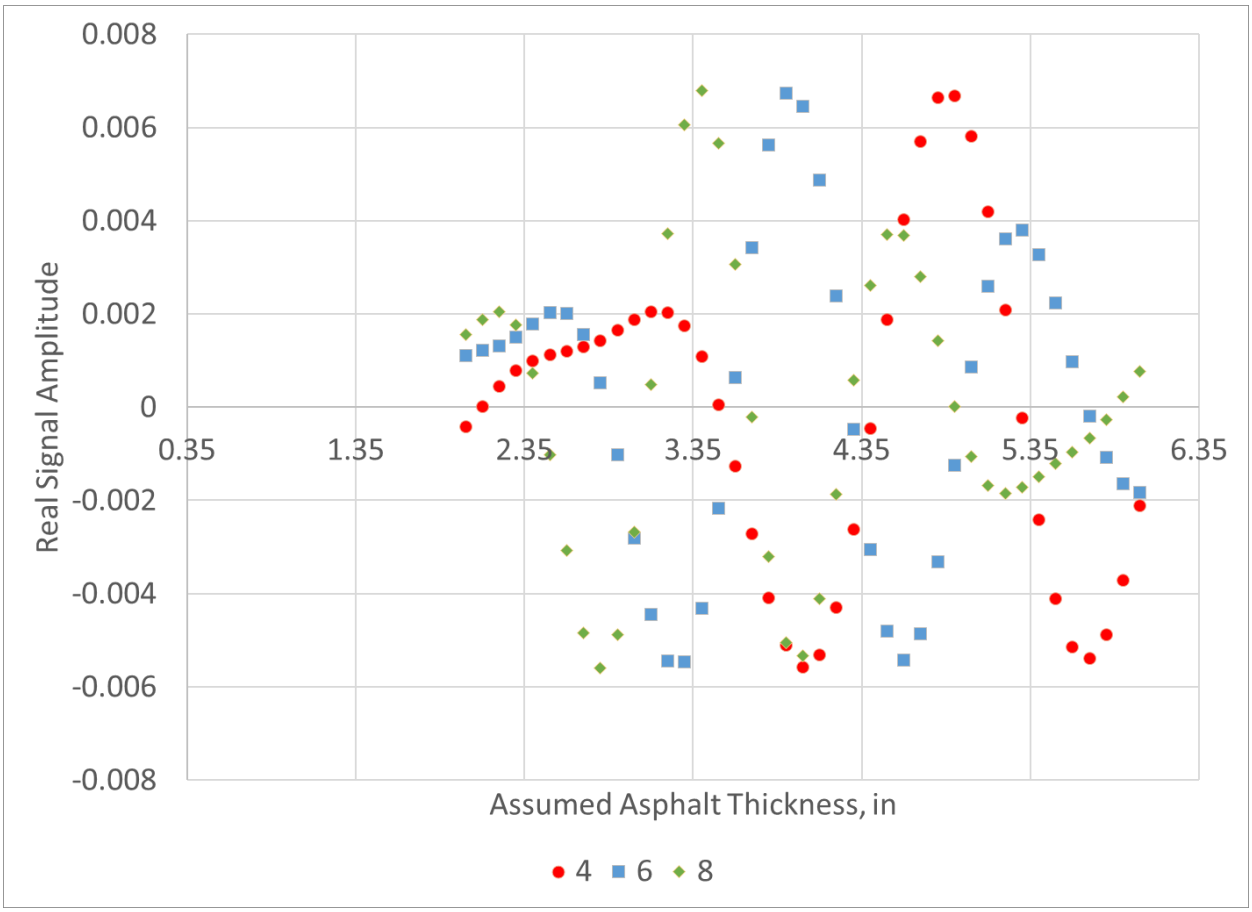

Figure 31. Total signal values of the reflections from the bottom asphalt surface for various assumed asphalt thicknesses and dielectric constants of asphalt equal to 4, 6, and 8.

This analysis was conducted for every value of the dielectric constant defined by the user. Figuer 32 presents the maximum values of the total signal magnitude and the corresponding asphalt thicknesses for every value of the dielectric constant of the asphalt layer specified by the user. It can be observed that the dielectric values of 5.8, 6.4, and 8.0 resulted in the highest values for the signals equal to 0.006792, 0.006795, and 0.006789, respectively. The corresponding asphalt layer thicknesses are equal to 4.0, 3.8, and 3.4 in, respectively. Since the maximum value of the signal is equal to 0.006795, the procedure select the thickness and dielectric constant for the asphalt layer at this point, i.e., trigger number in the longitudinal direction and the common point for this antenna group in the transverse direction, to be equal to 3.8 in and 6.8, respectively, but a small noise in the data could affect the resulting values.

Figure 33 shows computed asphalt thicknesses and dielectric values for the same trigger but different groups of antennas and, respectively, different common points in the transverse direction. It can be observed that the computed asphalt thicknesses are fairly consistent.

Finally, Figure 34 presents the computed asphalt thicknesses from the data collected by one antenna group for triggers between 1 and 500. It can be observed that, with a small

number of exceptions, the computed thickness were varied between 2.6 and 5.4 in. Nevertheless, there is a substantial scatter in the results collected even for the neighboring triggers. This might be attribute to the observation made from the analysis of Figure 32 several combinations of the asphalt thicknesses and dielectric constant may result in very similar maximum values of the total signal and a small noise in the signals may cause error in the thickness determination. This issue should be addressed in future studies.

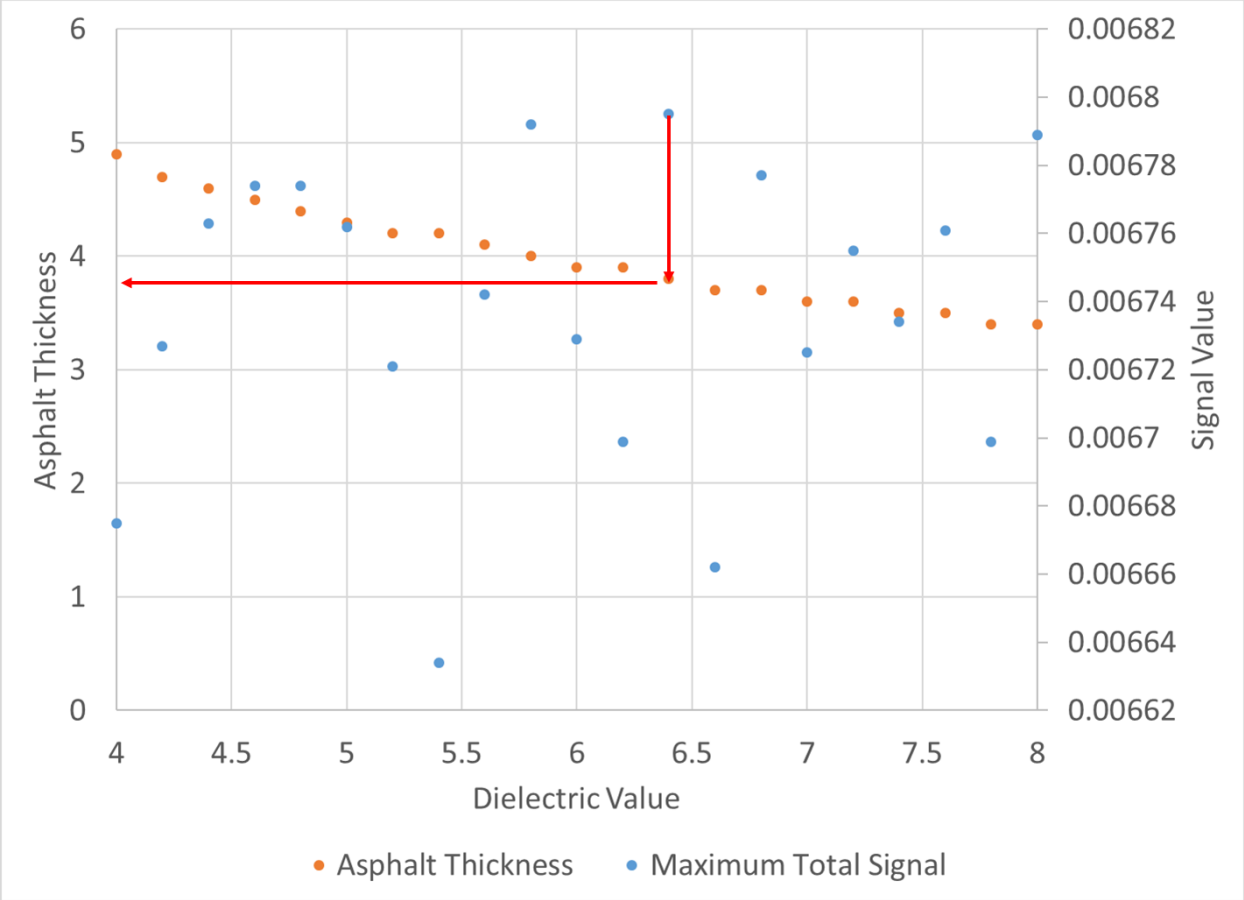

Figure 32. The maximum values of the total signals and the corresponding asphalt thicknesses for various assumed values of the dielectric constants of asphalt.

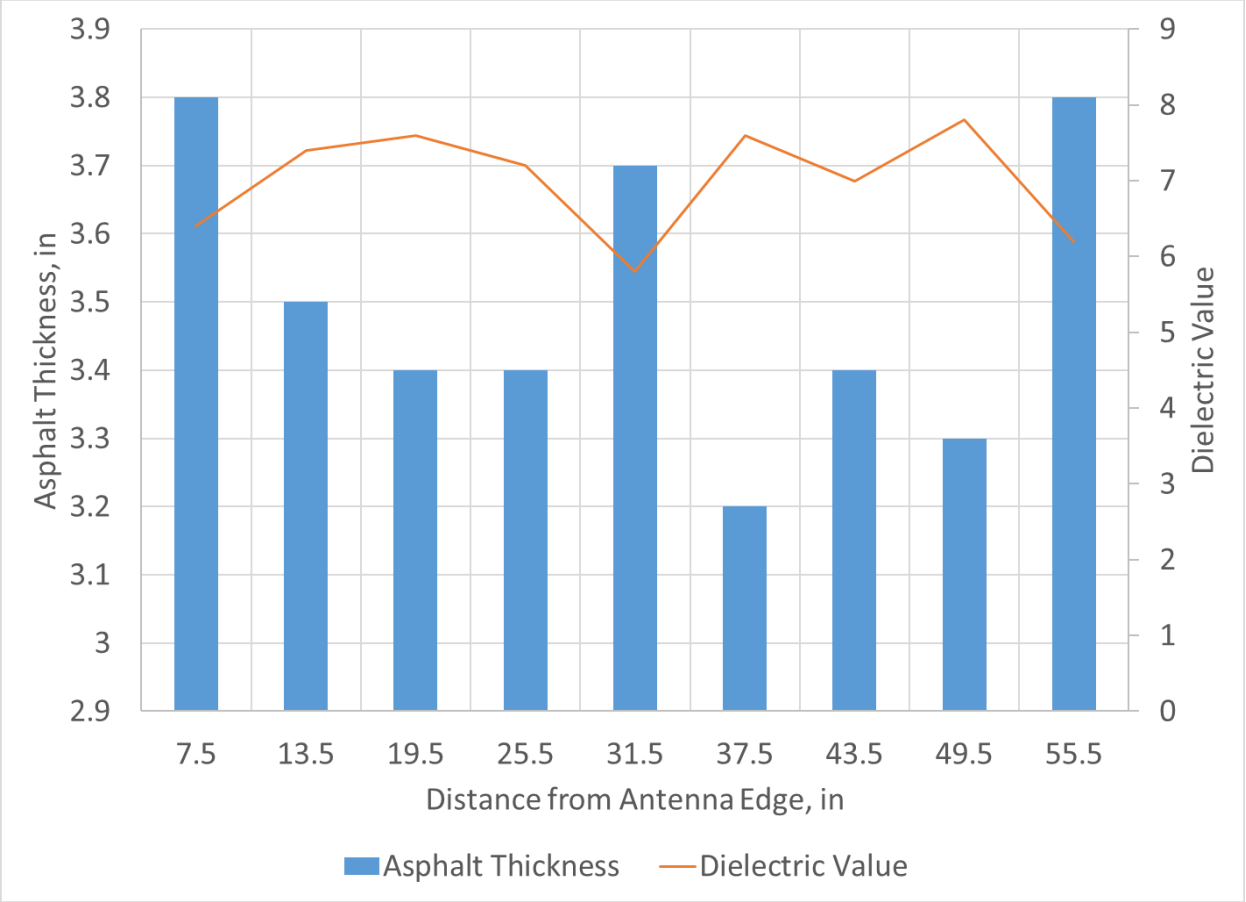

Figure 33. Computed asphalt thicknesses and dielectric values from time histories from every antenna pair groups and the same trigger.

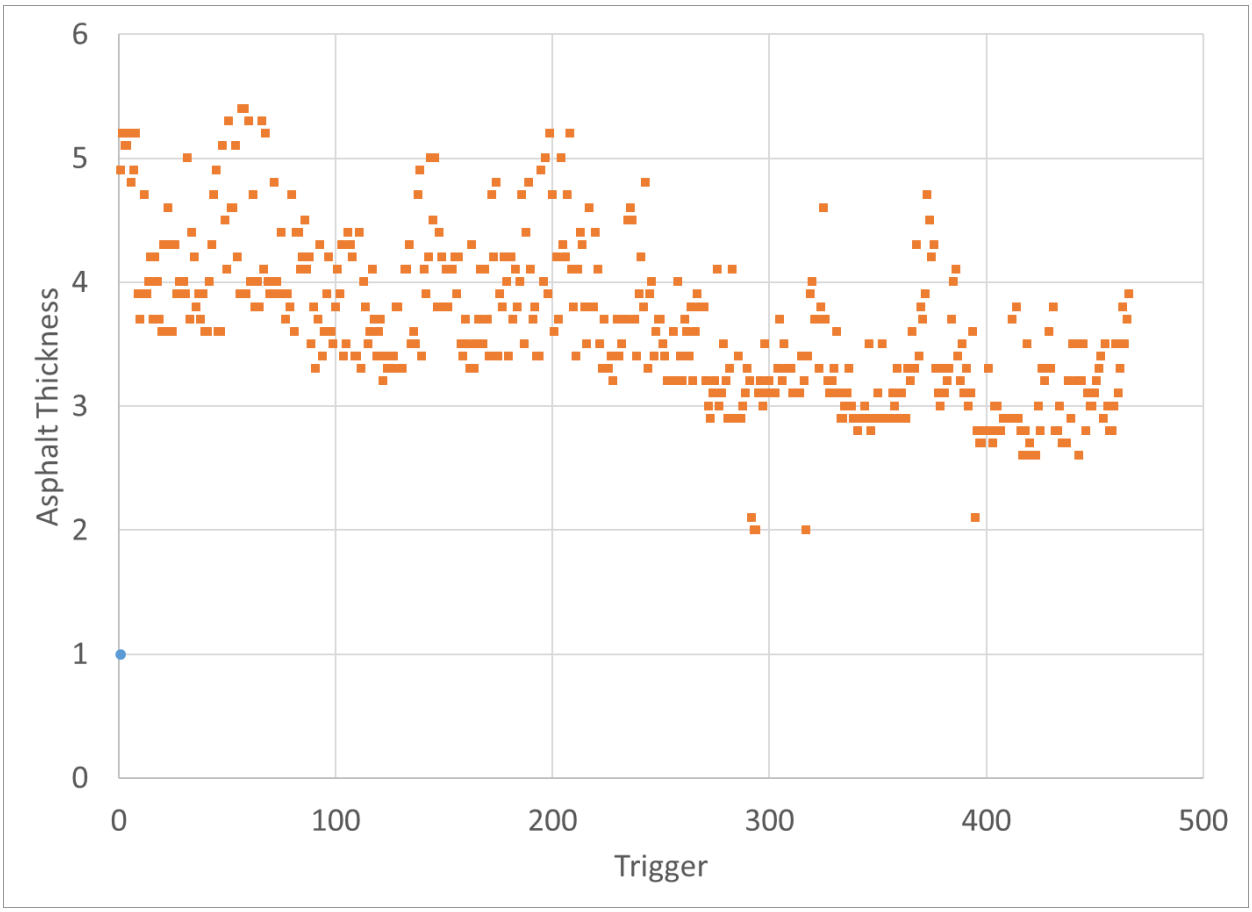

Figure 34. Computed asphalt thicknesses for one antenna group but different triggers

CHAPTER 6: CONCLUSIONS

Currently, thickness assessment is done by MnDOT either by core removal or with single antenna ground penetrating radar (GPR) testing. Conventional GPRs provide nondestructive evaluation of pavement thickness but restrict testing during one pass to a single test line. Recent advancements in GPR technology provide significant potential for improvement of nondestructive assessment of transportation infrastructure. The 3D RADAR step-frequency linear array system enables coverage of a 1.5-meter wide area at 75-mm spacing in the transverse direction, which improves data collection productivity and coverage. The 3D GPR has been incorporated into the RoadDoctor vehicle to further advance MnDOT's capabilities in continuous roadway evaluation technologies.

The main focus of this study was the development of a tool to determine asphalt layer thickness using data collected with the 3D Radar system. The DX antenna system used in this study has 11 transmitting and receiving antennas. Each receiving antenna may record signals from any transmitting antenna in the assembly. Therefore, 3D GPR scans are capable of providing information on the asphalt thickness for the entire scanned region. However, if all 121 measurements have to be made for one location, it makes the data collection process unnecessarily slow. To address this limitation, it was proposed to collect data using 27 transmitting and receiving antenna pairs focused on 9 points at the pavement surface.

The software developed in this study can analyze the data sets collected with either 121- or 27-transmitting and receiving pair configurations. It uses two approaches to determine asphalt thickness:

- Analysis of individual antennas pairs time histories along with the user-provided dielectric constant for the asphalt layer
- Analysis of groups of signals from transmitting and receiving antennas with various spacing but with a common mid-point using the Modified Extended Common Mid-Point (MXCMP) method (The MXCMP method is a generalization of the Extended Common Mid-Point (MXCMP) method for analysis of more than two antenna pair signals with the same mid-point.)

The software reports the results of the analysis in comma-separated text files that can be later analyzed by the user using Excel or other tools. The use of multiple antenna pairs focused on the same point at the pavement surface and two analysis methods provides redundancy and increases reliability of the results compared to the ones obtained with a single GPR antenna. The use of the proposed tool would facilitate utilization of continuous asphalt thickness evaluation at highway speed and minimize the need for coring.

REFERENCES

Al-Qadi, I., Lahouar S., & Loulizi. A. (2003). Successful application of ground-penetrating radar for quality assurance-quality control of new pavements. *Transportation Research Record: Journal of the Transportation Research Board, 1861*(1), 86–97.

Al-Qadi, I. L., & Lahouar, S. (2015). Measuring layer thicknesses with GPR – Theory to practice. *Construction and Building Materials*, *19*(10), 763-772. https://doi.org/10.1016/j.conbuildmat.2005.06.005

Blahut, R. E. (2004). *Theory of remote image formation.* Cambridge, UK: Cambridge University Press.

Cao, Y., Dai, S., Labuz, J. F., & Pantelis, J. (2017). *Implementation of ground penetrating radar* (Report No. MN/RC 2007-34). St. Paul, MN: Minnesota Department of Transportation.

Daniels, D. J. (1996). *Surface-penetrating radar* (Radar Series no. 6). London: ERA Technology, Institution of Electrical Engineers.

Daniels, D. J. (2005) *Ground penetrating radar*. Hoboken, NJ: John Wiley & Sons, Inc.

Eide, E. S. (2000). Ultra-wideband transmit/receive antenna pair for ground penetrating radar. *IEE Proceedings-Microwaves, Antennas and Propagation, 147*(3), 231–235.

Eide, E., & Sala J. (2012). High resolution step-frequency 3D GPR using wideband antenna arrays. *25th Symposium on the Application of Geophysics to Engineering and Environmental Problems 2012 (SAGEEP 2012), Proceedings of a meeting held 25-29 March 2012, Tucson, Arizona, USA.*

Grote, K., Hubbard, S., Harvey, J., & Rubin, Y. (2005). Evaluation of infiltration in layered pavements using surface GPR reflection techniques. *Journal of Applied Geophysics*, 57, 129–153.

Hoegh, K., Khazanovich, L., Dai, S., & Yu, T. (2015). Evaluating asphalt concrete air void variation via GPR antenna array data. *Case Studies in Nondestructive Testing and Evaluation*, *3*, 27-33. https://doi.org/10.1016/j.csndt.2015.03.002

Hu, J., Vennapusa, P. K. R., White, D. J., & Beresnev, I. (2016). Pavement thickness and stabilized foundation layer assessment using ground-coupled GPR. *Nondestructive Testing and Evaluation*, *31,* 267-287. https://doi.org/10.1080/10589759.2015.1111890

Jol, H. M. (2008). *Ground penetrating radar theory and applications.* Amsterdam: Elsevier.

Lahouar, S., Al-Qadi I., Loulizi A., Clark T., & Lee D. (2002). Approach to determining in situ dielectric constant of pavements: Development and implementation at Interstate 81 in Virginia. *Transportation Research Record: Journal of the Transportation Research Board, 1806*(1), 81–87.

Liu, H., & Sato M. (2014). In situ measurement of pavement thickness and dielectric permittivity by GPR using an Antenna Array. *NDT & E International*, *64,* 65–71.

Olhoeft, G. R., & Smith III, S. S. (2000). Automatic processing and modeling of GPR data for pavement thickness and properties. Paper presented at the 8th International Conference on Ground Penetrating Radar, Gold Coast, Australia.

Saarenketo, T., & Scullion, T. (2000). Road evaluation with ground penetrating radar. *Journal of Applied Geophysics*, *43,* 119–138.

Sala, J., & Linford, N., W. (2012). Processing stepped frequency continuous wave GPR systems to obtain maximum value from archaeological data sets. *Near Surface Geophysics*, *10*(1), 3-10. https://doi.org/10.3997/1873-0604.2011046

Scullion, T. (2006). *Using rolling deflectometer and ground penetrating radar technologies for full coverage testing of jointed concrete pavements* (Report No FHWA-HIF-13-025). Washington, DC: Federal Highway Administration.

Stutzman, W. L., & Thiele G. A. (2012). *Antenna theory and design.* Hoboken, NJ: John Wiley & Sons.

Tompkins, D. M., Khazanovich, L., & Johnson, D. M. (2008). Benefits of the Minnesota Road Research Project. *Transportation Research Record: Journal of the Transportation Research Board*, *2087,* 12–19.

Uddin, W. (2006). *Ground penetrating radar study – Phase I* (Report No *FHWA/MS-DOT-RD-06-182*). Jackson, MS: Mississippi Department of Transportation.

Uddin, W. (2014). An overview of GPR applications for evaluation of pavement thickness and cracking. Paper presented at the 15th International Conference on Ground Penetrating Radar – GPR, Brussels.

Zhao, S. (2015). *Development of analysis approach utilizing extended common mid-point method to estimate asphalt pavement thickness with 3-D GPR*. Thesis, University of Illinois at Urbana-Champaign.

Zhao, S., Shangguan P., & Al-Qadi I. (2015). Application of regularized deconvolution technique for predicting pavement thin layer thicknesses from ground penetrating radar data. *NDT & E International*, *73,* 1–7.

APPENDIX A: USER GUIDE

3dRadarThickenss is a rudimentary software tool for determination of the asphalt layer thickness using the data collected with 3D RADAR Ground Penetrating Radar system. It contains two components:

- A Graphical User Interface (GUI) coded in JAVA. To execute the program, the Java Runtime Environment (JRE) 8 should be installed.
- A computational engine program coded in FORTRAN.

The GUI enables the user to provide appropriate inputs, such as the ranges for the asphalt layer thickness and dielectric constant, the files with the 3D RADAR data, and other information. When the require information is provided the GUI can execute the computational engine program and open output files.

SETUP INSTRUCTIONS

From Windows Explorer, double click on "setup.exe" file. The following screen will appear:

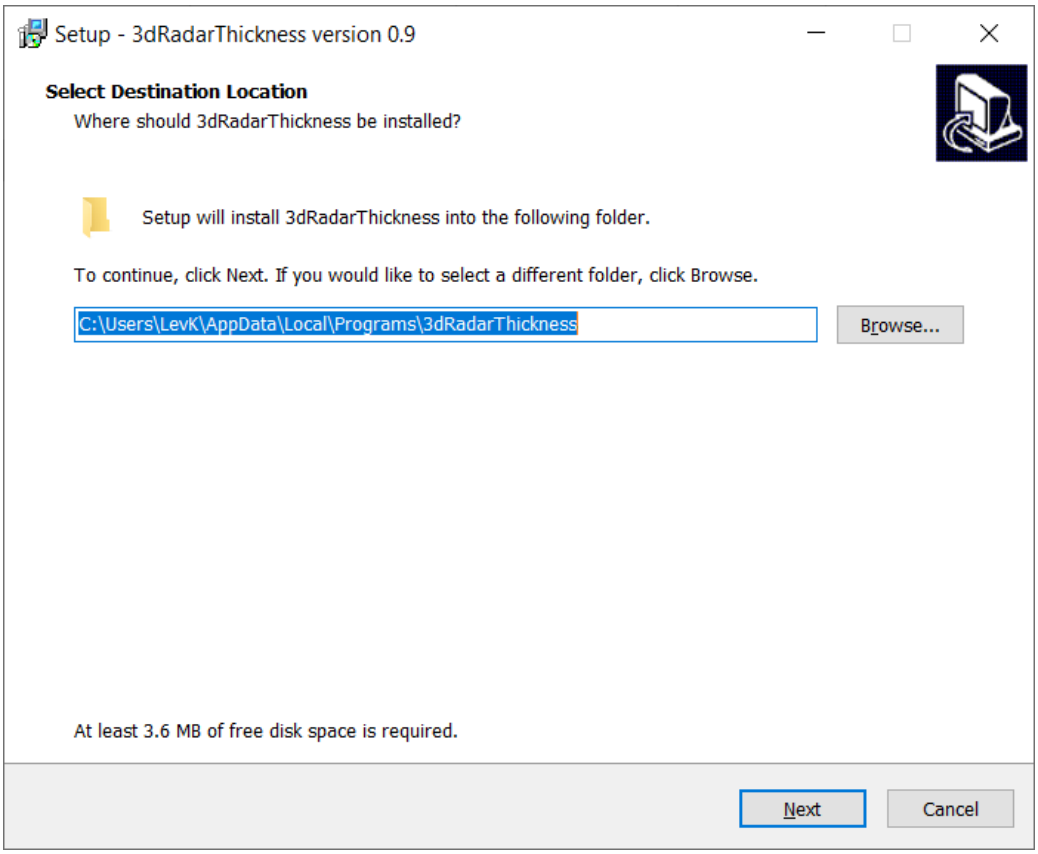

Click "Next". The Installation Wizard will prompt the user to select a destination directory for the 3dRadarThickness program.

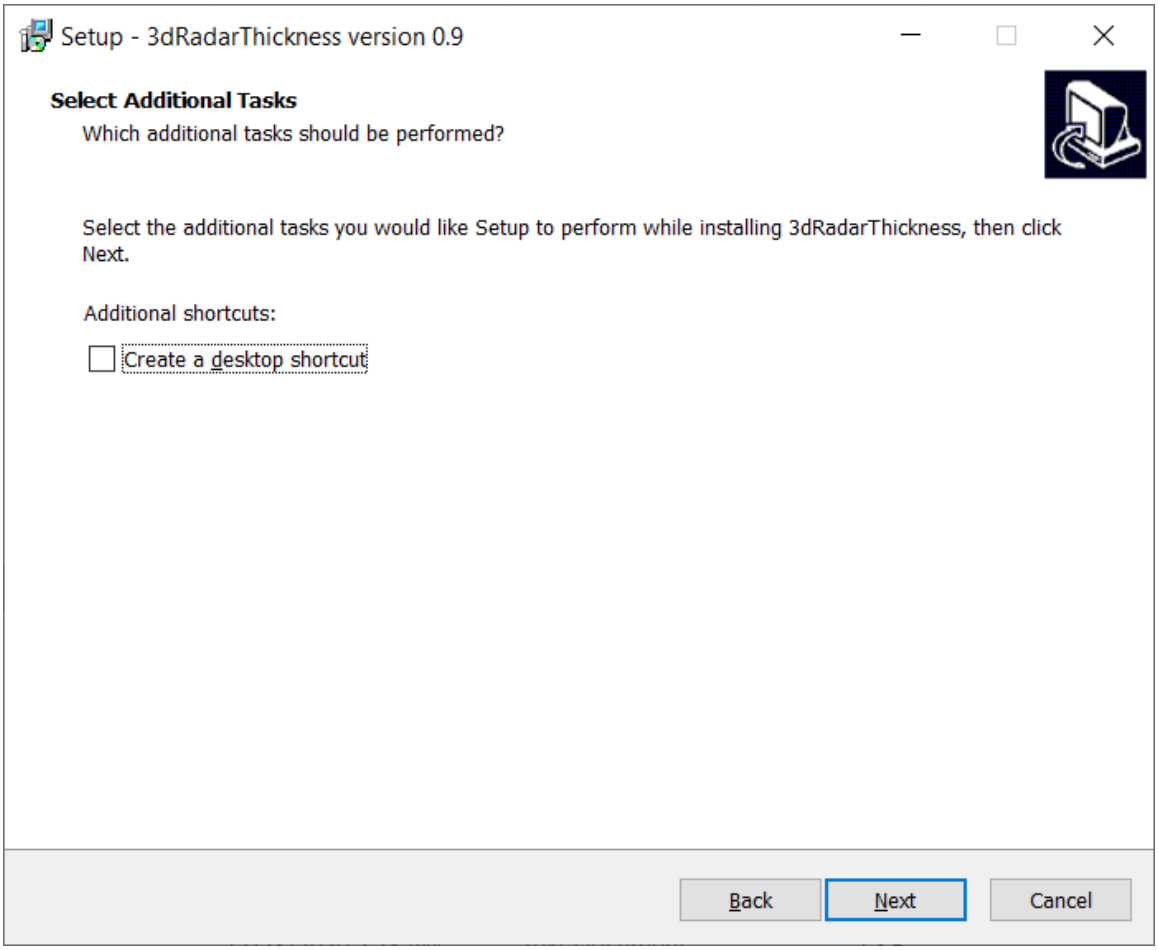

Click "Next" and the follow the on-screen instructions to complete the installation.

EXECUTING THE 3DRADARTHICKNESS PROGRAM

The application starts with the Main Window screen:

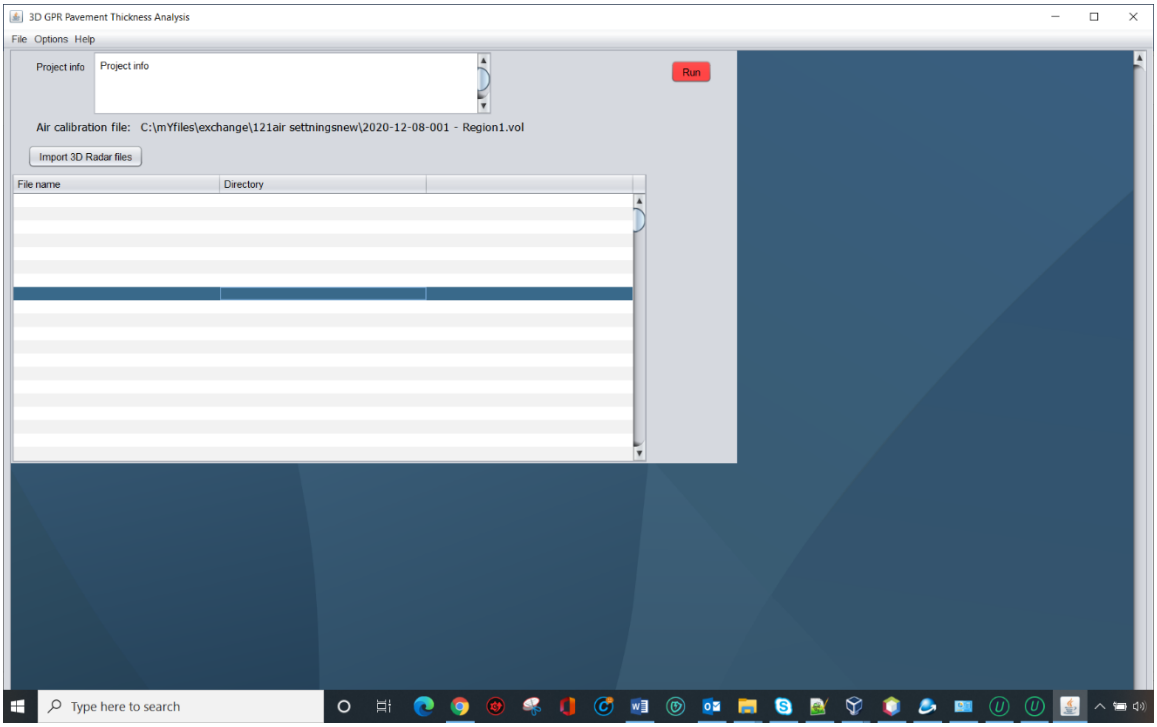

By default, a new empty project is created.

OPERATIONS WITH NEW PROJECTS

Importing 3D Radar Files

From the Main Window, click on the "Import 3D Radar files" button. A File Explorer will appear. Find and select the desirable file name(s).

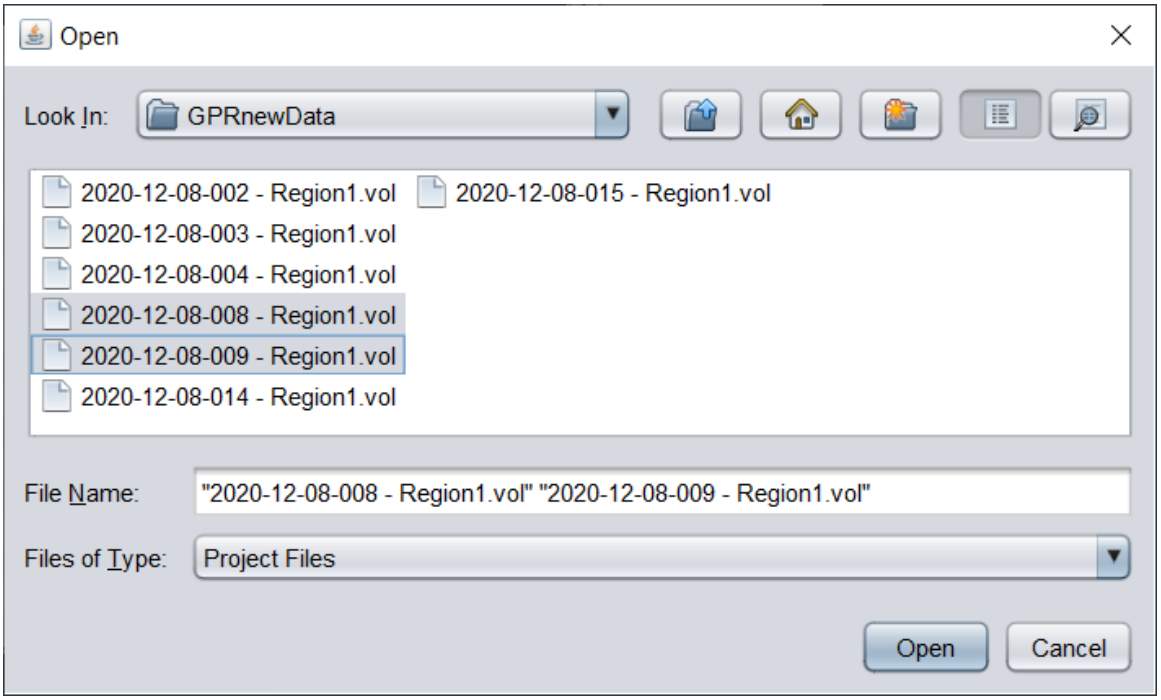

Click "Open" and the following screen will appear:

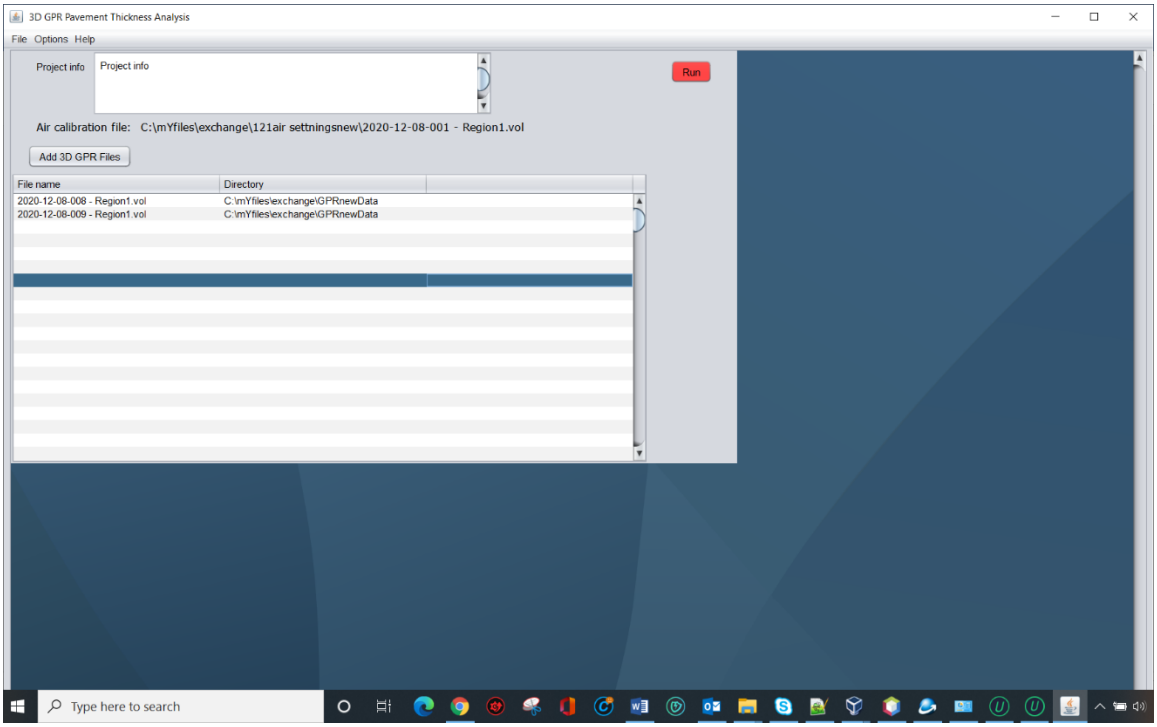

Note that the "Import 3D Radar files" button changed its name to "Add 3D Radar files" now (see above).

If desired, more files may be added to the table by clicking the "Add 3D Radar Files" button. They will be added to the bottom of the table.

Deselecting Some 3D Radar Files from the Project

If the user would like to deselect some or all of the files previously selected for the analysis, they need to select the files to be deleted, right-mouse click on them, and click the "Delete" button as shown in the following example:

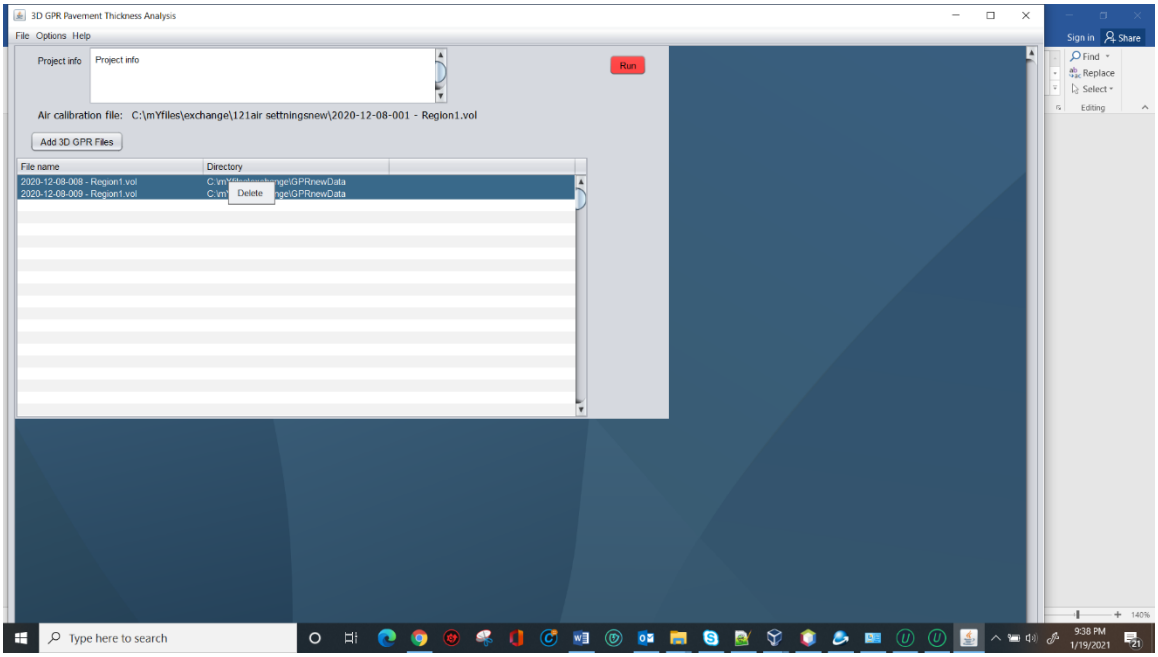

The prompt will appear asking the user to confirm the action:

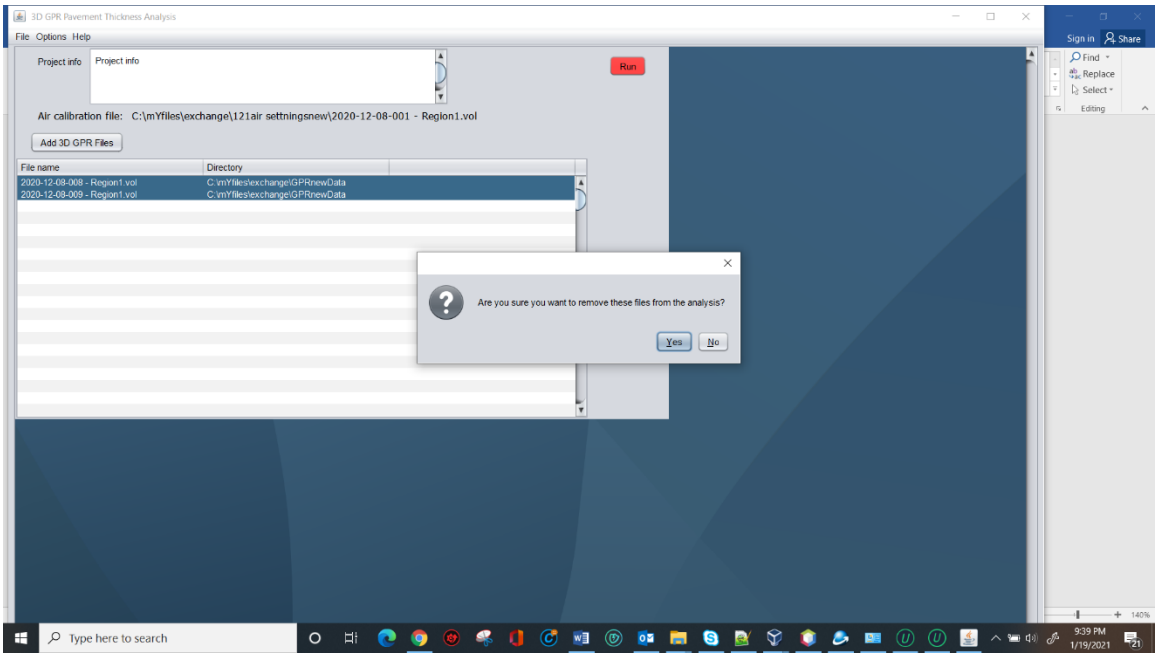

Click "Yes" to deselect the highlighted rows. Click "No" to cancel the operation.

Selecting Analysis Options

To conduct the analysis, the user should select the air calibration file and appropriate analysis settings.

To assign the analysis settings, the user should select "Options->Analysis Options" in the Main Window:

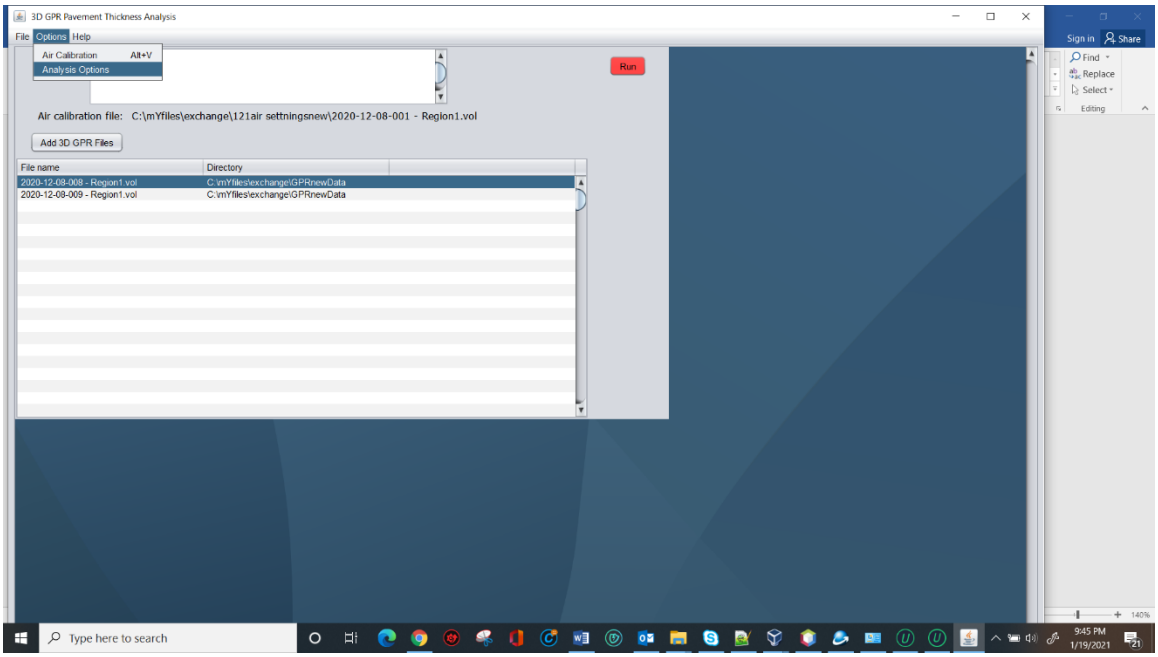

The following screen will appear:

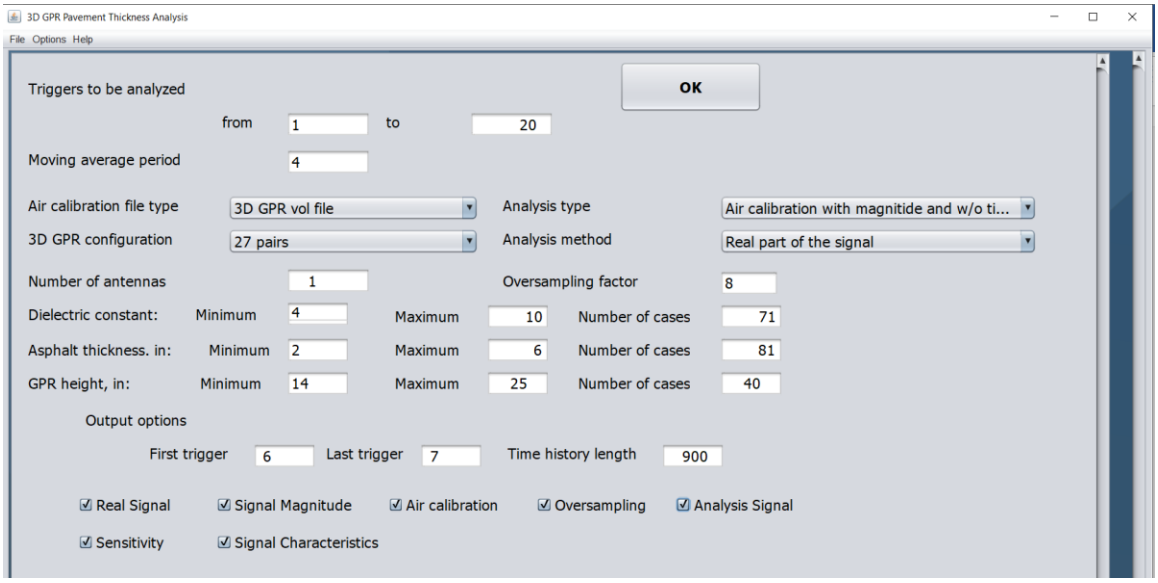

The user can specify/change the following options:

1. Range of triggers.

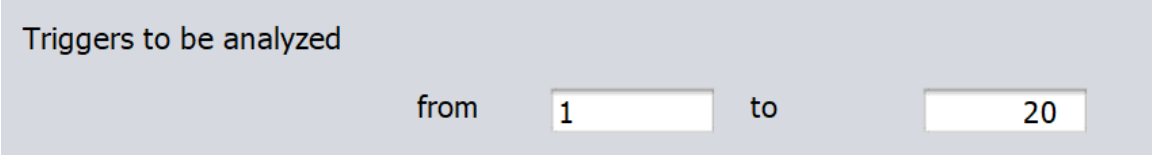

If a 3D GPR data file contains measurements made on many points along the road, its analysis may take substantial time. Sometimes, it is desirable to perform a preliminary analysis for a smaller set of the data. The user can specify the first and the last trigger to be analyzed, and the program will skip the data collected for the triggers outside of this range. If the user would like to analyze the data for all triggers in the file, the first trigger should be specified equal to 1 and the last trigger should be specified to a large number greater than the possible number of triggers in the file, for example, 999999.

2. Moving average period.

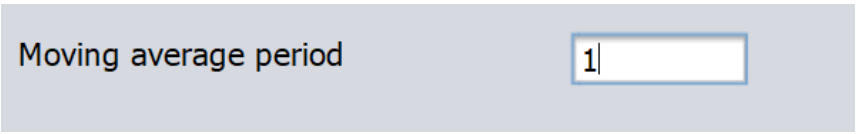

This parameter specifies how many time histories for the same antenna pair taken at subsequent triggers should be averaged prior to the data analysis. If this parameter is equal to one, then all the signals in the specified trigger range (see above) will be analyzed for the individual triggers.

3. Air calibration file type.

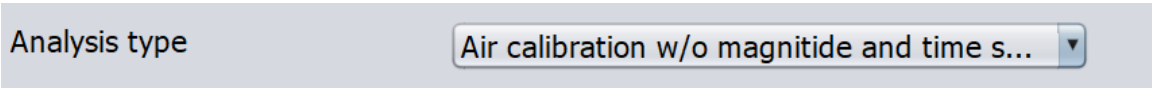

This analysis specifies the type of air calibration. The user can select from the following options:

1. No air calibration. In this case, the raw signals are analyzed
2. Air calibration w/o magnitude and time scaling. In this case, the corresponding air calibration signal time history is subtracted from each antenna pair signal time history.
3. Air calibration with magnitude but w/o time scaling. In this case, the corresponding air calibration signal time history adjusted to have the same first arrival peak magnitude is subtracted from each antenna pair signal time history.

4. Air calibration file type.

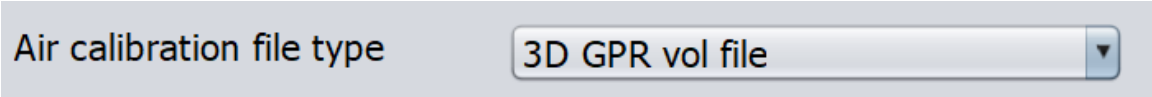

If the air calibration is specified in the analysis, then the user should provide an appropriate data file. The user can select from the following options:

1. No air calibration
2. Raw *.vol file.
3. Pre-analyzed *.csv file. This file is automatically generated by the program for each data analysis run and can be used for analysis of other data.

The selected air calibration file type should correspond to both the air calibration type and the specified air calibration file.

If no air calibration is specified in the analysis, then the program will ignore the air calibration file type parameter, or the user may select an option of “no air calibration.”

5. <u>3D GPR sensor configuration</u>

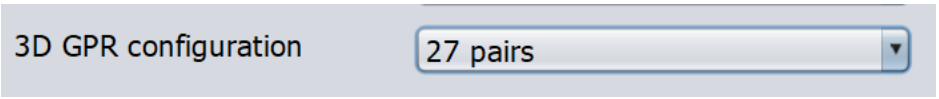

The program allows the user to specify two options for the GPR sensor configurations:

1. 121 pairs. In this case, all sensors are used to send or receive signals.
2. 27 pairs. In this case, time histories for the following sensor pairs are collected:

Signal number	Sensors	
	transmitting	receiving
1	1	3
2	2	2
3	2	4
4	3	1
5	3	3
6	3	5
7	4	2

Signal number	Sensors	
	transmitting	receiving
8	4	4
9	4	6
10	5	3
11	5	5
12	5	7
13	6	4
14	6	6
15	6	8
16	7	5
17	7	7
18	7	9
19	8	6
20	8	8
21	8	10
22	9	7
23	9	9
24	9	11
25	10	8
26	10	10
27	11	9

6. Analysis method

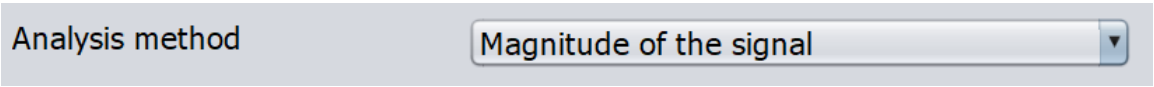

Two analysis method options are currently available:

1. Analysis of the real part of the signal
2. Analysis of the instantaneous magnitude of the signal.

7. Number of antennas

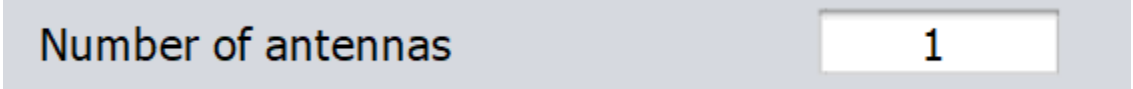

The user should specify the number of antennas used in the top layer thickness analysis. The recommended number is 3 antennas. For the 27-antenna configuration the number of antennas must be less than or equal to 3.

8. Oversampling factors

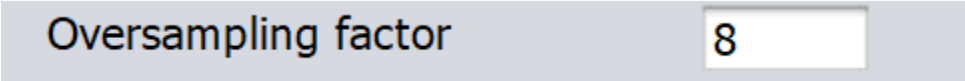

Each of the original intervals is divided into a number of subintervals for which the signals are reconstructed. The recommended value of this number is 8.

9. Dielectric constants used in the analysis

The user should specify the minimum and the maximum values of the dielectric constant for the top surface layer and the number of cases to be considered.

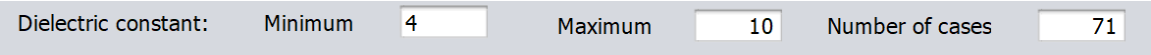

Based on this information, the program generates the set of dielectric values.
If the number of cases is greater than 1, then

$$\varepsilon_i = \varepsilon_{min} + \frac{\varepsilon_{max} - \varepsilon_{min}}{n-1}(i-1), i = 1,2,\cdots,n$$

where ε_{min} and ε_{max} are the minimum and the maximum dielectric values, and n is the number of cases.

If the number of cases is set to be equal to one, then $\varepsilon_i = \varepsilon_{min}$ and the maximum value is ignored.

10. Top layer thicknesses used in the analysis

The user should specify the minimum and the maximum values of the top surface layer thickness and the number of cases to be considered.

Asphalt thickness. in:	Minimum	2	Maximum	6	Number of cases	81

Based on this information, the program generates the set of the top layer thicknesses to be considered. If the number of cases is greater than 1, then

$$h_i = h_{min} + \frac{h_{max} - h_{min}}{m - 1}(i - 1), i = 1,2, \cdots, m$$

where h_{min} and h_{max} are the minimum and the maximum top layer thicknesses, respectively, and *m* is the number of cases.

If the number of cases is set to be equal to one, then $h_i = h_{min}$ and the maximum value is ignored.

11. Distances between the antennas and the pavement surface

The user should specify the minimum and the maximum values of the distance between the 3D GPR antennas and the pavement surface and the number of cases to be considered.

GPR height, in:	Minimum	14	Maximum	25	Number of cases	40

Based on this information, the program generates the set of the distances between the antennas and the pavement surface. If the number of cases is greater than 1, then

$$H_i = H_{min} + \frac{H_{max} - H_{min}}{k - 1}(i - 1), i = 1,2, \cdots, k$$

where h_{min} and h_{max} are the minimum and the maximum top layer thicknesses, respectively, and *k* is the number of cases.

If the number of cases is set to be equal to one, then $H_i = H_{min}$ and the maximum value is ignored.

12. Output options

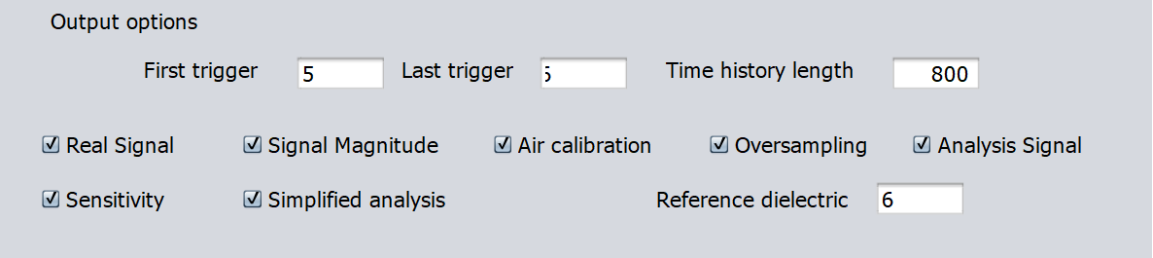

In addition to the main results, the program may output the optional detailed information. The user should specify the following parameters:

1. The first and the last trigger for which the detailed output information will be generated. If the value of the first output trigger is less than the value of the first trigger for which the analysis is conducted, then the latter will be used for the output. If the value of the last output trigger is greater than the value of the last output trigger specified for the analysis, then the latter value is used as the maximum value for the detailed output trigger.
2. Time history length – the maximum number of data points in the signal time histories outputs.
3. Real signal. If this checkbox is checked, then the raw signal will be reported for the range of the triggers specified for the detailed output.
4. Signal magnitude. If this checkbox is checked, then the calculated raw signal magnitude will be reported for the range of the triggers specified for the detailed output.
5. Air calibration signal. If this checkbox is checked, then the air calibration signal used in the analysis will be reported.
6. Oversampled signal. If this checkbox is checked, then the calculated oversampled signal used in the analysis will be reported for the range of the triggers specified for the detailed output. Depending on the specified analysis type, either the real part of the oversample signal or the signal magnitude will be reported.
7. Analysis signal. If this checkbox is checked, then the adjusted for the air calibration signal used in the analysis will be reported.
8. Sensitivity. If this checkbox is checked, then the program will report computed top layer thicknesses for each antenna pair for the entire set of the dielectric constants within the range of the specified triggers.
9. Simplified analysis– If this checkbox is checked, then the program will calculate the HMA layer thicknesses for the reference dielectric value for the HMA layer for each transmitter-receiver pair
10. Reference dielectric – dielectric constant for the HMA layer.

After all the options are selected or modified, user should press the “OK” button to save the selections and return to the main screen.

Selecting Air Calibration File

To select or modify the air calibration file, the user should select "Options->Air Calibration" in the Main Window:

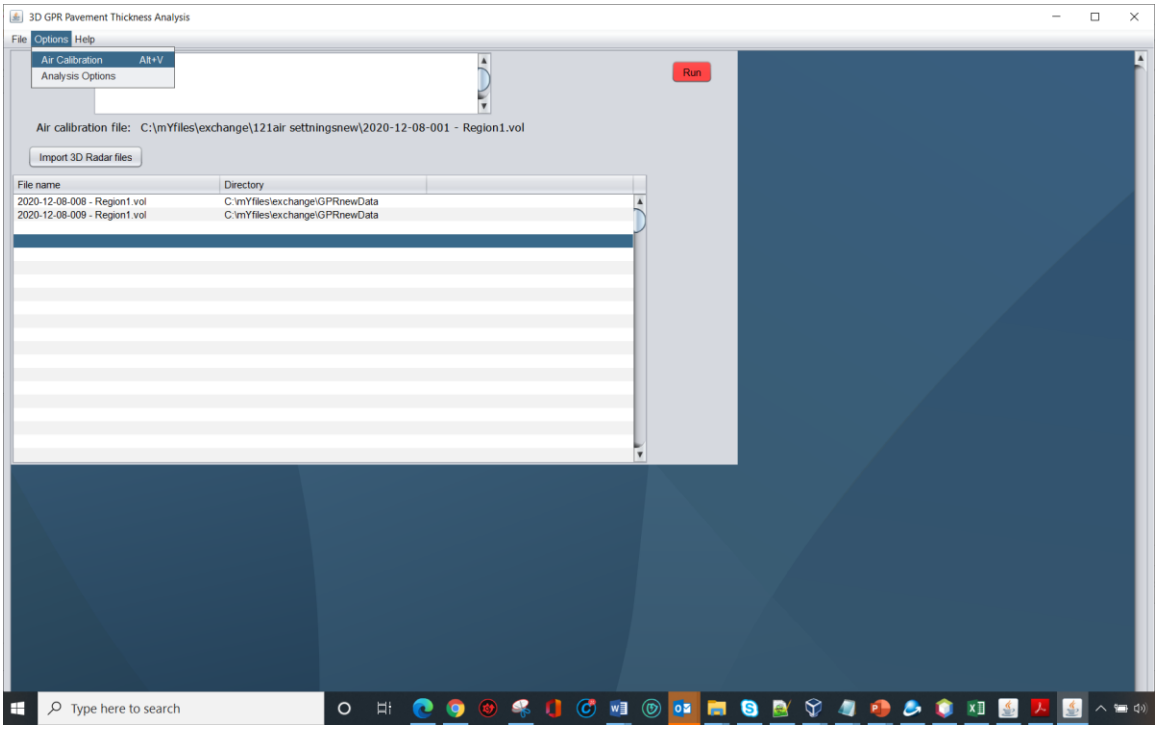

The following dialog box will appear:

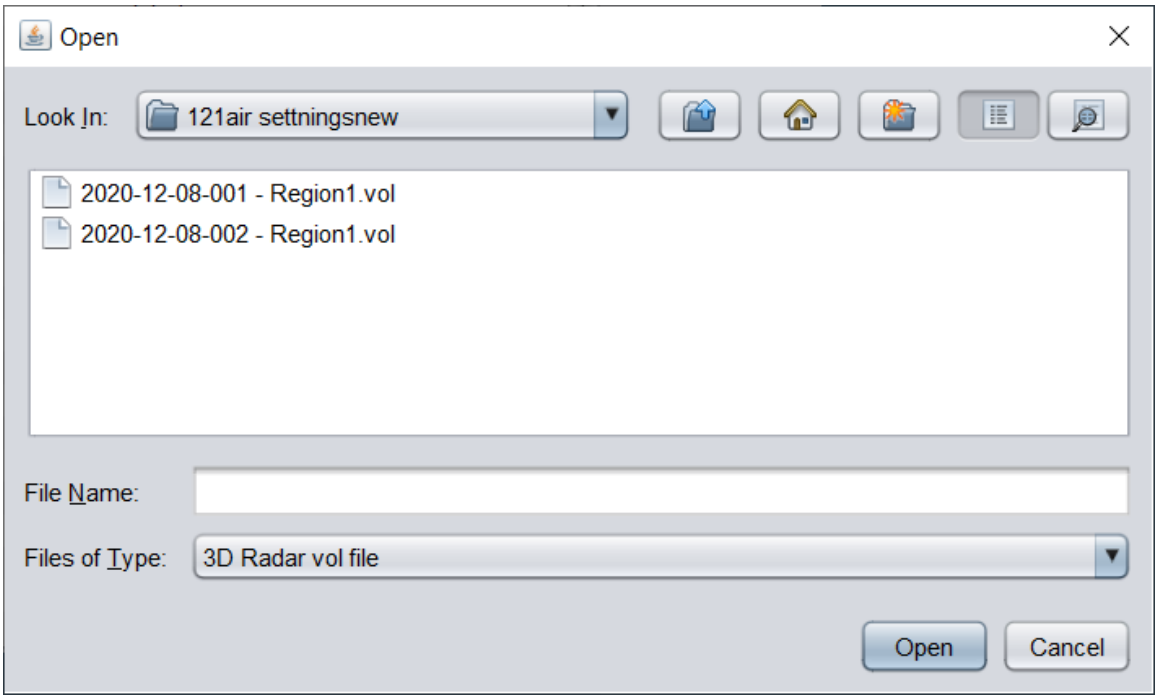

Once the appropriate file is selected, the user should press the “Open” button and the air calibration file name will be updated. The Main Window of the program will appear, and the air calibration file name and directory path will be displayed under the project info box.

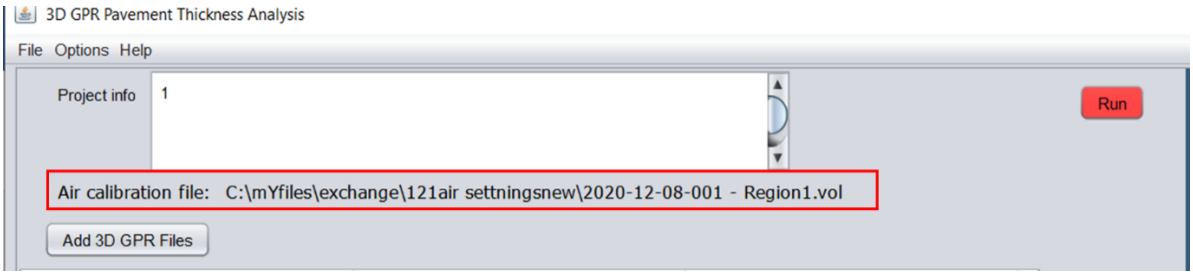

Executing Analysis

Once the 3D Radar data files, the air calibration file, and the analysis options have been selected, user can press the red "Run" button.

The table gets populated with the analysis status for each file; progress of the process is displayed:

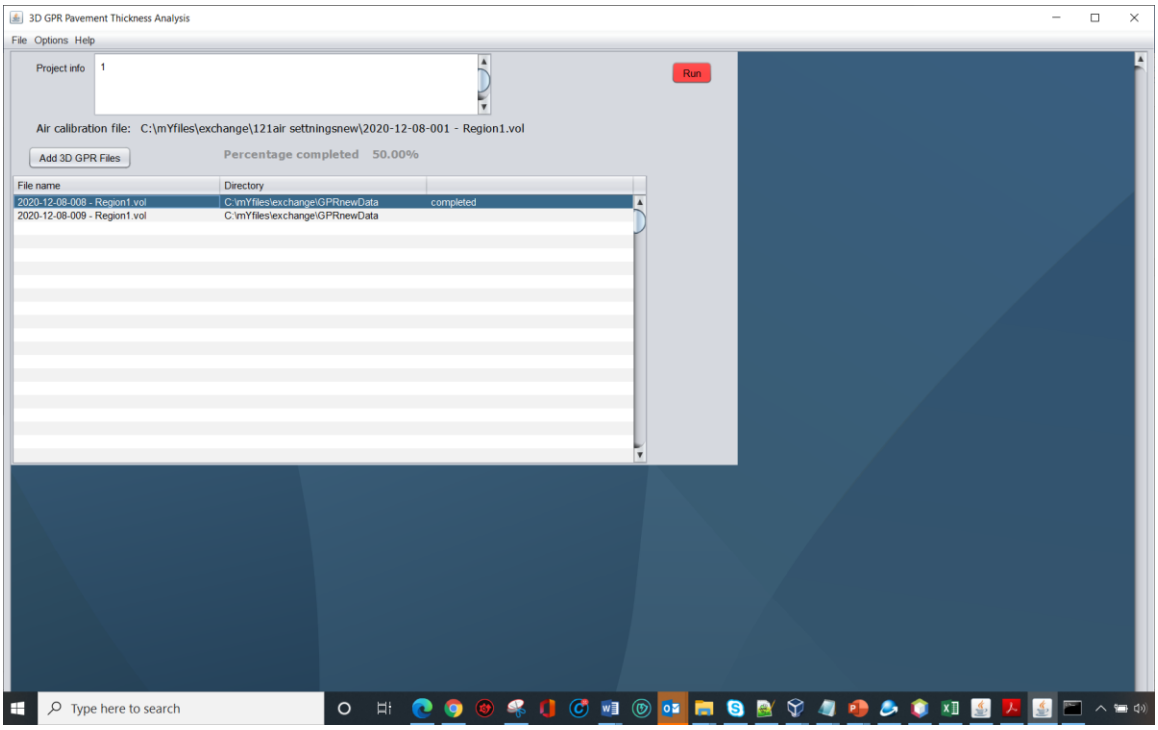

For each file_name.vol file, the program will generate an output file **File_name-XYZ_Thickness.csv** with computed top layer thickness, dielectric constant, and the distance from the 3D GPR antennas to the pavement surface for each antenna group. Indices XYZ denote the analysis method, air calibration type, and the moving average period, respectively.

If the proper output options are selected, the program will also generate the following files:

1. **File_name-XYZ_ RealSignal.csv** with real part time histories of the signals for each antenna pair and specified trigger.
2. **File_name-XYZ_ SignalMagnitude.csv** with the magnitude time history of the signals for each antenna pair and specified trigger.
3. **File_name-XYZ_ OversampledSignal.csv** with the oversamples real part or magnitude time history of the signals for each antenna pair and specified trigger.
4. **File_name-XYZ_FinalSignal.csv** with the oversamples real part or magnitude time history of the signals adjusted for the air calibration for each antenna pair and specified trigger.
5. **File_name-XYZ_air.csv** with the processed air calibration data used in the analysis.
6. **File_name-XYZ_sensitivity.csv** with the computed top surface thicknesses based on the individual antennas time histories for the entire range of dielectric constants.
7. **File_name-XYZ_sum1.csv** with the computed HMA thicknesses from each transmitting and receiving pair signals history without air calibration for the assumed reference dielectric value for the HMA layer.
8. **File_name-XYZ_sum2.csv** with the computed HMA thicknesses from each transmitting and receiving pair signals history with air calibration for the assumed reference dielectric value for the HMA layer.

After completion of the analysis for each *.vol file, the corresponding –XYZ_Thickness.csv file will be opened in notepad.

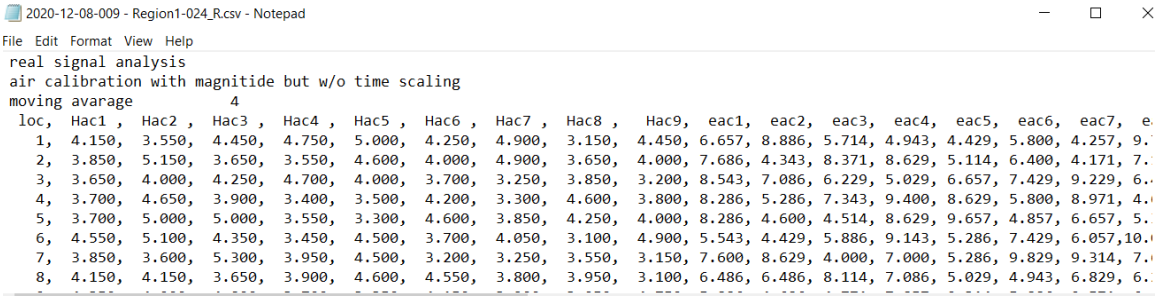

Saving Projects

To save the existing project, click "File" and "Save Project":

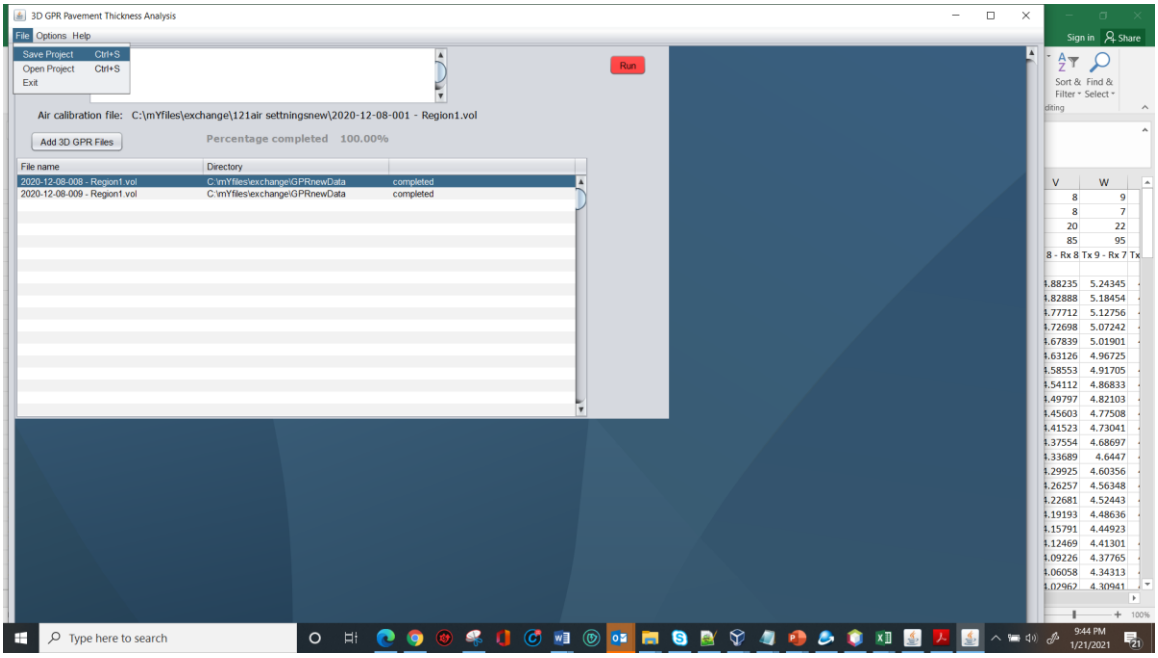

The prompt to save a file appears ("Specify a file to save"):

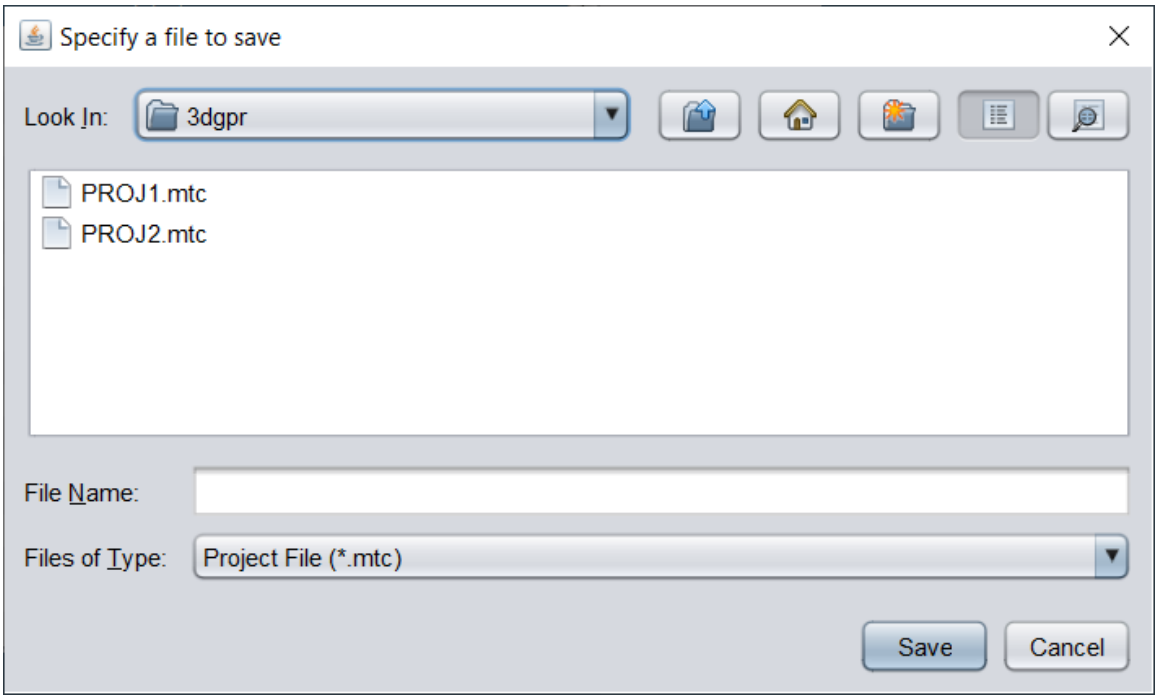

Work with Existing Projects

To reopen an existing project, click "File" and "Open Project":

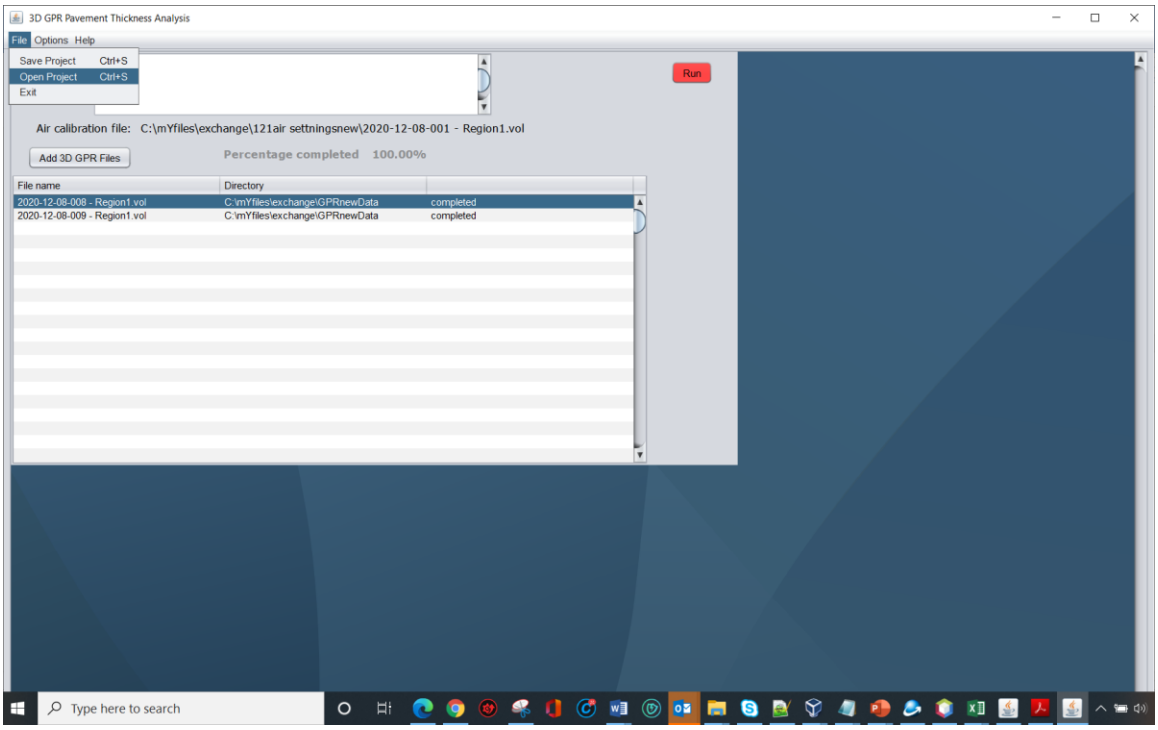

The prompt to open a file appears ("Specify a file to open"):

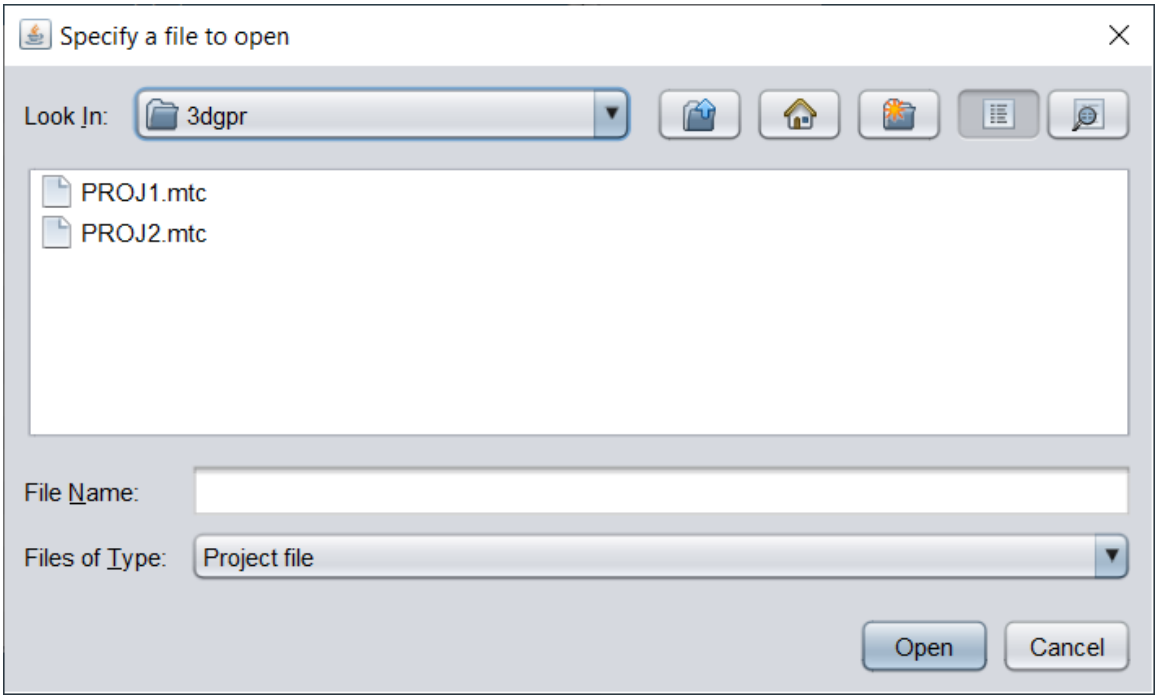

Select the desired file name(s) and click "Open".

The user now can add or delete 3D Radar files, change the analysis options, modify the project settings, and perform the analysis.